GEOLOGY AND MINERAL DEPOSITS OF THE CORNUDAS MOUNTAINS, OTERO COUNTY, NEW MEXICO

Virginia T. McLemore[1], Nels Iverson[1], Mason Woodard[1], Snir Attia[1], Haley Dietz[1], Evan J. Owen[1], Ethan B. Haft[1], Tristan Childress[2], Amy Trivitt[1], and Richard Kelley[1]

[1]New Mexico Bureau of Geology and Mineral Resources
New Mexico Institute of Mining and Technology
Socorro, NM 87801
virginia.mclemore@nmt.edu

[2]Texas Bureau of Economic Geology, Jackson School of Geosciences, The University of Texas at Austin, Texas 78713-8924 (now at U.S. Department of Energy, Morgantown, WV)

Open-file Report OF-619
ORIGINAL DECEMBER 2022

REVISED January 2024

2024

https://doi.org/10.58799/OFR-619

ABSTRACT

Re-examination of the rare earth elements (REE) deposits in the Cornudas Mountains is warranted in light of today's economic importance of critical minerals, including REE that are essential in most of our electronic devices. New mapping, petrography, $^{40}Ar/^{39}Ar$ geochronology, and geochemical analyses have provided a better understanding of the emplacement of these intrusions and associated mineral deposits. The Cornudas Mountains form the northern Trans–Pecos alkaline magmatic province in the southern part of the North American Cordilleran alkaline-igneous belt. The igneous rocks in the Cornudas Mountains were emplaced in two pulses at 37.14-34.5 and 32.48-26.95 Ma, just prior to or during the early phases of Rio Grande rift extension, and consist of 1) larger nepheline syenite–syenite laccoliths and plugs, 2) phonolite plugs, sills, and dikes, 3) smaller syenite plugs and dikes, and 4) volcanic breccia dikes that intrude Permian and Cretaceous sedimentary rocks. New USGS geophysical data indicate that some of these intrusions extend deep into the subsurface, with additional buried intrusions potentially at depth. The focus of REE exploration is along the basal unit (PEnsp2) of the Wind Mountain nepheline syenite laccolith, as well as within syenite–phonolite and volcanic breccia dikes, plugs and skarns and carbonate-replacement deposits in Chess Draw. Some samples contain as much as 3110 ppm total REE. REE could be leached from a mineral concentrate of the REE-bearing minerals (eudialyte, zircon, monazite, bastnäsite, calcio-catapleiite, vitusite, roumaite, xenotime). Niobium and zirconium are also found with the REE and have potential for economic recovery. Another potential mineral resource is nepheline syenite for use as ceramics, glass or other industrial use. We incorporate whole rock and clinopyroxene chemistry of each intrusion into the clinopyroxene-liquid geothermobarometer (Masotta, 2013) to determine the temperatures and pressures of emplacement. This thermometer provides higher crystallization temperature estimates for the syenite intrusions (857-1027^{o}C) than the phonolite sills (760-869^{o}C). We then use the barometric estimates (0.3-3.3 kbar) to calculate emplacement depths (1.2-12.3- km). Pairing these depths with the new geochronology, minimum exhumation rates for intrusions in the Cornudas Mountains are estimated that range from 0.04-0.34 mm/yr crystallization temperatures and exhumation rates provide additional information to aid in developing a model for the formation of REE deposits.

TABLE OF CONTENTS

LIST OF FIGURES

LIST OF TABLES

LIST OF ACRONYMS

BLM	U.S. Bureau of Land Management
BSE	Backscattered electron imaging
Earth MRI	Earth Mineral Resources Initiative
EO	Presidential Executive Order
GeMS	Geologic Map Schema
ICP-MS	Inductively coupled plasma mass spectrometry
MRDS	Mineral Resource Data System
MILS	Minerals Industry Location System
SQLS	MS SQL Server
NMBGMR	New Mexico Bureau of Geology and Mineral Resources
NMGRL	New Mexico Geochronology Research Laboratory
NMGS	New Mexico Geological Society
NMSHD	New Mexico State Highway Department
NMT	New Mexico Tech (New Mexico Institute of Mining and Technology)
REE	Rare earth elements
QA/QC	quality assurance and quality control
USBM	U.S. Bureau of Mines
USGS	U.S. Geological Survey
VAG	Volcanic arc granite
WAG	Within plate granite
WDS	Wavelength dispersive spectroscopy
XRD	X-ray diffraction
XRF	X-ray fluorescence

INTRODUCTION

The growing market for alternative technologies like solar panels, wind turbines, batteries, magnets, electric cars, desalination plants, and carbon capture and storage require non-traditional elements for their manufacture. In December 2017, a presidential executive order (U.S. Presidential Executive Order (EO) No. 13817) was signed that required the Departments of Interior, Energy, and Defense to develop a list of critical minerals. In May 2018, the U.S. Department of the Interior (U.S. Geological Survey, USGS) published its first list of 35 critical minerals. That list was revised in 2022. A critical mineral is a nonfuel mineral essential to the economic and national security of the United States that is from a supply chain that is vulnerable to disruption. Critical minerals are essential in the manufacture of products, the absence of which would have substantial consequences for the U.S. economy or national security. The term mineral used here is based upon the U.S. Mining Law of 1872, where minerals are defined as any mineral commodity of economic importance that could be removed from the ground. Most critical minerals are 75-100% imported into the U.S. (Committee on Critical Mineral Impacts of the U.S. Economy, 2008; Subcommittee on Critical and Strategic Mineral Supply Chains Committee on Environment, Natural Resources, and Sustainability, 2018) and many of these critical minerals are found in New Mexico (Fig. 1).

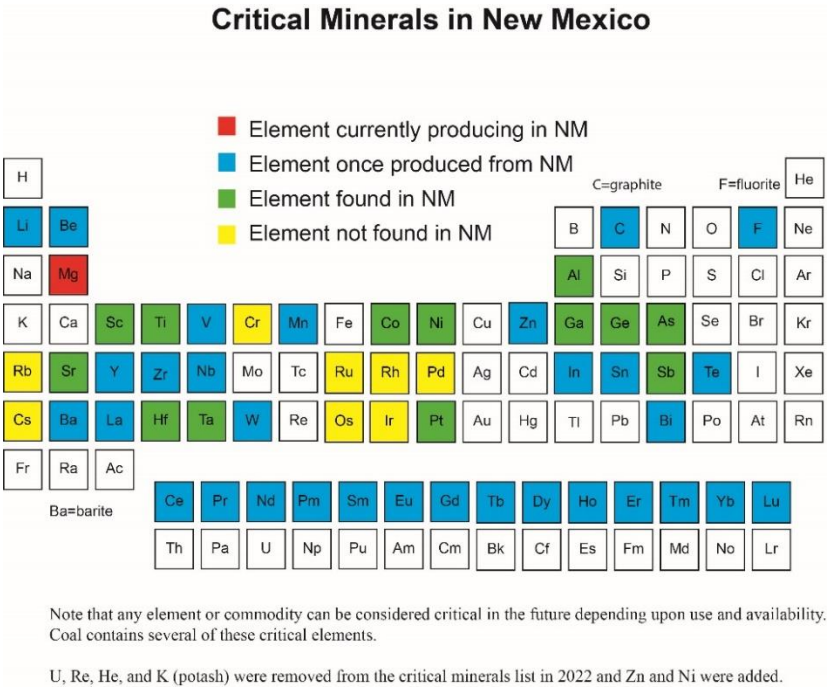

FIGURE 1. Critical minerals found in New Mexico.

Rare earth elements (REE) include the 15 lanthanide elements (La, Ce, Pr, Nd, Pm, Sm, Eu, Gd, Tb, Dy, Ho, Er, Tm, Yb, Lu, atomic numbers 57-71), yttrium (Y, atomic number 39), and scandium (Sc, atomic number 21) (Fig. 1) and are commonly divided into two chemical groups, the light REE (La through Eu) and the heavy REE (Gd through Lu and Y). REE, zirconium (Zr), niobium (Nb), and beryllium (Be), are critical minerals that are essential in most of our electronic devices, such as cell phones, laptops, computer chips, hybrid/electric cars, etc.

(Committee on Critical Mineral Impacts of the U.S. Economy, 2008; Long et al., 2010; McLemore, 2011, 2014). REE are used in magnets and batteries, and cerium is an important polishing agent. Other uses include wind turbines, solar panels, water purification, desalination, magnetic refrigeration, and more efficient light bulbs. Most of the current world production of REE comes from China, but the U.S. has significant REE resources that have a potential for future development. Zirconium is used as a refractory material in laboratory crucibles and metallurgical furnaces, and as an abrasive. Niobium is used in superconductors, batteries, and alloys. Beryllium is used in the defense, aerospace, automotive, medical, and electronics industries, in the cooling systems for nuclear reactors, and as shielding in nuclear reactors. Most of the world's beryllium comes from the U.S. and Brazil, but additional deposits need to be evaluated for sustainable future production. Some of the REE, Zr, Nb, and Be resources are located in New Mexico, but they have not been important exploration targets in the past because demand has been met elsewhere. However, with the projected increase in demand for critical minerals and the potential lack of available REE, Zr, and Nb production from China, the New Mexico deposits are being re-examined for their potential, and several areas in the state are undergoing current exploration.

A number of types of potential economic commodities, including REE, have been examined in the Cornudas Mountains in Trans-Pecos area, southern New Mexico and Texas. Of most interest to this study are potential economic deposits of REE, Zr, Nb, and Be (Schreiner, 1994; Nutt et al, 1997; McLemore, 2018). REE, Zr, Nb, and Be minerals are found in phonolite dikes, skarns, and the lower unit (PEnsp2) of the Wind Mountain nepheline syenite laccolith. In addition, the potential of one other type of mineral deposit has been studied, nepheline syenite for glass, ceramics, and sand blasting (McLemore and Guilinger, 1993). There has been no mineral production from the Cornudas Mountains except for test shipments of nepheline syenite in 1995. The mineral deposits found in the Cornudas Mountains require re-examination, specifically to better characterize the igneous system and associated mineralization and alteration in order to assess the economic potential in the Cornudas Mountains. The purpose of this study is to examine the geology and mineral-resource potential of the Cornudas Mountains by remapping specific mineralized and altered areas along with conducting detailed petrography, geochemistry, mineralogy, and geochronology.

The Cornudas Mountains are located along the North American Cordilleran alkaline-igneous belt in southern Otero County, New Mexico and northern Huspeth County, Texas (Fig. 2, 3) and form the northern extent of the Trans–Pecos alkaline magmatic province. This area is south and east of the McGregor Military Range and is part of the Otero Mesa-Diablo Platform between Rio Grande rift to the west and Salt Basin to the east (King and Harder, 1985; Nutt and O'Neill, 1998). The igneous rocks in the Cornudas Mountains were emplaced in two pulses at 37.14-34.5 and 32.48-26.95 Ma, just prior to or during the early phases of Rio Grande rift extension, and consist of 1) larger nepheline syenite to syenite laccoliths (Wind Mountain, Deer Mountain, San Antonio Mountain, Cornudas Mountain), 2) phonolite and nepheline syenite sills (Alamos Mountain, Flat Top Mountains, Chattfield Mountain, Washburn Mountain, and Black Mountain), 3) smaller syenite to nepheline syenite intrusions in Chess Draw, and 4) numerous syenite, nepheline syenite, volcanic breccia, and phonolite dikes that intrude Permian and Cretaceous sedimentary rocks (Table 1, Fig. 2). Other dikes, sills, and plugs are buried by sedimentary cover as indicated by subsurface drilling (King and Harder, 1985; Scaar, 1986), geophysical surveys (Bultman, 2021, 2022), and suggested by structural anomalies (i.e. folds, synclines, faults; U.S. Borax, 1986; Nutt et al., 1997; O'Neill and Nutt, 1998) in the overlying sedimentary rocks.

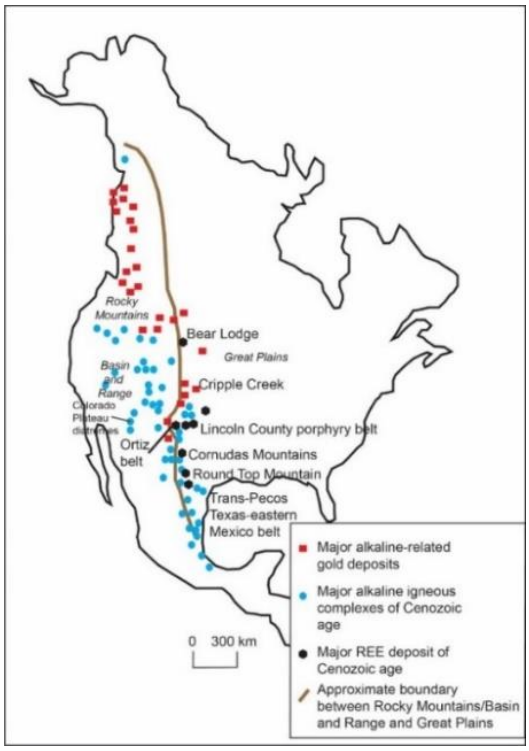

A.

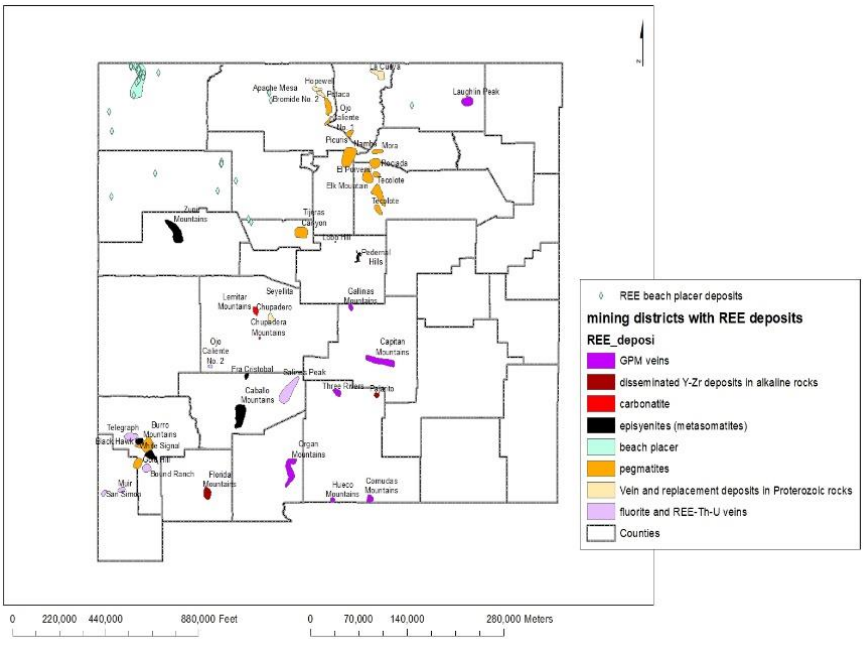

B.

FIGURE 2. A—Simplified map showing the extent of the North American Cordilleran alkaline-igneous belt (modified from Mutschler et al., 1991; McLemore, 1996, 2015a, b, 2018). B— Mining districts related to the North American Cordilleran alkaline-igneous belt (GPM or Great Plains Margin deposits), Rio Grande rift, calderas, and other Eocene-Miocene mining districts in New

Mexico (Chapin et al., 1978, 2004; McLemore, 1996, 2001, 2015a, b, c, 2018; Sims et al., 2002; McLemore et al., 2005a, b). GPM=Great Plains margin (GPM) deposits.

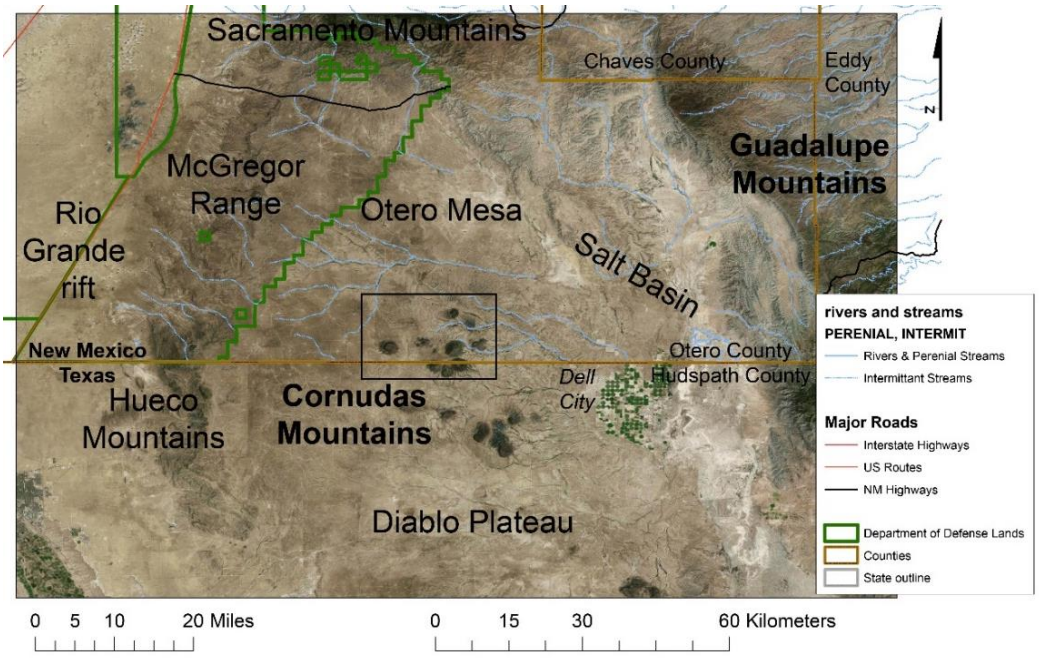

FIGURE 3. Location of Cornudas Mountains and regional physiographic features.

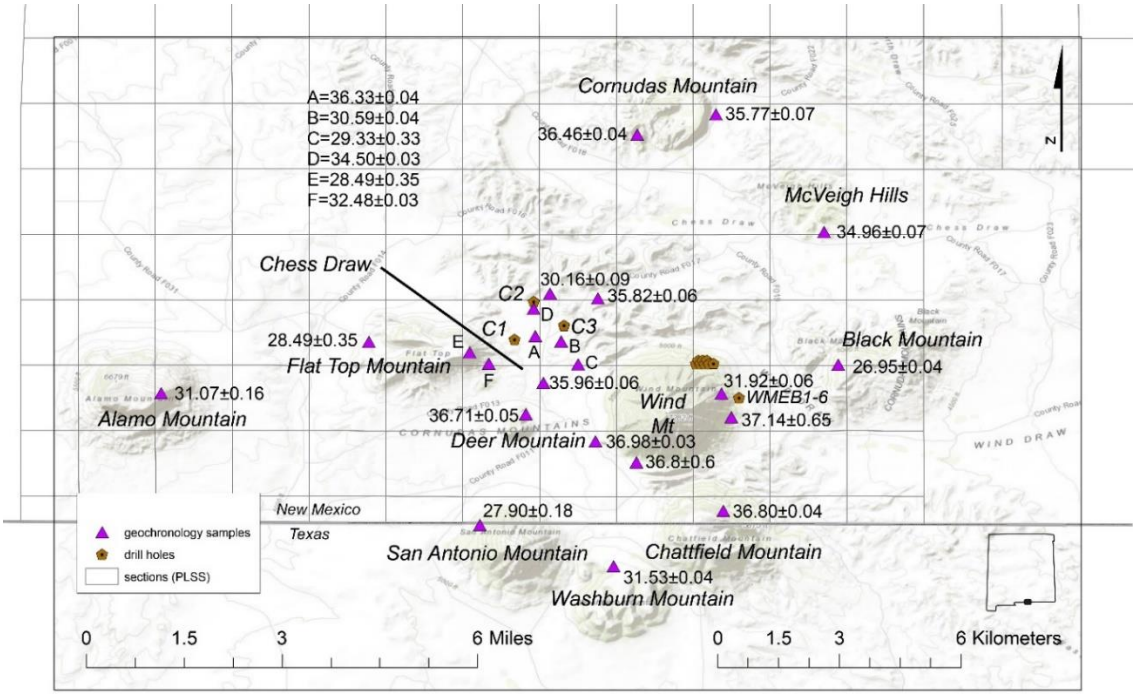

FIGURE 4. Intrusive bodies in the Cornudas Mountains, showing location of geochronology samples and drill holes. Summarized in Table 1.

TABLE 1. Intrusive bodies in the Cornudas Mountains, locations shown in Figure 4 (modified from Barker et al., 1977; McLemore, 2018; new mapping). Details of the geochronology are provided in a later section. *Note that fragments of phonolite are found in the Chattfield Mountain sill, indicating an older phonolite not identified at the surface (see description in a later section).

Locality, map unit	Predominant lithology	Form	Thickness (km)	Sample No. or reference for age date	Age (Ma)
Wind Mountain, PEnsp2	Nepheline syenite to syenite porphyry	Layered laccolith	0.25	McLemore (1996), CORN814	36.8±0.6, 37.14±0.65
Lil' Windy (west Wind Mountain), PEnsp3	Nepheline syenite	Laccolith	0.1	CORN4005	36.98±0.03
Chattfield Mountain, PEp*	Phonolite	Sill	0.15	CORN4015	36.80±0.04
Deer Mountain (Little Wind Mountain), PEns, PEm	Nepheline syenite	Laccolith	0.1	CORN2000	36.71±0.05
Sill west of Cornudas Mountain, PEp	Quartz syenite to syenite	Sill	0.1	CORN4019	36.46±0.04
Northwest Chess Draw augite syenite, PEas (Tas of Potter, 1996a, b), surrounded by PEs	Augite syenite inner zone, syenite outer zone, intruded by phonolite dike	Plug	0.1	CORN177	36.33±0.04
South Chess Draw nepheline syenite, PEnsc	Nepheline syenite	Sill	0.02	CORN20-10	35.96±0.06
Chess Draw, PEbx	Volcanic breccia	Dikes	0.01	nd	nd
Dike north of Wind Mountain, PEp	Phonolite	Dike	0.01	CORN181	35.82±0.06
Cornudas Mountain, PEqs, PEs	Quartz syenite to syenite	Plug or laccolith, sill	0.1	CORN112	35.77±0.07
McVeigh Hills, PEs, PEqs	Quartz syenite to syenite	Top of a laccolith or sill?	?	CORN226	34.96±0.07
Mesquite Hill (north Chess Draw), PEp	Phonolite	Dike	0.01	CORN4008	34.50±0.03
Dike east of Flat Top, PEp	Phonolite	Dike	0.01	CORN117	32.48±0.03
Wind Mountain dike, PEp	Phonolite	Dike	0.01	CORN805	31.92±0.06
Washburn Mountain, PEns	Nepheline syenite	Sill	0.15	CND208	31.53±0.44
Alamo Mountain, PEp, PEm	Phonolite	Discordant sheet or sill	0.25	CORN4002	31.07±0.16
Northeast Chess Draw (unnamed hill), PEpp	Phonolite	Plug	0.1	CORN4006	30.59±0.04
Chess Draw dike, PEp	Phonolite	Plug	0.01	CORN4007	30.16±0.09
East Chess Draw nepheline syenite, PEnsc	Nepheline syenite	Plug	0.01	CORN79	29.33±0.23
Flat Top, PEp	Phonolite	Sill (50-75 ft thick)	0.015-0.023	CORN4004	28.49±0.35
San Antonio Mountain, PEns	Nepheline syenite	Laccolith	0.15	CORN4013	27.90±0.18
Black Mountain, PEps	Nepheline syenite	Sill	0.07	CORN4011	26.95±0.04

REGIONAL GEOLOGIC AND TECTONIC SETTING

Lindgren (1933) was one of the first geologists who noted that a belt of alkaline-igneous rocks extends from Alaska and British Columbia southward into eastern New Mexico, Trans-Pecos Texas, and eastern Mexico (Fig. 2) and that these rocks contain relatively large quantities of critical minerals such as fluorine (F), Zr, Nb, REE, and other commodities such as gold and copper. Since then, the North American Cordilleran alkaline-igneous belt has been explored and exploited for numerous types of mineral deposits, especially gold and silver (Mutschler et al., 1985, 1991; Kelley and Ludington, 2002; Kelley and Spry, 2016), fluorite, and REE (Woolley, 1987; McLemore, 2018). Economic mineral deposits found within this belt have produced nearly 13% of the total lode gold production in the U.S. and Canada (Mutschler et al., 1991). Consequently, numerous companies have examined the belt for additional mineral deposits, including those related to REE, Zr, Nb, and Be deposits.

The North American Cordilleran alkaline-igneous belt in New Mexico (Fig. 2) coincides with exposures of alkaline intrusions and eastward lithospheric thickening, which follows the tectonic boundary between the stable Great Plains and the tectonically active Rocky Mountains and Basin and Range provinces from Colorado to Texas. The lithosphere of the Basin and Range and Southern Rocky Mountains is thinner, has a higher heat flow, and is more permeable and more fractured than the cooler, thicker lithosphere of the Great Plains (Prodehl and Lipman, 1989; McLemore, 1996; Keeley and Ludington, 2002; Chapin, 2012). The diversity of igneous rocks and associated mineral deposits within this belt (Mutschler et al., 1985, 1991; McLemore, 1996, 2018) suggests that the boundary between the Great Plains and Rocky Mountains and Basin and Range provinces is a region of highly fractionated and differentiated magmas (Thompson, 1991a, b; Allen and Foord, 1991).

In New Mexico, the North American Cordilleran alkaline-igneous belt extends from the Sangre de Cristo Mountains west of Raton, southward to the Cornudas Mountains (Fig. 2; North and McLemore, 1988; McLemore, 1996, 2001, 2018). The ages of alkaline-igneous rocks within this belt in New Mexico range from ~45 Ma through ~22 Ma and span the end of subduction-related tectonics through rifting and extension in New Mexico (Fig. 5). Significant mineral production, especially gold and tungsten, has come from New Mexico deposits spatially associated with Cenozoic alkaline-igneous rocks in the New Mexico portion of the alkaline-igneous belt (McLemore, 1996, 2001, 2017). These mineral deposits in New Mexico have been referred to as Great Plains Margin (GPM) deposits by North and McLemore (1988) and McLemore (1996, 2001, 2018). Alternative classifications by other workers include alkalic-gold or alkaline-igneous related gold deposits (Fulp and Woodward, 1991; Thompson, 1991a, b; Bonham, 1988; Mutschler et al., 1985, 1991; Richards, 1995), porphyry gold deposits (Wilson and Kyser, 1988), and Rocky Mountain gold province.

METHODS OF STUDY

Previous data

An important step in this study is to compile all published and unpublished data from existing mines and prospects within the Cornudas Mountains, including historical accounts from newspaper articles and older geologic reports. Mineral databases were examined, including the Mineral Resource Data System (MRDS) of the USGS (Mason and Arndt, 1996), the Minerals Industry Location System (MILS) of the U.S. Bureau of Mines (USBM) (U.S. Bureau of Mines, 1995), U.S. Forest Service Abandoned and Inactive Mines database, and AMLIS (U.S. Bureau of Land Management, BLM). Published and unpublished reports and files at the New Mexico Bureau of Geology and Mineral Resources (NMBGMR) were also examined. Using these data, mineral occurrences, deposits, mines, prospects, resources, and mills were identified, plotted, and entered in the NMBGMR New Mexico Mines Database (McLemore et al., 2005a, b; McLemore, 2010). Mines, prospects, and quarries in the Cornudas Mountains are identified by the unique mine identification number (NMOtxxxx, New Mexico Mines Database) throughout the report. Locational and other data are in the New Mexico Mines Database and summarized in Appendix 1.

Geologic mapping

Geologic mapping of the Cornudas Mountains was conducted by senior project personnel (McLemore, Attia, and Iverson) at scales ranging from 1:1,000 to 1:24,000 between 2020 and 2023 (Plate 1). Geologic maps were constructed onto USGS topographic base maps (portions of Alamo Mountain, Cornudas Mountain, McVeigh Hills). Previous geologic maps by O'Neill and Nutt (1998), Nutt et al. (1997), Clabaugh (1941), Zapp (1941), Tim (1941), Warner et al. (1959), Schreiner (1994), U.S. Borax (1986) and McLemore et al. (1996, including detailed mapping of Wind Mountain by P. Graseah in 1992) were used to guide new geologic map construction. Richard Kelly digitized the maps by O'Neill and Nutt (1998) and McLemore et al. (1996a, b), which were used to make the final geologic map for this report (Plate 1). Final map production was supervised by Phil Miller.

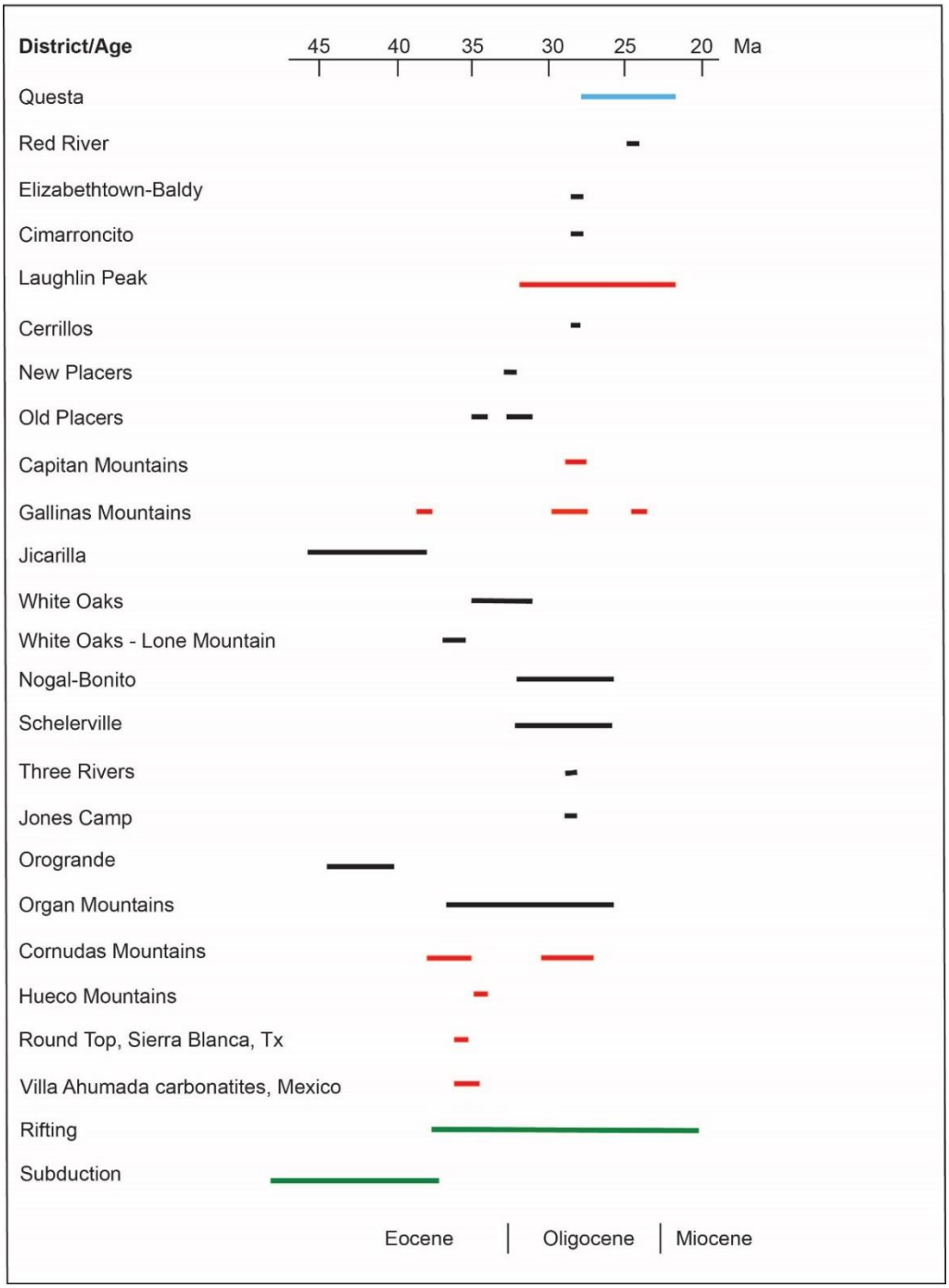

FIGURE 5. Ages of igneous rocks associated with North American Cordilleran alkaline-igneous belt (i.e. GPM districts) in New Mexico, Texas, and eastern Mexico, arranged from north to south (modified from McLemore, 2018 and McLemore et al., 2021, and includes ages obtained in this study). The blue line represents predominantly porphyry molybdenum deposits, black lines represent primary gold and base metals districts, and the red lines represent predominantly REE districts. The green lines represent rifting and subduction, and are from McMillan et al. (2000) and Chapin et al. (2004). Previous $^{40}Ar/^{39}Ar$ ages have been recalculated using the new

monitor age 28.201 Ma from Kuiper et al. (2008). Published ages are listed in McLemore (2018), Zimmerer et al. (2019), McLemore et al. (2021), and this report. Locations are in Figure 2.

Multiple traverses were made over both Chess and Wind Draws, Cornudas Mountain, and along the contact of the Wind Mountain laccolith to remap those areas in detail. After geophysical data were obtained, additional detailed mapping occurred in the McVeigh Hills. Additional newly recognized faults have been mapped. Geologic features could be determined in more detail than in previous mapping because of the use of handheld GPS units, which were used to accurately locate geologic features. Arial photographs were used in the revised mapping. Data were compiled and digitized in ArcMap version 10.7.1 using the GeMS format (https://ngmdb.usgs.gov/Info/standards/GeMS). Orientations of fractures, faults, dikes, veins, and bedding were recorded in the project databases.

In addition to regional mapping of the Cornudas Mountains, detailed geologic mapping of selected areas of alteration and mineral deposits was conducted at scales of 1:500 to 1:1,000 by McLemore (figures throughout this report). Pits, trenches, shafts, and adits have exposed some of the mineralized areas.

The revised geologic map (Plate 1) shows significant changes from previous mapping in the Chess Draw, Wind Mountain, Cornudas Mountain, and McVeigh Hills areas; however, much of the regional mapping surrounding these areas by O'Neill and Nutt (1998) was not significantly changed. The igneous intrusions are further subdivided into specific units (Plates 1, 2). Mapping of the Texas portion of the southern Cornudas Mountains is in progress and will be presented in a future report by the Texas Bureau of Economic Geology.

Project databases

Databases were developed for this project (McLemore et al., 2022). Initially, data were collected and stored in MS Access databases. During the course of the project, to increase reliability, efficiency and security, data were migrated to MS SQL Server (SQLS) and the Access "front end" forms were reworked to connect to the external database server. Mapping components and other spatial data are in ESRI ArcMap geodatabases (Plate 1). Some of the appendices are taken from the project databases. Locational and other information of photographs taken in the field, thin sections, and hand samples are recorded in the SQLS database. Location and descriptions of samples referred to in this report are in the SQLS database.

Drill core

Drilling has occurred in the Cornudas Mountains and is summarized in Table 2 and locations are shown in Figure 4. U.S. Borax drilled three holes in the Chess Draw area in 1985 (C-1, C-2, C-3; Scaar, 1986); this core is stored at the NMBGMR core facility and was relogged as part of this study (Appendix 2). Selected samples were collected for chemical analyses and mineralogical study. AddWest Minerals, Inc. drilled eight holes in 1992 at the southwest end of Wind Mountain (near the Wind Mountain adit, NMOt0014). McLemore examined that core in the field while drilling was performed, but did not sample any of the core. Geovic Mining Corp. drilled 12 winkie holes on the northern portion of Wind Mountain in 2010, east of the State Lease (NMOt043, NMOt0437). The JS Group entered a joint agreement with Geovic and the joint venture drilled four additional angled holes on eastern portion of Wind Mountain, north of the Jones prospects (NMOt0011) in 2015. McLemore logged three of the holes and sampled

selectively from all four holes. All three companies provided NMBGMR with their drill reports and chemical analyses; however, AddWest did not perform any geochemistry on their core. Description of selected core is provided in a later section.

TABLE 2. Summary information on drill holes in the Cornudas Mountains. Holes C1, C2, and C3 are stored at the NMBGMR core facility. AddWest=AddWest Minerals Inc. Locations shown in Figure 4. Coordinate system=NAD27.

Hole No	Latitude	Longitude	Elevation (ft)	Depth (ft)	Core size	Inclination	Azimuth	Company	Comments
C1	32.041631	-105.54926	5175	900	NX	Vertical		U.S. Borax	Core, chemistry available
C2	32.05	-105.545	5110	800	NX	Vertical		U.S. Borax	Core, chemistry available
C3	32.044699	-105.53826	5155	800	NX, BX	Vertical		U.S. Borax	Core, chemistry available
WM-1	32.016264	-105.520744	5500	21.3		Vertical		AddWest	
WM-2	32.016264	-105.520744	5500	26		Vertical		AddWest	
WM-3	32.016264	-105.520744	5500	11.6		Vertical		AddWest	
WM-4	32.016264	-105.520744	5470	57		Vertical		AddWest	
WM-5	32.016264	-105.520744	5470	69		Vertical		AddWest	
WM-6	32.016264	-105.520744	5470	25		Vertical		AddWest	
WM-7	32.016264	-105.520744	5530	102		Vertical		AddWest	
WM-8	32.016264	-105.520744	5530	96		Vertical		AddWest	
WM-01A	32.036231	-105.508971	5202.3	182	Winkie	Vertical		Geovic	Chemistry available
WM-02	32.036932	-105.508497	5053.801	170.5	Winkie	Vertical		Geovic	Chemistry available
WM-03	32.036234	-105.508007			Winkie	Vertical		Geovic	Chemistry available
WM-04	32.036935	-105.507532	5055.341	138.5	Winkie	Vertical		Geovic	Chemistry available
WM-05	32.036238	-105.507043			Winkie	Vertical		Geovic	Chemistry available
WM-06	32.036945	-105.50655	5051.621	123.5	Winkie	Vertical		Geovic	Chemistry available
WM-07	32.036242	-105.506079			Winkie	Vertical		Geovic	
WM-08	32.036246	-105.505116			Winkie	Vertical		Geovic	
BM-01	32.029649	-105.477638			Winkie	Vertical		Geovic	
BM-02	32.032273	-105.477183			Winkie	Vertical		Geovic	
WMEB-1	32.028683	-105.499442	4879		NX	45	270	Geovic-JS	Chemistry available
WMEB-2	32.028683	-105.499442	4879		NX	90		Geovic-JS	Chemistry available
WMEB-4	32.028683	-105.499442	4879		NX	45	245	Geovic-JS	Chemistry available
WMEB-6	32.028683	-105.499442	4879		NX	55	295	Geovic-JS	Chemistry available

Drill core was photographed and logged describing the lithology, color, mineralogy, phenocryst size and shape, alteration, fracture intensity, and hardness. Grain size cards were used to determine phenocryst shape and rounding, and tables were used to determine alteration and fracture intensity. All core was photographed with hole, box, and depth information and then replaced in the original position. Select drill core samples were split in half using a drill core splitter or saw. One half of the core was returned to the box to preserve the core. The other half was split into sufficient sizes for thin section preparation and chips for chemical analysis. Sampled intervals are indicated in the core box by a note denoting person, date, purpose, project, hole, box, and depth. Appendix 2 is a summary of drill logs and chemical analyses are in Appendix 3.

Sample collection

Samples from outcrops, mine waste rock piles, mine workings, drill core, and rarely subcrop or float were collected by project personnel, analyzed, and used to supplement published and unpublished data. Unaltered igneous intrusions, mineralized and altered samples were collected for geochronological, mineralogical, and geochemical analyses. Appendix 3 contains chemical analyses of drill core and Appendix 4 contains chemical analyses of surface samples. Mineralized and altered areas were previously sampled and analyzed in 1980 and 2009-2010 by McLemore, in 1995 by the USBM (Schreiner, 1995), and in 2016-2020 by Geovic. These data were combined and used in the chemical interpretations. Since none of these legacy samples were available for petrographic analyses, some sites were resampled for this study. Location, type of sample, and other descriptive data were entered into the project database. Most samples were composite samples (i.e. combination of individual samples over an outcrop, generally 0.3-1 m in diameter), although select (high-grade or highly mineralized) or chip (i.e. combination of individual samples over a specified length) samples of mineralized and altered areas were collected for specific analyses. Samples were sawed and scanned. Samples (sawed samples, thin sections, hand samples, mineral separates, probe samples) are archived at NMBGMR for future examination.

Geochemical analyses

Geochemical data are a critical part of geologic mapping and for evaluation for critical mineral resources central to the mission of the Earth Mapping Resources Initiative (Earth MRI). Geochemical analyses of samples collected for this study were determined by the USGS laboratory (see Appendix 5) and by ALS Laboratory (description of methods can be found at ALS Geochemistry Fee Schedule USD (2).pdf). Unweathered, fist-sized samples or small chips were selected in the field specifically for chemical analyses. Weathered surfaces and organic material were removed. Samples were submitted to the laboratories where sample preparation occurred. Duplicate samples and standards were analyzed and uncertainty of analyses is generally <5%. Specific analytical methods for each element and additional quality assurance and quality control (QA/QC) are discussed in Appendix 5. Published geochemical analyses by Barker et al. (1977), Schreiner (1994), Potter (1996a, b), McLemore et al. (1996a), New Mexico Bureau of Mines and Mineral Resources et al. (1998), and unpublished geochemical analyses by Geovic Mining Corp. were combined with the new analyses to form an extensive geochemical data set (Appendix 4). Chemical analyses also were provided by the Texas Bureau of Economic Geology (determined by the USGS) for completeness of the data set, even though the Texas

portion of the Cornudas Mountains was not mapped for this study. Chemical plots were created using ioGAS-64 (ioGAS™ - REFLEX (reflexnow.com) and GCDkit (GCDkit, home).

Petrography and mineralogy

Hand sample descriptions of both sawed samples and thin sections were entered into the project's SQLS database. Polished thin sections of selected samples of the igneous, altered, and mineralized rocks were made by Quality Thin Sections. Thin sections were scanned in both plane and plane polarized light, and selected photomicrographs were taken. Mineralogy of selected samples was determined by visual and petrographic, X-ray diffraction (XRD), and electron microprobe methods (Table 3). Igneous rock lithologies were identified on the basis of mineralogy and chemistry as defined by Le Maitre (1989).

X-ray powder diffraction (XRD) analysis was performed on either whole rock or mineral separates performed on a PANalytical X- Pert PRO® diffractometer at the NMBGMR X-ray Diffraction Laboratory. Analyses were conducted using 45 kV X-ray beam tension and 40 mA X-ray beam current. XRD scans were identified using X'Pert HighScore Plus® software, which identifies intensity peaks and matches patterns to a Powder Diffraction File database. XRD data are in Appendix 6.

Petrographic descriptions, including mineralogy and texture, of thin sections using plane, plane polarized, and reflective light were entered into the SQLS database. Modal analyses of major and minor minerals were estimated by standard percentage charts (Walker and Cohen, 2009, section 6.2). However, most minerals listed in Table 3, including potential economic minerals, are found only in trace amounts. The particle size and abundances of potential economic minerals were not determined in this study because of insufficient funding and time. Whole-rock geochemical analyses can act as analogs for abundance of some minerals (for example; Zr for eudialyte, F for fluorite, Nb for pyrochlore, total REE for eudialyte), but that assumes all of the element is found in only one mineral. Additional methods are required to determine abundances of trace elements, as discussed in the recommendations section.

$^{40}Ar/^{39}Ar$ Geochronology

Biotite, amphibole, and groundmass concentrates were prepared using conventional techniques at the New Mexico Geochronology Research Laboratory (NMGRL). Samples were crushed using a jaw crusher and disk mill crusher. The crushed samples were sieved into three size fractions using 1.41 and 0.420 mm (14 and 40 mesh) sieves and the 14-40 mesh size fraction was washed in deionized water. Crushed materials were sonicated in hydrochloric acid, rinsed and then sonicated in hydrofluoric acid to break apart and clean clumped grains as well as remove fines. Cleaned samples were separated using a Frantz Isodynamic Magnetic Separator. If needed, separated samples were filtered using heavy liquids (LMT) to concentrate biotite and amphiboles. Altered mineral grains were removed and clean biotite or amphiboles were picked using a binocular microscope. In samples that lacked either phase, groundmass grains that were mostly homogenous and did not contain large crystals were picked for analysis.

Picked samples were loaded into 8-hole aluminum disks to be irradiated. Irradiation NM-316 contained five samples for this project and was conducted at the USGS TRIGA reactor in Denver, Colorado. They were irradiated for 16 hours and returned to NMGRL. Irradiations NM-322 and NM-324 contained nine and twelve samples, respectively and were irradiation for 24 and 21 hours at the Oregon State University TRIGA reactor in Corvallis, Oregon. Samples were

co-irradiated with flux monitor FC-2 sanidine crystals using the age 28.201 Ma (Kuiper et al, 2008) and the decay constant of $5.463x10^{-10}$/yr (Min et al., 2001).

Following irradiation, feldspar monitors were loaded into 421 stainless steel laser trays and degassed as single-crystal fusions by a 55-watt CO_2-laser and analyzed on a high-sensitivity ARGUS VI multi-collector mass spectrometer. Cornudas samples were loaded into 37-hole stainless steel trays, placed under vacuum, and step heated with ten steps using a Photon Machines 810 nm diode laser at NMGRL. The samples were then analyzed using the Helix MC Plus multi-collector mass spectrometer. Atmospheric air ($^{40}Ar/^{36}Ar$ = 295.5, Neir, 1950), blank air, cocktail (internal reference gas with a $^{40}Ar/^{39}Ar$ ratio of 6.71), and blank cocktail measurements were taken between each sample to aid in calibration and assist in data reduction. Data was reduced using PyChron software (Ross, 2014) and ages were assigned by either step-heating spectral analysis or inverse-isochrons. The preferred age was a plateau age as defined by Fleck et al. (1977). If no plateau was available, the inverse isochron age was selected as the preferred age. Additional information on analytical procedures, age calculations and instrumentation can be found in the footnotes of Appendix 7.

Electron microprobe studies

Samples with high measured total REE and Zr concentrations were analyzed for the major and minor element compositions of feldspars, zirconosilicates and REE-bearing phases. All preparation work was completed at the NMBGMR electron microprobe lab. Rock samples were cut to billet size, set in plastic ring molds, backfilled with Spurr 4-part epoxy, and cured at 80ºC for four hours. Some of the samples dated using the $^{40}Ar/^{39}Ar$ dating method needed further characterization and a subset of the picked grains were analyzed on the electron microprobe. These samples were mounted in leucite 4-hole mounts, backfilled with Spurr 4-part epoxy and cured. Cured samples were then polished using diamond polishing wheels (168 µm, 63 µm and 30 µm) and finished with diamond polishing powder slurry on Buehler polishing cloth (15 µm, 6 µm) down to 1 µm and coated with approximately 20 nm of carbon.

Prepared samples were analyzed using the Cameca SX-100 electron microprobe with four wavelength dispersive spectrometers (WDS) located at the NMBGMR. Backscattered electron (BSE) images were used to observe textures, identify phases with high mean atomic number, and assess REE phase abundance. WDS qualitative element scans and WDS X-ray maps were used to identify the mineral phases. Major, minor, and trace element concentrations were collected on specific mineral phases using a 20 nA beam current and an accelerating voltage of 15 kV. Eudialyte, bastnäsite, and feldspars were analyzed with a 10 µm beam diameter, 10 µm for pyroxenes and monazite, and 5 µm for calciocatapleiite due to their small size in most samples. The microprobe was calibrated using kaersutite and Kakanui hornblendes, orthoclase, and albite standards. Calibration minerals, counting times, and spectrometers crystals can be found in the footnote of Appendix 8.

EXPLORATION HISTORY

The Cornudas Mountains are 18 mi (29 km) northwest of Dell City, Texas and were prominent landmarks on historic maps as early as the 1860s. Cornudas Mountain was once a stage coach stop on the Butterfield Overland Mail route from about 1858 to 1861; the Cornudas spring provided water for travelers. Springs on Washburn Mountain (Washburn and Persimmon springs) were shown on 1860s and 1870s maps, but were dry by 1980.

There has been no mineral production from the Cornudas Mountains except for a test shipment of nepheline syenite in 1993 for industrial mineral use from the Wind Mountain nepheline syenite adit (NMOt0014). Prospect pits and shallow shafts were found and described during mapping in Chess Draw, Wind Mountain, and McVeigh Hills (Appendix 1). One of the earliest historical accounts of mineral exploration in the Cornudas Mountains was in 1882 for lead (New Southwest and Grant County Herald, 1882). Beryllium was first reported from the Cornudas Mountains during the 1940s (Zapp, 1941; Fleischer and Cameron, 1946; Warner et al., 1959). In the 1950s, prospectors located several areas of anomalously high radioactivity in the Cornudas Mountains and attributed it to the presence of uranium and thorium. Shallow prospect pits and one adit were constructed on many of the claims in the area, but assay results were low and the claims were later dropped with no production (Collins, 1958; Warner et al., 1959; Holser, 1959; McLemore, 1983; Schreiner, 1994). In 1956, the U.S. Atomic Energy Commission examined the area to evaluate the potential for uranium (Collins, 1958). Assays ranged from 0 to 0.8% U_3O_8 (Collins, 1958) and 13-351 ppm Th (Schreiner, 1994). No further work was recommended. Woodrome (1980) collected samples from the Cornudas Mountains to evaluate the area for uranium and thorium, but reported low concentrations.

In 1958, the USBM examined the area for beryllium and suggested the occurrence of tin, nickel, rubidium, and lithium from spectrographic analyses (NMBGMR file data, 5879_mf). A few samples assayed as much as 0.2% BeO (Warner et al., 1959). The only beryllium minerals identified so far is epididmite, which is found in trace amounts in miarolitic cavities (Table 3). Northwest of Wind Mountain, one sample contains ~150 ppm Be, whereas the remaining samples from that area contain less than 100 ppm Be (Appendix 6; Warner et al., 1959; Scaar, 1986). The abundant rare mineralogies in the Cornudas Mountains (Table 3) suggest the area has potential for undiscovered deposits of REE, Nb, and Zr. A few companies have examined the Cornudas Mountains unsuccessfully for similar deposits, including gold and silver.

TABLE 3. Minerals and summary of their occurrence reported from the Cornudas Mountains. *Identified or confirmed by NMBGMR thin section, XRD (Appendix 6) or electron microprobe (Appendix 8). Additional references include Tschernich (1992), Northrop (1996), and DeMark (1989). na=not analyzed

Mineral	Occurrence	Chemical formulae	Reference
*Actinolite	Nepheline syenite, syenite	$Ca_2(Mg,Fe)_5Si_8O_{22}(OH)_2$	This study
*Aegirine-augite (acmite)	Miarolitic cavities, prismatic crystals locally in phonolite dikes and nepheline syenite, skarns	$NaFe_3Si_2O_6$	Boggs (1985, 1987)
*Aenigmatite	Nepheline syenite	$Na_2Fe_5^{2+}Ti\ (Si_6O_{18})O_2$	Barker and Hodges (1977)
*Albite	Platy to tabular crystals in most igneous intrusions	$Na(AlSi_3O_8)$	Boggs (1985, 1987)
*Analcime	Replaces nepheline, lines vugs, vesicles and miarolitic cavities, skarns, alteration of nepheline	$Na(AlSi_2O_6) \cdot H_2O$	Barker and Hodges (1977), Boggs (1985)

Mineral	Occurrence	Chemical formulae	Reference
*Anatase	Nepheline syenite, syenite	TiO_2	This study
*Arfvedsonite	Miarolitic cavities, prismatic crystals	$[Na][Na_2][Fe^{2+}{}_4Fe^{3+}]Si_8O_{22}(OH)_2$	Mindat.Org
*Apatite	Accessory mineral in igneous rocks	$Ca_{10}(PO_4)_6(OH,F,Cl)_2$	This study
*Aqualite (Eudialyte group)	Skarn north of Wind Mountain (CORN104)	$(H_3O)_8(Na,K,Sr)_5Ca_6Zr_3Si_{26}O_{66})(OH)_9Cl$	This study
*Barite	Skarns	$BaSO_4$	Mindat.Org
*Bastnäsite	Hexagonal crystals, disseminated in nepheline syenite	$(Ce,La)(CO_3)F$	This study
*Biotite	Nepheline syenite, syenite	$K(Mg,Fe)_3AlSi_3O_{10}(F,OH)_2$	This study
Brockite	Vugs in nepheline syenite	$(Ca,Th,Ce)PO_4 \cdot H_2O$	Mindat.Org
*Calcite	Colorless to white, skarns	$CaCO_3$	This study
*Calderite	Nepeheline syenite, Chess Draw	$Mn^{2+}{}_3Fe^{3+}{}_2(SiO_4)_3$	This study
*Cancrinite	Skarn east of Wind Mountain (CORN108), nepheline syenite Wind Mountain (CORN812), alteration of nepheline	$Na_6Ca_2[(CO_3)_2\|Al_6Si_6O_{24}]\cdot 2H_2O$	This study
*Catapleiite (calciocatapleiite)	Miarolitic cavities, platy to tabular , disseminated in nepheline syenite	$Na_2Zr(Si_3O_9) \cdot 2H_2O$	Boggs (1985)
Chabazite	Miarolitic cavities	$(Ca,K_2,Na_2,Mg)Al_2Si_4O_{12}\cdot 6H_2O$	Boggs (1985)
*Chlorite	Skarns, altered phonolite dikes	$(Mg,Fe)_3(Si,Al)_4O_{10}(OH)_2\cdot (Mg,Fe)_3(OH)_6$	This study
*Clinoptilolite	Disseminated in nepheline syenite	$Ca_3(Si_{30}Al_6)O_{72}\cdot 20H_2O$	Mindat.Org
*Diopside-hedenbergite	Nepheline syenite	$MgCaSi_2O_6$	This study
*Dolomite	Skarns, carbonate-replacement deposits, minor alteration in some igneous rocks	$CaMg(CO_3)_2$	This study
Elpidite	Prismatic, in miarolitic cavities	$Na_2ZrSi_6O_{15}\cdot 3H_2O$	Michayluk and Cone (2017b)
Epididmite	Psuedohexagonal plates	$Na_2Be_2Si_6O_{15}\cdot H_2O$	Michayluk and Cone (2017b)
*Epidote	Skarns	$Ca_2(Al_2,Fe)(SiO_4)(Si_2O_7)O(OH)$	This study
*Eudialyte	Dikes, sills, and laccoliths and in miarolitic cavities	$Na_4(Ca, Ce)_2(Fe^{2+}, Mn^{2+})YZrSi_8O_{22}(OH,Cl)_2$	Barker and Hodges (1977), Clabaugh (1950), Boggs (1985, 1987)
*Fayalite (olivine, aenigmatite)	Nepheline syenite, phonolite	Fe_2SiO_4	This study
*Fluorite	Breccia, skarns	CaF_2	Barker et al. (1977), Schreiner (1994)
Gaidonnayite	Miarolitic cavities	$Na_2Zr(Si_3O_9) \cdot 2H_2O$	Michayluk and Cone (2017b)
*Galena	Dikes, nepheline syenite Wind Mountain	PbS	Schreiner (1994), this study
*Georgechaoite	Miarolitic cavities, coatings on microcline or acmite, from south side of Wind Mountain	$NaKZrSi_3O_9\cdot 2H_2O$	Boggs (1985), Boggs and Ghose (1985)
Gonnardite	Miarolitic cavities	$(Na,Ca)_2(Si,Al)_5O_{10}\cdot 3H_2O$	Mindat.Org

Mineral	Occurrence	Chemical formulae	Reference
*Grosslar garnet	Yellow hexagonal crystals (CORN4011)	$Ca_3Al_2(SiO_4)_3$	This study
*Gyrolite	Disseminated in nepheline syenite	$NaCa_{16}Si_{23}AlO_{60}(OH)_8•64(H_2O)$	This study
*Hastingsite (pyroxene)	Skarn	$NaCa_2(Fe^{2+}_4Fe^{3+})(Si_6Al_2)O_{22}OH_2$	This study
*Hematite	Common alteration mineral	Fe_2O_3	This study
Heulandite-Ca	Miarolitic cavities	$(Ca,Na)_5(Si_{27}Al_9)O_{72}•26H_2O$	Michayluk and Cone (2017b)
Hochelagaite	Nepheline syenite	$(Ca,Na,Sr)(Nb,Ti,Si,Al)_4O_{11}•8H_2O$	Mindat.org
*Hornblende	Nepheline syenite and syenite	$(Ca,Na)_{2-3}(Mg,Fe,Al)_5(Al,Si)_8O_{22}(OH,F)_2$	This study
* Hydroxy-manganopyrochlore	Phonolite dike	$(Mn^{2+},Th,Na,Ca,REE)_2(Nb,Ti)_2O_6(OH)$	This study
*Ilmenite	Nepheline syenite, augite syenite	$FeTiO_3$	This study
*Johannsenite (clinopyroxene)	Wind Mountain nepheline syenite	$CaMn^{2+}Si_2O_6$	This study
*Kaersutite (amphibole)	Nepheline syenite, syenite, phonolite	$NaCa_2(Mg_3Ti^{4+}Al)(Si_6Al_2)O_{22}(OH)_2$	This study
*Kaolinite	Skarns, altered areas	$Al_2(Si_2O_5)(OH)_4$	This study
*Kerimasite (garnet group)	Wind Mountain nepheline syenite	$Ca_3Zr_2(SiO_4)(Fe^{3+}O_4)_2$	This study
*K-feldspar	Crystals in most igneous intrusions	$KAlSi_3O_8$	Boggs (1985, 1987)
Lavenite	Miarolitic cavities	$(Na,Ca)_2(Mn^2,Fe^2)(Zr,Ti)(Si_2O_7)(O,OH,F)_2$	Michayluk and Cone (2017a)
Lemoynite	Miarolitic cavities	$(Na,K)_2CaZr_2Si_{10}O_{26}•H_2O$	Michayluk and Cone (2017b)
*Lizardite (serpentine group)	Nepheline syenite, skarns	$Mg_3(Si_2O_5)(OH)_4$	This study
*Lueshite	Phonolite dike	$NaNbO_3$	This study
*Maganoeudialyte	Skarn east of Wind Mountain (CORN108), nepheline syenite Wind Mountain	$Na_{14}Ca_6Mn_3Zr_3[Si_{26}O_{72}(OH)_2](H_2O,Cl,O,OH)_6$	This study
*Magnetite	Crystals in most igneous intrusions	Fe_2O_3	This study
*Magnesioferrite	Skarn	$MgFe^{3+}_2O_4$	This study
*Microcline	Crystals in most igneous intrusions	$K(AlSi_3O_8)$	This study
*Molybdenite	Disseminated in nepheline syenite	MoS_2	Michayluk and Cone (2017a)
*Montmorillonite	Skarns, altered rocks	$(Na,Ca)_{0.33}(Al,Mg)_2(Si_4O_{10})(OH)_2 \cdot nH_2O$	This study
*Monazite	Miarolitic cavities, disseminated in nepheline syenite, skarns	Ce, La, Nd(PO_4)	Boggs (1985)
*Muscovite	Crystals in most igneous intrusions, fine-grained alteration	$KAl_2(AlSi_3O_{10})(OH)_2$	Mindat.Org
*Natrolite	Prismatic crystals replaces nepheline and feldspars	$Na_2Al_2Si_3O_{10}•2H_2O$	Barker and Hodges (1977)
*Nepheline	White hexagonal crystals in many igneous intrusions	$(Na,K)AlSiO_4$	This study
Niobian rutile	Vugs, miarolitic cavities	$(Ti,Nb)O_2$	Schreiner (1994)

Mineral	Occurrence	Chemical formulae	Reference
Nordstrandite	Spherical aggregates	$Al(OH)_3$	Mindat.Org
*Olivine	Mineral aggregates of ferromagnesian minerals and magnetite	M_2SiO_4 M = Ca, Fe, Mn, Ni, Mg	Barker and Hodges (1977)
*Oxynatropyrochlore (Pyrochlore group)	Skarn	$(Na,Ca,U)_2Nb_2O_6(O,OH)$	This study
Parakeldyshite	Nepheline syenite, Wind Mountain	$Na_2ZrSi_2O_7$	McLemore et al. (1996a)
*Parasite-Ce	Disseminated nepheline syenite	$CaCe_2(CO_3)_3F_2$	Michayluk and Cone (2017b)
*Phlogopite	Alteration in skarns and igneous rocks	$KMg_3AlSi_3O_{10}(F,OH)_2$	This study
*Pigeonite (clinopyroxine group)	Nepheline syenite	$(Ca_xMg_yFe_z)(Mg_{y1}Fe_{z1})Si_2O_6$ Where $0.1 \leq x \leq 0.4$, $x + y + z = 1$ and $y1 + z1 = 1$	This study
Polylithionite	Miarolitic cavities	$KLi_2Al(Si_4O10)(F,OH)_2$	Michayluk and Cone (2017b)
*Pyrite	Within mineral aggregates of ferromagnesian minerals in syenite dike and skarn in Chess Draw, Wind Mountain nepheline syenite	FeS_2	Schreiner (1994), McLemore et al. (1996a), this study
*Pyrochlore	Nepheline syenite	$(Na,Ca)_2Nb_2O_6(OH,F)$	This study
*Pyrolusite	Phonolite dike	$Mn^{4+}O_2$	This study
*Quartz	Rare in area, disseminated within quartz syenite, along edges of phonolite dikes, within skarn, vugs in syenite	SiO_2	Schreiner (1994), Boggs (1985, 1987)
*Rheniite?	In Wind Mountain nepheline syenite (CORN812), needs confirmation	ReS_2	This study, sample contains 0.002 ppm Re (higher than most)
*Roumaite	In Wind Mountain nepheline syenite (CORN260)	$(Ca,Na,REE)_7(Nb,Ti)[Si_2O_7]_2OF_3$	This study
*Sepiolite	Nepheline syenite	$Mg_4Si_6O_{15}(OH)_2 \cdot 6H_2O$	This study
*Sergevanite (eudialyte group)	Nepheline syenite	$Na_{15}(Ca_3Mn_3)(Na_2Fe)Zr_3Si_{26}O_{72}(OH)_3 \cdot H_2O$	This study
*Siderite	Skarns, altered dikes	$FeCO_3$	This study
*Sodalite	Phonolite dikes, Wind Mountain nepheline syenite	$Na_8(Al_6Si_6O_{24})Cl_2$	This study
*Sphalerite	Disseminated in Wind Mountain nepheline syenite and dikes	(Zn,Fe)S	Schreiner (1994), this study
*Svanbergite	Nepheline syenite	$SrAl_3(PO_4)(SO_4)(OH)_6$	This study
Thomosonite (Ca)	Radiating balls in miarolitic cavities	$NaCa_2(Al_5Si_5O_{20}) \cdot 6H_2O$	Zapp (1941), Boggs (1985)
*Titanite	Crystals in most igneous intrusions	$CaTi(SiO_4)O$	This study
*Titanomagnetite	Phonolite dike	$Fe^{2+}(Fe^{3+},Ti)_2O_4$	This study
*Tuperssuatsiaite	Alteration clay mineral	$NaFe^{3+}{}_3Si_8O_{20}(OH)_2 \cdot H_2O$	This study
*Vitusite	Wind Mountain nepheline syenite	$Na_3(Ce,La,Nd)(PO_4)_2$	This study
Windmountainite	Vesicles in phonolite dike, nepheline syenite and phonolite sills	$Fe^{+3}{}_2Mg_2\ 2Si_8O_{20}(OH)_2(H_2O)_4 \cdot 4H_2O$	Leung and McDonald (2020)
Yofortierite?	In nepheline syenite, but identification not confirmed	$Mn_5Si_8O_{20}(OH)_2 \cdot 8\text{-}9H_2O$	Michayluk and Cone (2017a)
*Xenotime	Nepheline syenite	$(Y,Th,U,Dy,Yb.Er,Gd)PO_4$	This study
*Zircon	Nepheline syenite, syenite	$ZrSiO_4$	Schreiner (1994)

In 1984, Leonard Minerals Co. in conjunction with U.S. Borax Corp. conducted an exploration program for REE, Nb, Be, and Zr. Mapping, sampling, and drilling (Table 2, Appendix 2) in Chess Draw northeast of Wind Mountain failed to discover any significant mineralized zones (Goodell et al., 2002; NMBMMR files). Chemical analyses were low (up to 0.06% total REE, 10-1400 ppm Nb, 10-3000 ppm Zr, 230-13,000 ppm F) (Appendix 3). An analysis of a dike reported by McLemore et al. (1988a, b) contained 1235 ppm Ce, 700 ppm La, 270 ppm Nd, and 242 ppm Y (sample number 7368, Appendix 4). Analyses reported by Schreiner (1994) are also low and subeconomic at the time; as much as 3790 ppm total REE, 2332 ppm Nb, 92 ppm Be, and 3137 ppm F (Appendix 4). Zirconium silicates are common in the area and assays as high as 9919 ppm Zr are reported (Schreiner, 1994).

In 1991, the BLM designated part of the Cornudas Mountains an "Area of Critical Environmental Concern" because of endangered species and visual and cultural resources. The area is part of one of the largest remaining Chihuahuan desert grasslands in the U.S. There are many petroglyphs scattered throughout the Cornudas Mountains. Future exploration and mining activities will be required to develop plans in coordination with the BLM in order to protect these resources.

AddWest Minerals, Inc. began exploration and development of the outer zone of the Wind Mountain nepheline syenite ($PENSP_2$) in 1991-1995 for use in manufacturing amber-colored beverage containers, flatware, and ceramics and for use as an abrasive and as roofing granules (McLemore et al., 1994; McLemore and Guilinger, 1996; McLemore et al., 1996a). Drilling occurred (Table 2, Appendix 2) and an adit was constructed in the laccolith (NMOt0014). Several small shipments of nepheline syenite were sent for testing for use as sand blasting material. Mining was by underground, room and pillar methods. Processing was planned to involve crushing, grinding, magnetic separation, and screening. At full production, Wind Mountain was expected to process 3,000 short tons per day or 700,000 short tons per year. Current proven, probable, and inferred reserves total 200 million short tons for a mine life of more than 100 years (Industrial Minerals, 1995). In 1996, the company changed focus and dropped the project but retained the mining claims around the adit (NMOt0014).

In 2010 and 2011, Geovic Mining Corp. filed mining claims in the Wind Mountain area and began exploration for REE and Zr. Drilling occurred in 2011-2012 and 2015 (Table 2; Appendix 2, 3). Geovic formed a joint venture with The JS Group. Bench scale metallurgical tests are being conducted to separate REE from eudialyte and other REE-bearing minerals.

PREVIOUS WORK IN THE CORNUDAS MOUNTAINS

Shumard (1886) was one of the earliest references mentioning the igneous intrusions forming the Cornudas Mountains. The first geological mapping of the area was by three students from the University of Texas in Austin in 1941 (Zapp, 1941; Clabaugh, 1941: Timm, 1941). These three theses were the first to accurately describe the stratigraphy, igneous petrology and mineralized areas in the Cornudas Mountains.

During the 1970s and 1980s, Barker (1977, 1979, 1980, 1987) and Barker et al. (1977) began mineralogical and geochemical studies of the igneous rocks in the Trans-Pecos area, including the Cornudas Mountains. Henry et al. (1986, 2010), Henry and McDowell (1986), Rubin et al. (1987, 1988, 1990), Rubin and Price (1989), Price et al. (1987, 1990), Potter (1996a, b) continued that geochemical work. The USBM examined the mineralized areas in the early 1990s (Korzeb and Kness, 1994; Korzeb et al., 1995; Schreiner, 1994).

The USGS mapped the area in 1997 (Nutt et al., 1997; Nutt and O'Neill, 1998). Miller (1997) conducted an environmental study of water samples from the area and concluded the primary environmental concerns are the presence of saline water due to gypsum and halite, neutral to slightly acid groundwaters due to dedolomitization or reduction of sulfate, and elevated concentrations of nitrate, possibly due to leaching of cattle wastes in the vicinity of well sites. Klein and Rodriguez (1997) conducted an electrical resistivity survey in the Cornudas Mountains and concluded that the area was underlain by carbonate rocks and that a sill or flexture may underlie the area between Flat Top and Cornudas Mountain. Cretaceous stratigraphy in the Cornudas Mountains was described by Kues and Lucas (1993). Regional geologic reports of southern New Mexico include King and Harder (1985), Black (1987), New Mexico Bureau of Mines and Mineral Resources et al. (1998), and Kelley et al. (2020).

The Cornudas Mountains, especially Wind Mountain, has been a favorite mineral collecting locality for many years. Several reports and abstracts have been published and are cited in Table 3. Wind Mountain is the type locality of georgechaoite and windmountainite.

STRATIGRAPHY AND DESCRIPTION OF LITHOLOGIC UNITS

Organization of this section is generally arranged from oldest (Permian) to youngest (Quaternary); sedimentary units are described first, followed by descriptions of the igneous intrusions. The map symbols from Plate 1 are in parentheses. The oldest rocks in the Cornudas Mountains are Permian limestones of the Hueco, Yeso, and San Andres formations and Cretaceous sedimentary rocks of the Campagrande Formation, Cox Sandstone, and Muleros-Mesilla Valley Formation (undivided). Dikes, sills, and laccoliths of varying compositions, ages, and dimensions intruded the Permian and Cretaceous sedimentary rocks (Table 1). Quaternary surficial deposits are found along drainages and slopes in the Cornudas Mountains. A simplified geologic map is in Figure 6 and a correlation chart is shown in Figure 7. Locations of samples and photographs are in the SQL database.

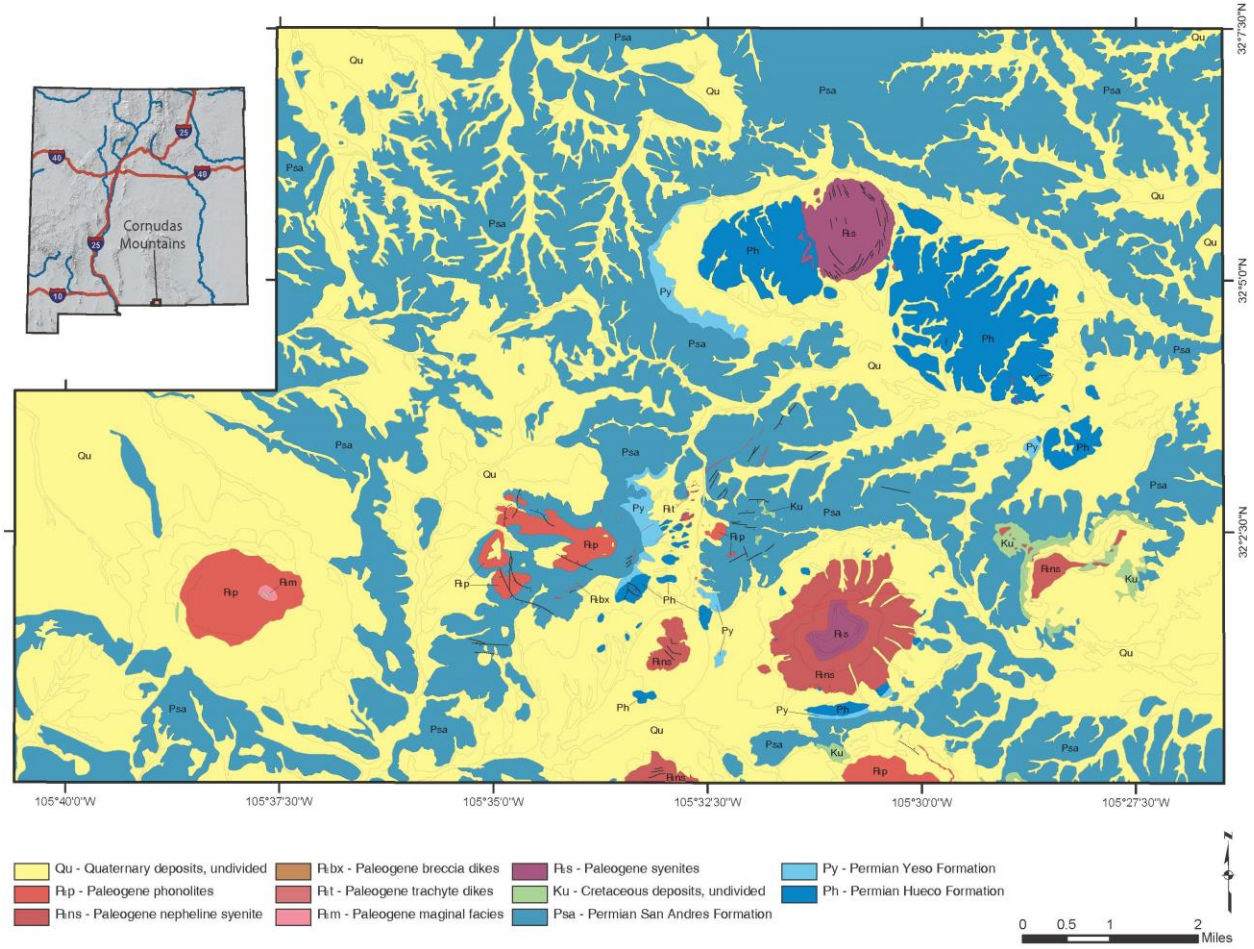

FIGURE 6. Geologic map of the Cornudas Mountains, Otero County, New Mexico based upon new mapping for this study (Plate 1) with incorporation of published maps (McLemore et al., 1996a, b; McLemore and Guilinger, 1996; O'Neill and Nutt, 1998; Nutt and O'Neill, 1998).

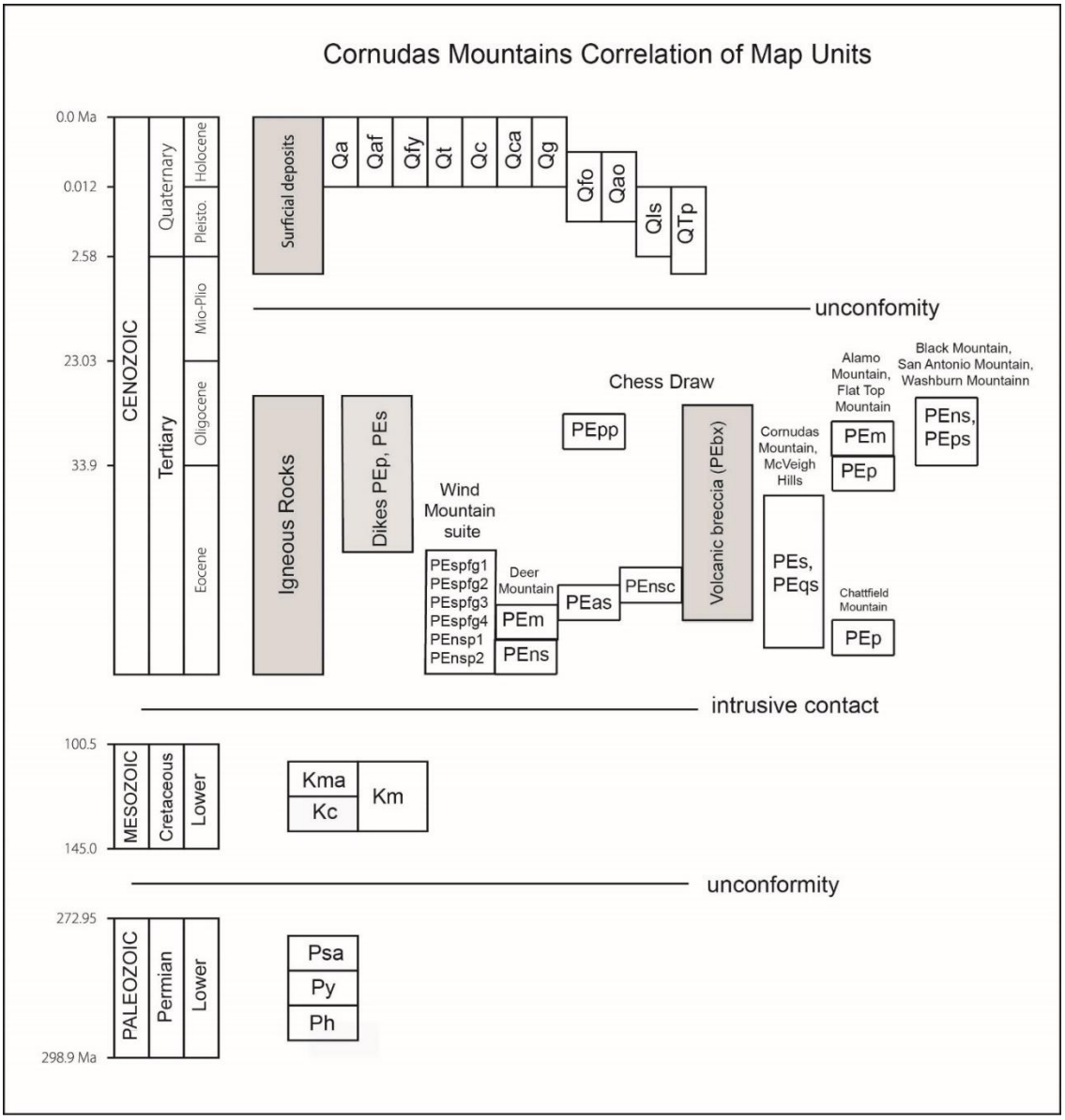

FIGURE 7. Correlation chart for rock units exposed in the Cornudas Mountains (Plate 2).

Proterozoic rocks

Proterozoic rocks are not exposed in the Cornudas Mountains, but numerous oil and gas wells have penetrated Proterozoic rocks in the area, especially on Otero Mesa. Proterozoic rocks are relatively shallow because of the erosion of Pennsylvanian and Paleozoic rocks. Proterozoic metamorphosed sedimentary rocks intruded by granite plutons and gabbro dikes and sills are exposed in the Sacromento Mountains (New Mexico Bureau of Mines and Mineral Resources et al., 1998). The oldest know Proterozoic rocks belong to the 1350 Ma Chaves granite (Black, 1973). Proterozoic metamorphosed sedimentary rocks were deposited on this terrain, forming the DeBaca metamorphic terrain.

Permian sedimentary rocks

The oldest sedimentary rocks exposed in the area belong to the Permian Hueco Formation (Ph), which form hills and mesas in the Cornudas Mountains. The Hueco Formation consists of light- to dark-gray, fine-grained, thin- to medium-bedded cherty limestones interbedded with minor gray shales and white fine- to coarse-grained sandstones and siltstones. Locally the Hueco limestone contains dark gray to black chert nodules and stringers. It is 400 to 1500 ft (122-457 m) thick in the McGregor Range area (New Mexico Bureau of Mines and Mineral Resources et al., 1998), but is typically less than 200 ft (61 m) in the Cornudas Mountains.

The Yeso Formation (Py, Leonardian) conformably overlies the Hueco Formation and is 0 to 1800 ft (0-548 m) thick in the McGregor Range area (New Mexico Bureau of Mines and Mineral Resources et al., 1998) and as much as 2,410 ft (734.4 m) in the subsurface of the Guadalupe Mountains (Kelley et al., 2020), but less than 200 ft (61 m) in the Cornudas Mountains. The Yeso consists primarily of interbedded tan to red-brown to orange siltstone and shale, white to gray finely crystalline dolostone and limestone, white to gray gypsum, and red to gray fine-grained sandstone. The Yeso Formation pinches out in the southern Cornudas Mountains and has not been reported south of the Cornudas Mountains (Nutt and O'Neill, 1998). The Yeso rocks grade into carbonate rocks of the Victorio Peak and Bone Spring formations in Texas and Guadalupe Mountains (Black, 1975; Kelley et al., 2020). The Yeso Formation was deposited in marine to continental environments.

FIGURE 8. Yellow and red siltstone beds of the Yeso Formation overlain by light gray limestones of the San Andres Formation on the east side of Flat Top Mountain, looking west.

The San Andres Formation (Psa, Leonardian) conformably overlies the Yeso Formation and is 0 to 750 ft (0-229 m) thick in the McGregor Range area (New Mexico Bureau of Mines

and Mineral Resources et al., 1998) and 847 ft (258 m) thick in the Otero Mesa (Black, 1973), but less than 500 ft (152 m) in the Cornudas Mountains. It consists of brown to dark-gray to olive-gray, thin- to medium-bedded marine dolomitic limestone and minor olive-gray dolomite. Thin beds of fine- to medium-grained quartzose sandstones are locally present in the lowermost 120 ft (36 m; Pray, 1961). The San Andres Formation in the western Cornudas Mountains grades into the Bone Springs Limestone (King, 1934; Nutt and O'Neill, 1998). In the eastern Cornudas Mountains, the San Andres Formation grades into the Victorio Peak carbonates of the Capitan reef complex (Pray, 1969; Nutt and O'Neill, 1998).

Cretaceous stratigraphy

Cretaceous sedimentary rocks are found scattered throughout the Cornudas Mountains (Fig. 6, Plate 1) at Alamo, San Antonio, Chattfield, and Black Mountains, mostly at the top of anticlines. The oldest Cretaceous rocks are metamorphosed, yellow-white to pale-green, fine-grained calcareous rocks that rest on the Alamo Mountain sill (Km). At San Antonio Mountain, the base of the Cretaceous is the Campagrande Formation (Kc), which consists of a thin siliceous conglomerate of black, gray, and red quartz, chert, and lithic pebbles that are overlain by thin beds of yellow to yellow-orange siltstone and calcarenite (Kues and Lucas, 1993; O'Neill and Nutt, 1998). The Cox Sandstone overlies the Campagrande Formation and consists of chert pebble conglomerate and silty to sandy, light gray, limestone and orange to reddish-brown calcareous quartz sandstone. The Muleros and Mesilla Valley formations (Kma) are the youngest of the Cretaceous rocks and consist of yellow to gray limestone, marl, and pebbly conglomerate and interbedded sandstone. The Cretaceous rocks are less than 300 ft (91 m) thick in the Cornudas Mountains.

FIGURE 9. Campagrande Formation, which consists of a thin siliceous conglomerate of black, gray, and red quartz, chert, and lithic pebbles.

Quaternary sedimentary units

The Quaternary units are typically unconsolidated and relatively thin. Calcium carbonate or caliche commonly coats sand and gravel, along fractures, and as cement. Many drainages are deep, indicating erosion from storm events. The oldest units are pediment alluvium (QTp, Pleistocene-Pliocene?) consisting of angular boulder to gravel set in finer-grained matrix deposited on gently sloping surfaces, and preserved as isolated, flat-topped deposits on flanks of Alamo, Black, and Chattfield Mountains and Flat Top at elevations near 4,900 ft (1,470 m).

Landslide deposits (Qls, Pleistocene) consisting of angular fragments of bedrock mixed with soil, or a heterogeneous mixture of boulders and finer-grained material derived from adjacent hillslopes. They are characterized by irregular-shaped, hummocky topography and numerous closed depressions. Landslides are mainly confined to areas underlain by Cretaceous sedimentary rocks found adjacent to Eocene-Oligocene igneous intrusions. Landslide deposits surround Alamo and Black Mountains.

Old alluvium (Qao, Holocene-Pleistocene) consist of dissected terraces underlain by sand, silt, clay, and pebble to cobble gravel and is preserved as small, isolated hills 3-10 ft (0.9-3.0 m) above active stream valley floors. Maximum thickness is unknown.

Old alluvial fan deposits (Qfo, Holocene-Pleistocene) consisting of poorly sorted silty sand and gravel are deposited in dissected, abandoned alluvial fans that no longer receive sediment. Maximum thickness is unknown.

Colluvial and alluvial gravel (Qg, Holocene?) consists of angular to subrounded pebbles and cobbles of fine grained calcareous rocks. The unit is mapped locally covering benches on Flat Top and underlain by phonolite (PEp), where it is interpreted as the erosional remnants of metamorphosed calc-silicate rocks (Km). These deposits are less than 2 ft (0.6 m) thick.

Colluvial and alluvial deposits, undivided (Qca, Holocene) consist of colluvium (Qc) that is partly reworked and dissected by intermittent streams infilled with young alluvium (Qa) and is restricted to the south-central part of the map area, which is drained by tributaries of University Draw to the south. Maximum thickness is unknown.

Colluvium (Holocene, Qc) consists of weakly to strongly cemented caliche soil developed in residual deposits of sand, silt, clay, and angular pebbles and cobbles. These deposits commonly cover the San Andres Formation (Psa) in the northwestern part of the map area, which is drained by tributaries of Shiloh Draw to the north. Thickness generally is less than 1-2 ft (0.3-0.6 m).

Talus deposits (Qt, Holocene) consist of unsorted, unstratified angular pebbles to boulders with maximum diameters of 30 ft (9 m) and covers flanks of steep slopes of hills and mountains underlain by resistant bedrock. The maximum thickness is unknown.

Young alluvial fan deposits (Qf, Holocene) consisting of poorly sorted silty sand and gravel are deposited in small alluvial fans along valley margins and around hills and mountains. Locally, these deposits include minor colluvium (Qc) where exposures are too small to differentiate on map. Maximum thickness is unknown.

Alluvial and fluvial deposits (Qaf, Holocene) consist of sand, silt, clay, and pebble to cobble deposited in narrow stream channels and on broad alluvial slopes at base of low hills and the mountain fronts. Generally, they are less than 15 ft (4.5 m) thick.

The youngest deposits are stream floodplain alluvium Qa (Holocene), consisting of sand, silt, and clay, with a maximum exposed thickness of approximately 20 ft (6 m). Some of these drainages are very deep (10-20 ft; 3-6 m) and difficult to cross.

Paleogene Igneous Rocks

The igneous rocks are intrusive and Eocene to Oligocene (Paleogene) in age. The following description of the igneous rocks is generally organized by age (oldest to youngest), then by area with descriptions of hand samples, thin sections (if available), modal analyses (if available), and geochemical characterization. The map symbols from Plate 1 are in parenthesis. Sample locations are in the SQLS database and Plate 1. A summary of the intrusions in the Cornudas Mountains is in Table 2. A detailed description of the new $^{40}Ar/^{39}Ar$ dating results is provided in a later section. The relative ages of the igneous rocks in the Cornudas Mountains are not obvious everywhere because few contact relationships exist, except in drill core, and alteration has obscured some igneous lithologies, especially in Chess Draw, McVeigh Hills, and east of Cornudas Mountain.

The nomenclature of igneous rocks in this report conforms to the International classification proposed by Le Bas et al. (1986) and Le Maitre (1989), where the primary classification of igneous rocks is based upon mineralogy and, if too fine-grained, by the use of whole-rock geochemical analyses using the TAS diagram (total alkali-silica; Le Bas et al. 1986; Le Maitre, 1989). According to the definition of volcanic and plutonic rocks proposed by Le Maitre (1989), the laccoliths and some sills in the Cornudas Mountains are plutonic (i.e. fine- to coarse-grained, equigranular matrix), thus mineralogy and the TAS plutonic classification diagram (Cox et al. 1979 adapted by Wilson 1989) is used. However most of the sills and dikes are fine-grained and the TAS volcanic diagram (Le Maitre, 1989) is used. Schreiner (1993) used the term *malignite* (nepheline syenite containing more than 50% mafic minerals) for some of the coarser mafic dikes and plugs at Wind Mountain and in Chess Draw. However, we are using the more accepted term *phonolite* if found in a dark fine-grained dike or plug, and *nepheline syenite* if coarse grained.

Field relationships indicate that these rocks are clearly intrusive. A laccolith generally is a dome- or mushroom-shaped igneous intrusion that forms at shallow depths in between layers of sedimentary rocks (Maynard, 2005). In contrast, plutons or batholiths are typically larger intrusions that formed at greater depths than laccoliths. A sill is generally smaller than a laccolith and intruded in between sedimentary rocks. The sills lack prominent vesicles and other features that would indicate an extrusive flow.

Foliation representing magma flow is common in many of the intrusions. The foliation of sills is typically parallel to subparallel to the sedimentary hosts. Plugs and dikes have steep foliation parallel to the intrusive contacts. The laccoliths typically have steep to variable foliation along the intrusive contact to more horizontal foliation towards the top of the intrusion.

Contacts between the larger intrusions and sedimentary rocks are commonly covered by talus material. Where the contacts are exposed, they are sharp. The sedimentary rocks adjacent to laccoliths are steeply dipping away from the laccoliths, whereas they realtively flat lying adjacent to the sills.

Detailed paragenesis is beyond the scope of this project, but a few observations are noted. Nepheline, K-feldspar, and biotite are generally some of the earliest minerals formed. Hornblende formed before actinolite, and aegirine formed before arfvedsonite. Hematite, sericite (white phyllosilicates), and zeolites are predominant alteration minerals.

Wind Mountain

The Wind Mountain laccolith is a prominent peak in the Cornudas Mountains (7280 ft, 2219 m elevation), is the oldest intrusion in the Cornudas Mountains, and consists of six mineralogical and textural zones (Table 4; Fig. 6, 10; McLemore et al., 1996a, b; McLemore and Guilinger, 1996). The margin of the laccolith is locally foliated. The foliation dips steeply away from the center of the intrusion (Fig. 11, 12). The laccolith is typically gray to cream colored and weathers to darker colors and consists of alkali feldspars (albite), nepheline, biotite, and a variety of accessory minerals (Fig. 13; Table 5). Varying amounts of pyroxene (aegirine-augite to aegirine to diopside-hedenbergite) and amphibole (arfvedsonite) minerals form dark-colored aggregates dispersed throughout the rock. Pegmatitic zones are common (Fig. 14). Plagioclase is rare. Some zones are red in color due to the abundance of eudialyte and other Zr and REE minerals (discussed in a later section).

Lil' Windy, a small hill southwest of Wind Mountain, is nepheline syenite and similar in texture, chemistry, and mineralogy to the Wind Mountain laccolith. It is mapped as a separate unit (PEnsp3; Table 4; Fig. 6, 10) and consists of anorthoclase, aegirine-augite, nepheline, and accessory titanomagnetite (Appendix 8, sample CORN4005).

Portions of the flanks of Wind Mountain were mapped in detail (maps provided in a later section below). The nepheline syenite intruded the limestones of the Hueco Formation, forming steep dips, as much as 70-80° along the eastern (Fig. 12) and western flanks and as much as 40-60° along the northern and southern flanks. The limestones decrease in dip within meters of the intrusive contact. Locally, phonolite dikes intrude along the limestone-nepheline syenite contact. Thin aplite dikes locally intruded the Wind Mountain nepheline syenite (Fig. 10, 12).

Chemically, most of the Wind Mountain samples plot as nepheline syenite or syenite, as mapped (Fig. 15). Chondrite-normalized REE patterns are light-REE enriched with a negative Eu anomaly (Fig. 16). Chemical variations among the individual map units within the laccolith cannot be readily discerned by utilizing major element analyses (Appendix 4; McLemore et al., 1996a, b). However, slight chemical differences in Ba and Sr between the nepheline syenite and syenite units are observed (Fig. 17). The syenites contain slightly more Ba and Sr than the nepheline syenites (McLemore et al., 1996a, b). These chemical analyses of the Wind Mountain laccolith suggest that the zonation appears to be controlled by crystal fractionation, volatile separation, and cooling history, not different pulses of magma (McLemore et al., 1996b). Feldspar crystallization under initially subsolvus conditions can account for most of the variations in the zones. The feldspar-rich solid forms at or migrates towards the top of the magma chamber and forms a capping syenite. Differential cooling of the magma resulted in the textural variations at Wind Mountain. The outer zone ($PEnsp_2$) is most suitable for use in manufacturing amber-colored beverage containers, flatware, and ceramics. Higher concentrations of REE and Zr are found in the lower unit (PEnsp2) and higher concentrations of Nb are found in the lower unit (PEnsp2) on the western edge of the laccolith.

Several black to greenish black phonolite dikes (PEp) intrude the limestones and the nepheline syenites on Wind Mountain, discussed in detail in a later section. One of the longest phonolite dikes is east-west trending and intrudes the northern Wind Mountain nepheline syenite. It is 1.5 mi (2.4 km) long.

TABLE 4. Description of the textural units comprising the Wind Mountain laccolith (modified from P. Graseah, field mapping, July 1992).

Map symbol	Name	Description	Comments
PEspfg1	Syenite porphyry	Fine-grained, contains minor analcime, aegrite, Na amphibole, biotite and magnetite in a plagioclase rich groundmass	Top of laccolith
PEspfg2	Syenite porphyry	Fine-grained, contains predominant plagioclase, aegirite, Na amphibole, biotite	
PEspfg3	Syenite porphyry	Fine-grained, contains predominant plagioclase, aegirite, Na amphibole, biotite but is more mafic than Tspfg2	
PEspfg4	Syenite porphyry	Fine-grained, contains analcime, aegrite, Na amphibole, biotite and magnetite in a plagioclase rich groundmass	
PEnsp1	Nepheline syenite porphyry	Coarse-grained, contains K-feldspar phenocrysts in a matrix of plagioclase, nepheline, analcime, with accessory aegerite, Na amphibole, minor magnetite	
PEnsp2	Nepheline syenite porphyry	Medium-grained, contains K-feldspar phenocrysts in a matrix of plagioclase, nepheline, minor analcime, with accessory aegerite, Na amphibole, minor magnetite	Base of laccolith
PEnsp3 (Lil' Windy)	Nepheline syenite porphyry	Medium-grained, contains blocky, vertical K-feldspar phenocrysts in a matrix of plagioclase, nepheline, with accessory arfvedsonite - aegerite, minor magnetite	Hill southwest of Wind Mountain

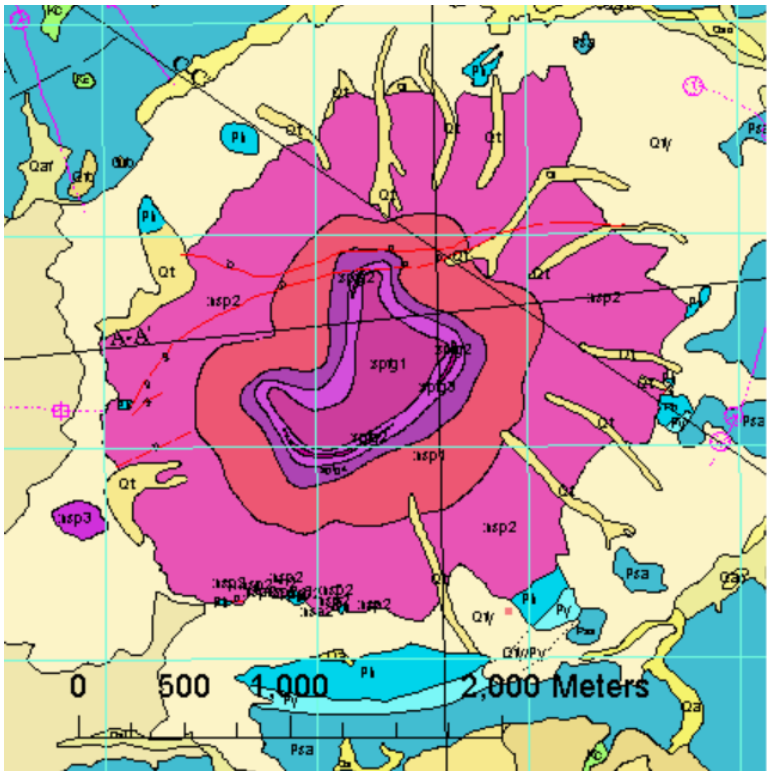

FIGURE 10. Geologic map of Wind Mountain (modified from P. Graseah, field mapping, July 1992). See Plate 1, Figure 11, and Table 4 for descriotion of geologic map units.

FIGURE 11. Wind Mountain, looking east. Note the dipping foliation near the top of the laccolith.

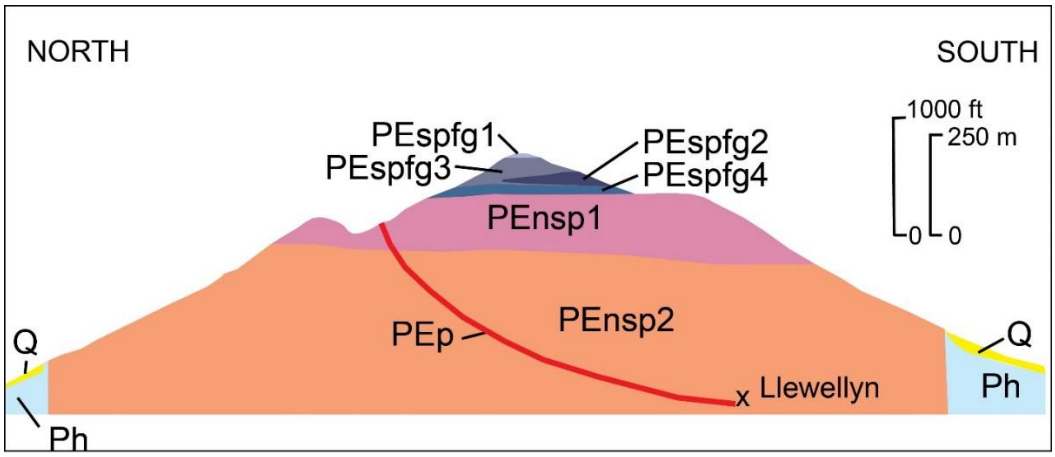

FIGURE 12. Cross section of Wind Mountain laccolith (along cross section B-B' on plate 1). See Figure 10 and Table 4 for description of units.

FIGURE 13. Close-up of Wind Mountain nepheline syenite (PEnsp2, sample CORN20-07).

FIGURE 14. Amphibole-rich pegmatite cutting nepheline syenite (PEnsp2, drill hole WMEB-4, depth 400 ft, total REE=703.86 ppm, 2991 ppm Zr).

TABLE 5. Modal analyses of Wind Mountain nepheline syenite and phonolite.

Mineral	CORN121	CORN123	CORN4005	CORN190
Lithology	Nepheline syenite (PEnsp2)	Phonolite (PEp)	Nepheline syenite (PEnsp2)	Nepheline syenite, altered (PEnsp2)
K-feldspar		6	34	9
Perthite		23		
Plagioclase			1	
Hornblende			18	
Aegirine-augite	40	18	4	17
Augite				2
Arfvedsonite		1	1	
Clinopyroxine	4			
Natrolite		16		29
Analcime		6		13
Windmountainite			1	
Nepheline	2	2	16	10
Pyrochlore			3	
Sodalite	42			
Biotite			2	
Cancrinite		4		
Phlogopite			5	
Clay	12	15		13
Calcite				1
Hematite		9	7	6
Sericite			8	
Total	100	100	100	100

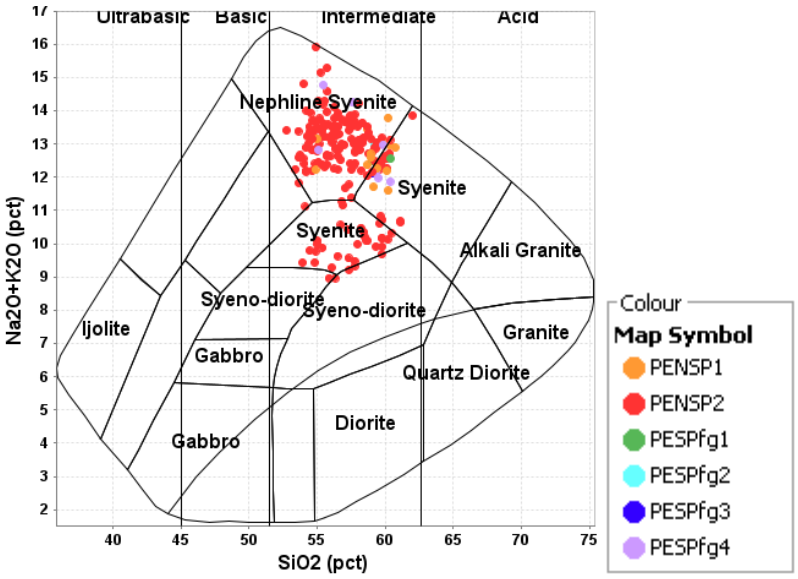

FIGURE 15. TAS plutonic classification plot for samples from Wind Mountain (Cox et al. 1979 adapted by Wilson 1989). The curved line separates the alkaline (above the curve) from subalkaline (below the curve) rocks (Irvine and Baragar, 1971). Chemical analyses are in Appendix 4.

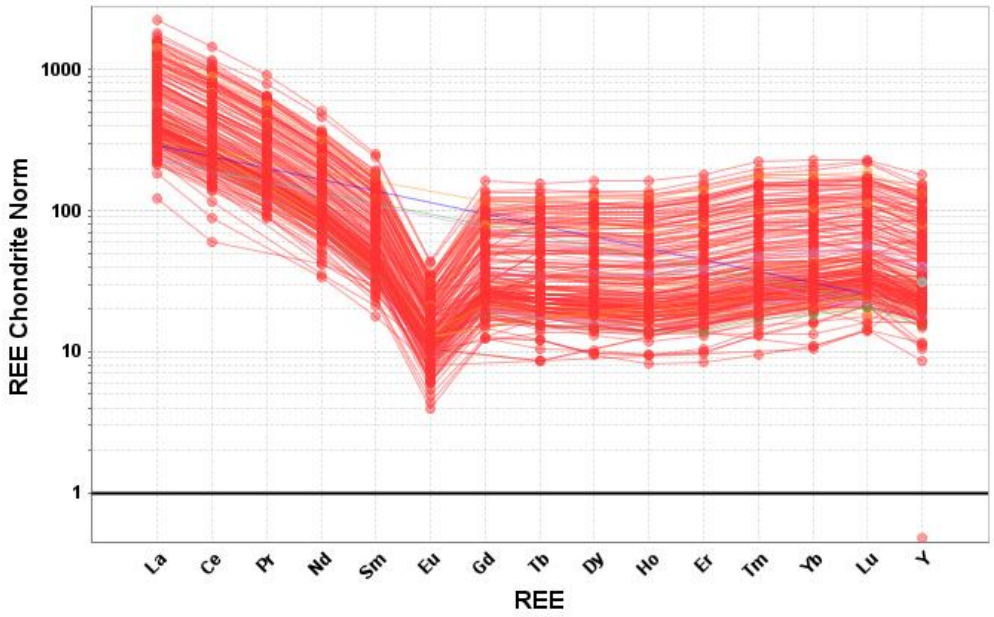

FIGURE 16. REE chondrite-normalized plot for samples from Wind Mountain (chondrite values from Taylor and McLennan, 1985). Chemical analyses are in Appendix 4.

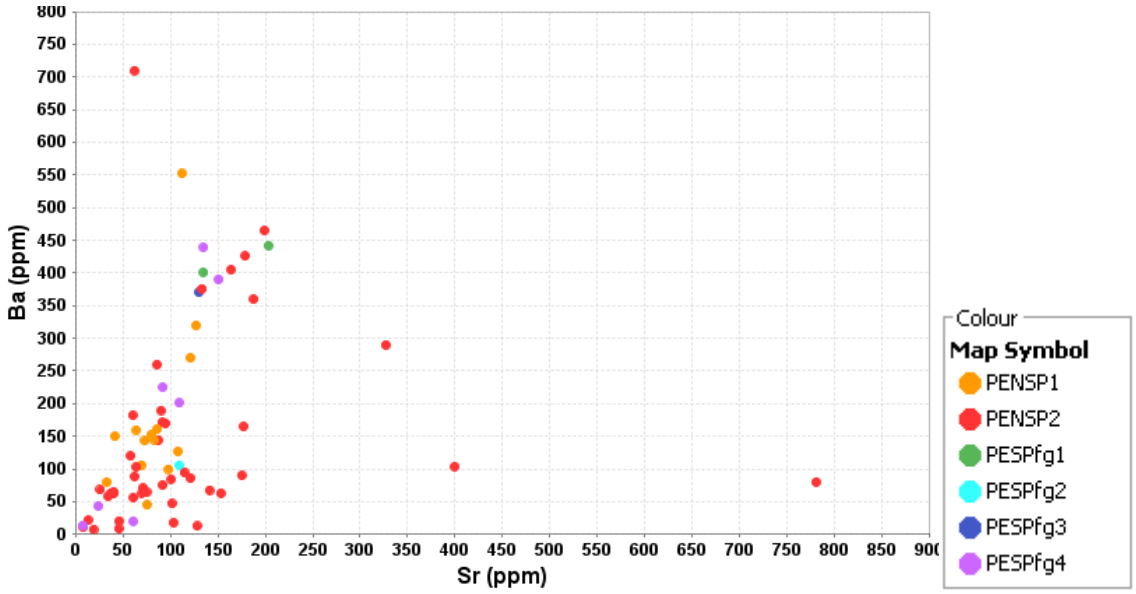

FIGURE 17. Ba-Sr plot of samples from Wind Mountain laccolith. Chemical analyses are in Appendix 4.

Chattfield Mountain (PEp)

Chattfield Mountain is a prominent peak in the Cornudas Mountains (6247 ft, 1904 m elevation) that is formed by a near-horizontal, dark green to black, aphanitic phonolite sill (Fig.

18; PEp) with local well-developed magmatic foliation. The sill consists of aegirine-augite, anorthoclase, albite, analcime, nepheline, and minor arfvedsonite and titanomagnetite (Table 6, Appendix 8, sample CORN4014). The fine-grained matrix locally has a trachytic texture formed by anorthoclase. Small fragments of phonolite are found in the sill (Fig. 19), indicating older phonolite intrusions at depth.

Chemically, samples plot as phonolite (Fig. 20). Chondrite-normalized REE patterns are light-REE enriched with a negative Eu anomaly (Fig. 21).

FIGURE 18. Wind Mountain left, Chattfield Mountain middle, San Antonio Mountain right, looking southeast across southern Chess Draw.

FIGURE 19. Close-up of Chattfield phonolite sill. Note the dark black phonolite fragments.

TABLE 6. Modal analyses of Chattfield phonolite.

Mineral	CORN4015	CORN4014
Lithology	Phonolite	Phonolite
K-feldspar	15	24
Actinolite	1	
Aegirine	20	10
Arfvedsonite	4	4
hornblende		7
aenigmatite	1	1
hastingsite	1	1
Nepheline	30	12
natrolite	14	
pyrochlore	2	4
Biotite	1	1
magnetite		3
Cancrinite		1
Tuperssuatsiaite - Windmountainite		2
sodalite		10
zeolite		4
calcite	2	
Hematite	4	
Sericite (white phyosilicate)	5	8
Total	100	

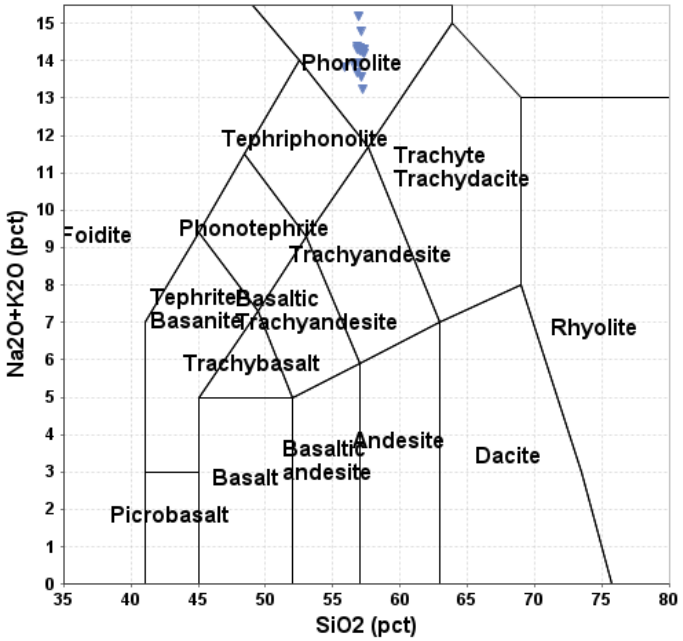

FIGURE 20. TAS (total alkali vs silica) plot of samples from Chattfield sill (La Maitre, 1989). Chemical analyses are in Appendix 4.

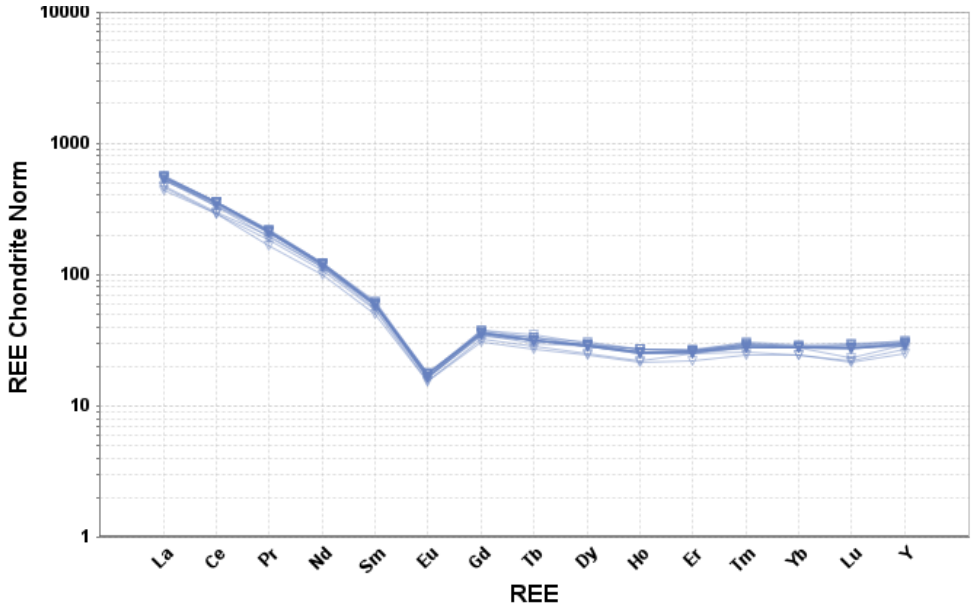

FIGURE 21. REE chondrite-normalized plot for samples from Chattfield Mountain (chondrite values from Taylor and McLennan, 1985). Chemical analyses are in Appendix 4.

Deer Mountain (PEns, PEm)

Deer Mountain (also known as Little Wind Mountain, Fig. 22) is in the southern portion of Chess Draw and consists of light gray to pinkish gray, coarse- to fine-grained, equigranular analcime nepheline syenite to syenite with nepheline, analcime, aegirine-augite, pyroxene, perthitic feldspar, and albite with minor amounts of biotite, apatite, calcite, and titanite. Clabaugh (1941) reports a sample from the top of Deer Mountain is fine-grained nepheline syenite and contains olivine. The nepheline syenite comprising Deer Mountain does not appear to vary in mineralogical or chemical composition, although a finer-grained border facies (PEm) is present locally along the western margin (Plate 1). From geophysical data, the Deer Mountain nepheline syenite is a laccolith as first described by Clabaugh (1941).

Marginal facies (PEm) of Deer Mountain intrusion is near external contacts of limestones and is gray-green, aphanitic to very fine grained, equigranular to slightly porphyritic mafic syenite. Generally, it consists of phenocrysts of feldspar and amphibole, up to 0.5 inches (15 cm) long in groundmass.

Two phonolite dikes (PEp) intrude Deer Mountain: a north-trending dike in the northern portion, approximately 0.5-1 m wide and 4 m long, and a second east-west-trending dike in the southern portion, approximately 1-2 m wide and 15 m long. Both dikes contain abundant inclusions of nepheline syenite. The phonolites are dark greenish black, fine-grained, holocrystalline and consist of anorthoclase, aegirine, analcime, and magnetite. The southern dike also consists of fragments of the Deer Mountain nepheline syenite, some as large as 10 cm in diameter. The nepheline syenite fragments appear to be unaltered.

A syenite dike (PEs) intrudes the Deer Mountain nepheline syenite in the southern portion near the phonolite dike. This dike is orange to bluff and consists of blocky white phenocrysts of feldspar now altered to clay.

West of Deer Mountain a small northwest-trending dark greenish black, porphyritic phonolite dike (PEp) intrudes a small outcrop of limestone. This phonolite contains abundant,

tabular white and pink feldspar and clear nepheline phenocrysts surrounded by the fine-grained greenish matrix.

Chemically the Deer Mountain samples plot as nepheline syenite to syenite (Fig. 23). Chondrite-normalized REE patterns are light-REE enriched with a slight negative Eu anomaly (Fig. 24). The syenite dikes are similar in major element composition to the main nepheline syenite at Deer Mountain, but the syenite dike samples are slightly higher in REE than the nepheline syenite (Fig. 24).

FIGURE 22. Deer Mountain, looking west with San Antonio Mountain to the left and Flat Top Mountain to the right.

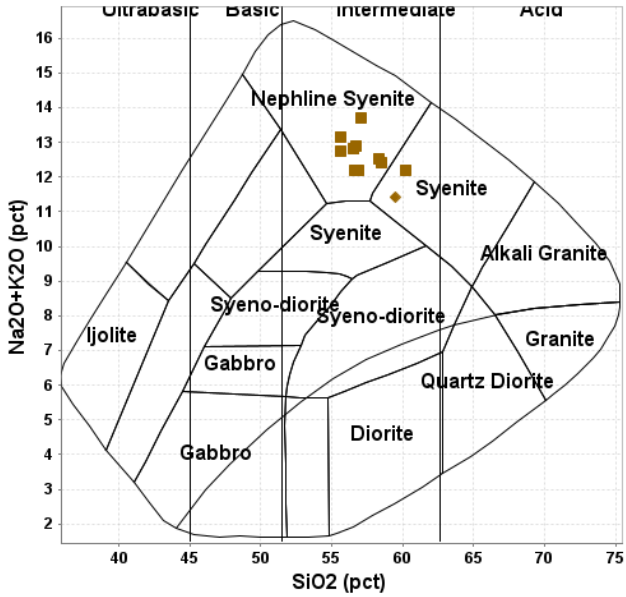

FIGURE 23. TAS plutonic classification plot for samples from Deer Mountain (Cox et al. 1979 adapted by Wilson 1989). The curved line separates the alkaline (above the curve) from subalkaline (below the curve) rocks (Irvine and Baragar, 1971). Chemical analyses are in Appendix 4. Squares=nepheline syenite (PEns). Diamond=syenite dike (PEs).

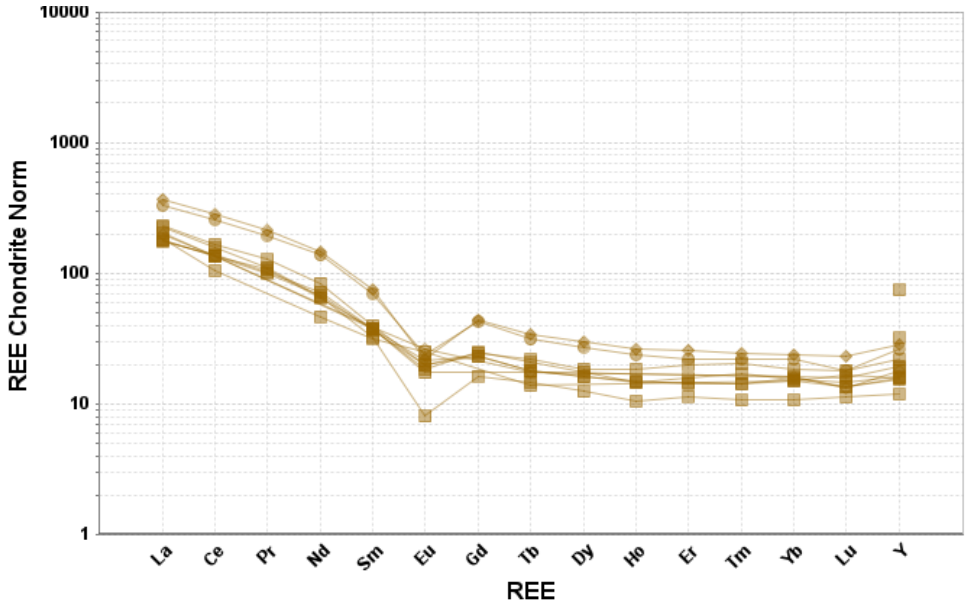

FIGURE 24. REE chondrite-normalized plot for samples from Deer Mountain (chondrite values from Taylor and McLennan, 1985). Chemical analyses are in Appendix 4. Squares=nepheline syenite (PEns). Diamond=syenite dike (PEs). Note that syenite dike samples are slightly higher in REE than the nepheline syenite.

Chess Draw intrusions

The Chess Draw area spatially includes the southern part of Chess Draw between Wind Mountain and Flat Top Mountain. Chess Draw includes numerous phonolite (PEp), syenite (PEs), trachyte (PEt), nepheline syenite (PEns), and volcanic breccia (PEbx) plugs, sills, and dikes (Table 1, Plate 1). The phonolite dikes found north of Wind Mountain, Mesquite Hills, north and east of Flat Top Mountain, and northern Chess Draw area also are included as part of Chess Draw. The intrusions are discussed together, although they are of different ages (Table 1, 36.33±0.04 to 29.33±0.23 Ma; discussed in more detail in a later section).

The oldest and largest outcrop of syenite (PEas) in Chess Draw forms a low hill in the northwestern portion (Fig. 25). The center of the stock is light gray to orange gray, medium–grained, equigranular, augite-bearing syenite to diorite (Tas of Potter, 1996a, b) consisting of anorthoclase, zoned plagioclase, augite, nepheline, magnetite, hornblende and biotite with accessory analcime, apatite, titanite, and hematite. The medium-grained augite-bearing syenite grades into a border of darker gray more mafic, porphyritic syenite (PEs) with slightly more mafic composition. The border facies contains rock fragments (limestone, sandstone, syenite) and phenocrysts. A dark greenish black, fine-grained, holocrystalline phonolite dike (PEp) intrudes the augite-bearing syenite and consists of anorthoclase, aegirine, analcime, magnetite, with minor calcite. This phonolite does not exhibit a trachytic texture and is not porphyritic. The contact between the augite-bearing syenite and phonolite is sharp with no alteration. Several small dikes of syenite to trachyte, many very altered, surround the augite-bearing nepheline syenite stock (Plate 1).

Chemically the augite-bearing syenite plots as syenite to syeno-diorite (Fig. 26). Chondrite-normalized REE patterns are light-REE enriched with no Eu anomaly (Fig. 27).

FIGURE 25. Northwestern Chess Draw augite-bearing syenite (PEas) in middle ground, looking west. Taken from northeastern Chess Draw phonolite. Flat Top Mountain in background. Phonolite dike is in the foreground.

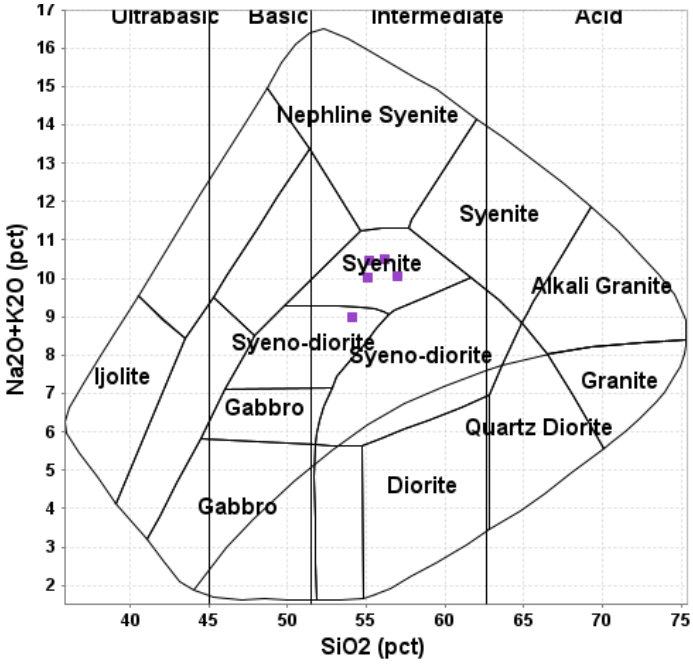

FIGURE 26. TAS plutonic classification plot for augite-bearing syenite from Chess Draw (Cox et al. 1979 adapted by Wilson 1989). The curved line separates the alkaline (above the curve) from subalkaline (below the curve) rocks (Irvine and Baragar, 1971). Chemical analyses are in Appendix 4.

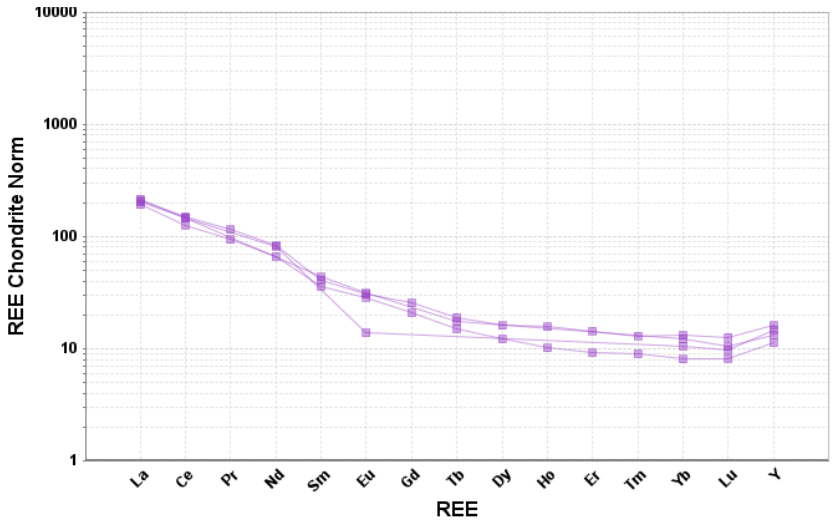

FIGURE 27. REE chondrite-normalized plot for augite-bearing syenite from Chess Draw (chondrite values from Taylor and McLennan, 1985). Chemical analyses are in Appendix 4.

Nepheline syenite (PEnsc) in southern Chess Draw forms a small sill (Fig. 28, 29, 30) that is exposed along five ridges (Plate 1). The nepheline syenite is coarse- to medium-grained and consists of feldspars, amphiboles, biotite, nepheline and accessory minerals (Fig. 29; Table 7).

Chemically the samples plot as nepheline syenite (Fig. 31). Chondrite-normalized REE patterns are light-REE enriched with a negative Eu anomaly (Fig. 32).

FIGURE 28. Nepheline syenite from southeastern Chess Draw (sample CORN20-08).

FIGURE 29. Close-up of nepheline syenite from southeastern Chess Draw (sample CORN20-11).

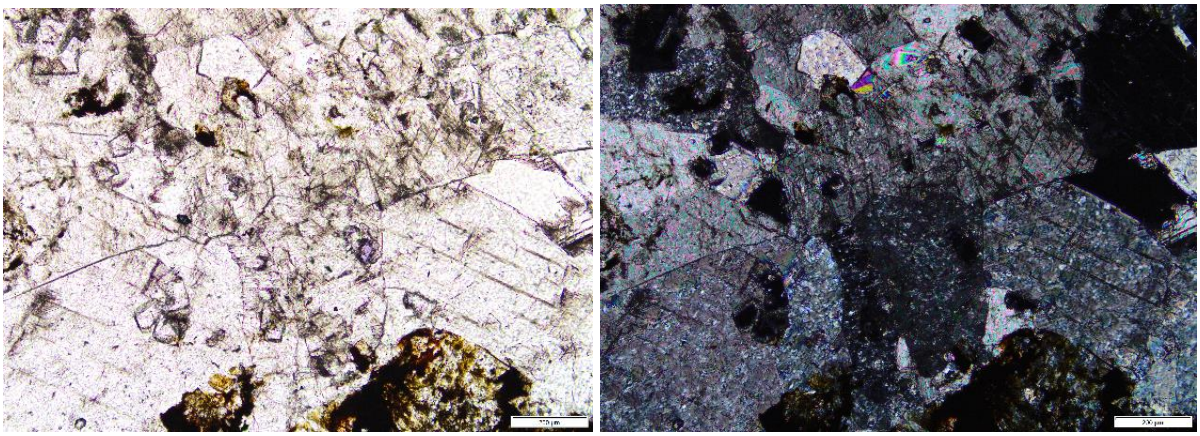

FIGURE 30. Photomicrograph of nepheline syenite: cubic purple fluorite disseminated in dolomite, green-brown aegerine (CORN79, left is plane polarized light, right is crossed polarized light).

TABLE 7. Modal analysis of Chess Draw nepheline syenite.

Mineral	CORN197
Lithology	Nepheline syenite
K-feldspar	8
Perthite	22
Aegirine-augite	18
Aenigmatite	1
Natrolite	30
Nepheline	4
Clay	9
Chlorite	1
Hematite	7
Total	100

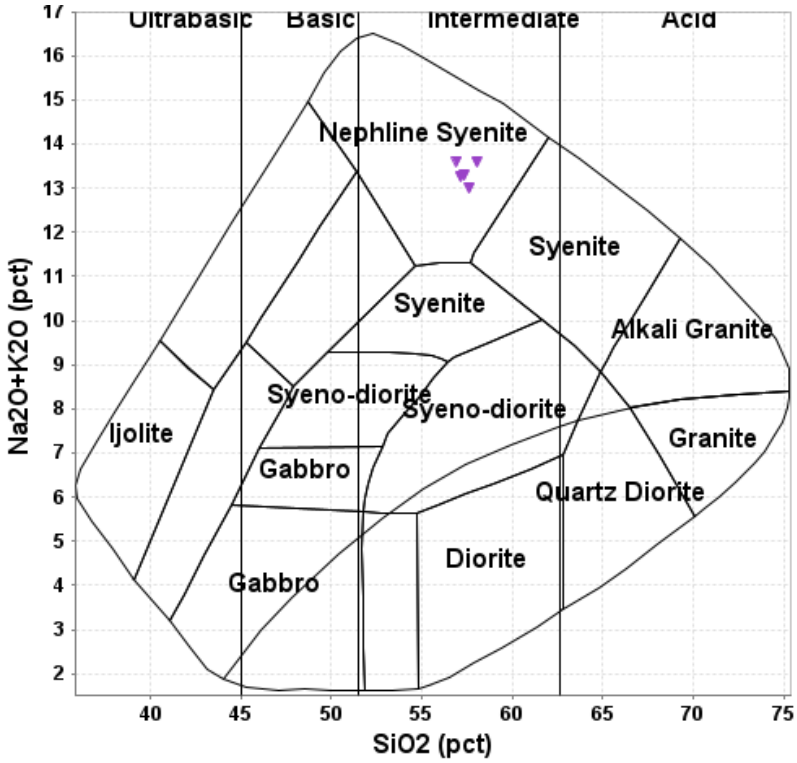

FIGURE 31. TAS plutonic classification plot for nepheline syenite from southeastern Chess Draw (Cox et al. 1979 adapted by Wilson 1989). The curved line separates the alkaline (above the curve) from subalkaline (below the curve) rocks (Irvine and Baragar, 1971). Chemical analyses are in Appendix 4.

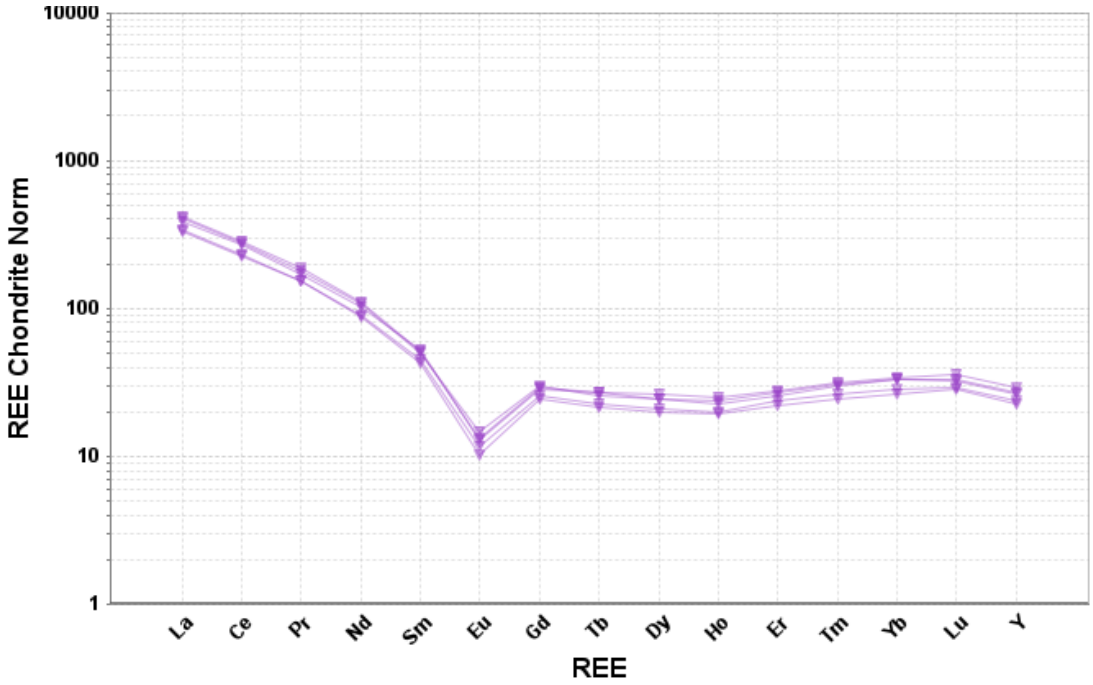

FIGURE 32. REE chondrite-normalized plot for nepheline syenite samples from southeast Chess Draw (chondrite values from Taylor and McLennan, 1985). Chemical analyses are in Appendix 4.

Aphanitic phonolite (PEp/PEpp) plugs (PEpp) and dikes (PEp) consist predominantly of alkali feldspar, nepheline, clinopyroxene, and riebeckite (Table 8). They vary in color from black to gray-black to green-black (Fig. 28-31). Locally they are porphyritic with xenocrysts of olivine, clinopyroxene, and biotite. The large plug in northeast Chess Draw is included with these rocks (PEpp, Fig. 32). Phonolite dikes and plugs are variable in width (meters) and length (as much as 1 mi long), and range in age from 35.82±0.06 to 30.16±0.09 Ma (discussed in a later section).

Chemically, the phonolite dikes plot as phonolite, tephriphonolite, trachyte, and trachyandesite (Fig. 33). Chondrite-normalized REE patterns are light-REE enriched with a negative Eu anomaly (Fig. 34) and samples from Wind Mountain and McVeigh Hills contain both the highest and the lowest concentrations of REE in the area.

FIGURE 33. Dark gray phonolite dike intruding San Andres limestones in northern Chess Draw, looking northeast.

FIGURE 34. closeup of dark gray phonolite dike in Figure 33 intruding San Andres limestones in northern Chess Draw, looking southwest (CORN20-21).

FIGURE 35. Close-up of dark gray phonolite dike in Figure 34 intruding San Andres limestones in northern Chess Draw, looking southwest (CORN20-21).

FIGURE 36. Phonolite plug in the southern Chess Draw (sample CORN20-10). Wind Mountain in the background.

FIGURE 37. Large phonolite plug in northeast Chess Draw (PEpp, CORN4006), Wind Mountain in background.

FIGURE 38. Nepheline syenite rock fragment in phonolite plug (CORN4006).

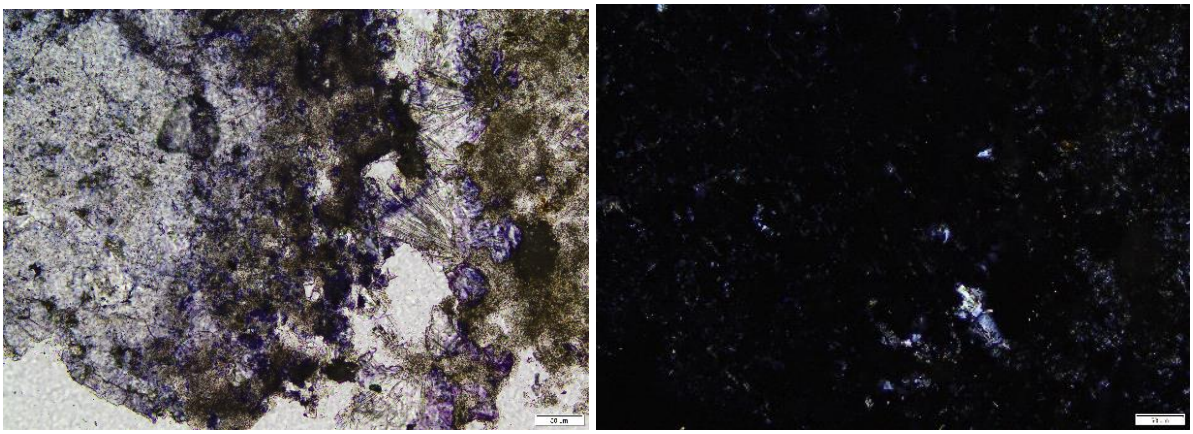

FIGURE 39. Photomicrograph of phonolite plug in Chess Draw: purple fluorite, carbonate, clay, bladed zeolites (right), and windmountainite (acicular brown) associated with an altered nepheline phenocryst (left) (CORN45, left is plane polarized light, right is crossed polarized light).

TABLE 8. Modal analyses of Chess Draw phonolite.

Mineral	CORN117	CORN40	CORN4008	CORN4006	CORN4007
Lithology	phonolite	phonolite	phonolite	phonolite	Phonolite
groundmass		45			
K-feldspar	76		45	10	65
orthoclase		5			
albite		15			
Hornblende	1				
Aegirine-augite	14	5			25
Actinolite				16	
Aenigmatite				1	
Natrolite	5				
Analcime	1				
Windmountainite	1				
Nepheline		10	15	15	
apatite		2			
Zircon				1	
Biotite	1	2			
Magnetite		3			
Calcite/dolomite		2	3	2	
Kaolinite			5	35	
Hematite	1	6	5		
Muscovite					
Sericite (white phyllosilicate)			27		15
Chlorite				20	
Titanomagnetite	tr				
Rock fragments		5			
Total	100				

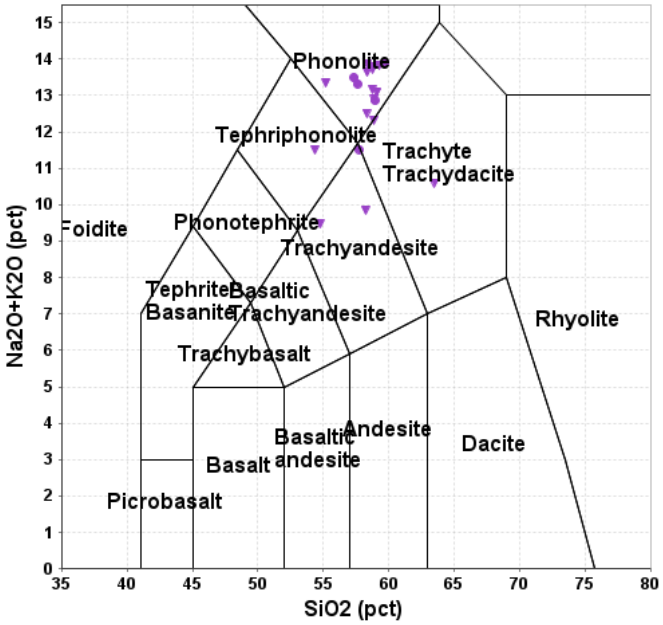

FIGURE 40. TAS (total alkali vs silica) plot of phonolite dike samples from Chess Draw (La Maitre et al., 1989). Chemical analyses are in Appendix 4.

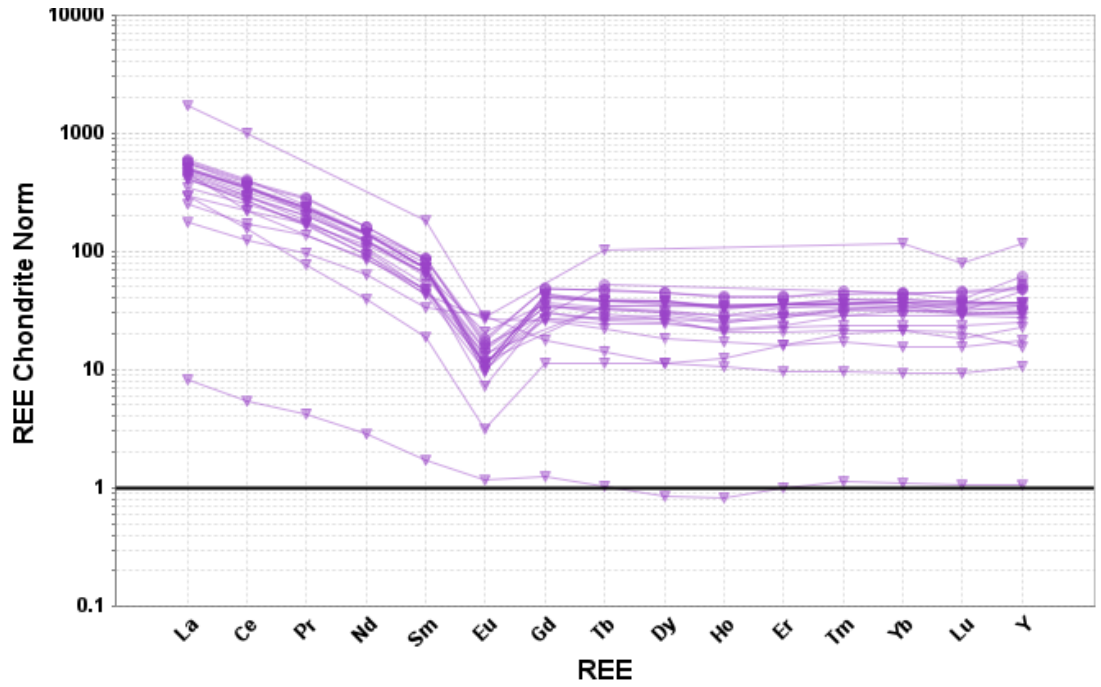

FIGURE 41. REE chondrite-normalized plot for phonolite dike samples from Chess Draw (chondrite values from Taylor and McLennan, 1985). Chemical analyses are in Appendix 4.

Syenite and nepheline syenite dikes (PEs) are common in Chess Draw, McVeigh Hills, east of Cornudas Mountain, and around the margins of Wind Mountain (Plate 1). They are medium- to fine-grained and composed predominantly of alkali feldspar, nepheline, clinopyroxene, and riebeckite (Fig. 39-41; Table 9). Groundmass consists of feldspar, amphiboles, and quartz, and is typically altered to iron oxides and clay where exposed at the surface. They vary in color from orange to cream to light gray and altered at the surface (Fig. 39). Locally they are porphyritic with xenocrysts of feldspar. The dikes are 1 inch (2.5 cm) to 50 ft (15 m) wide and as much as 500 ft (152 m) long.

Chemically the dikes plot as syenite to nepheline syenite to diorite to gabbro, reflecting the alteration of many dikes (Fig. 42). Chondrite-normalized REE patterns are light-REE enriched with a negative Eu anomaly (Fig. 43).

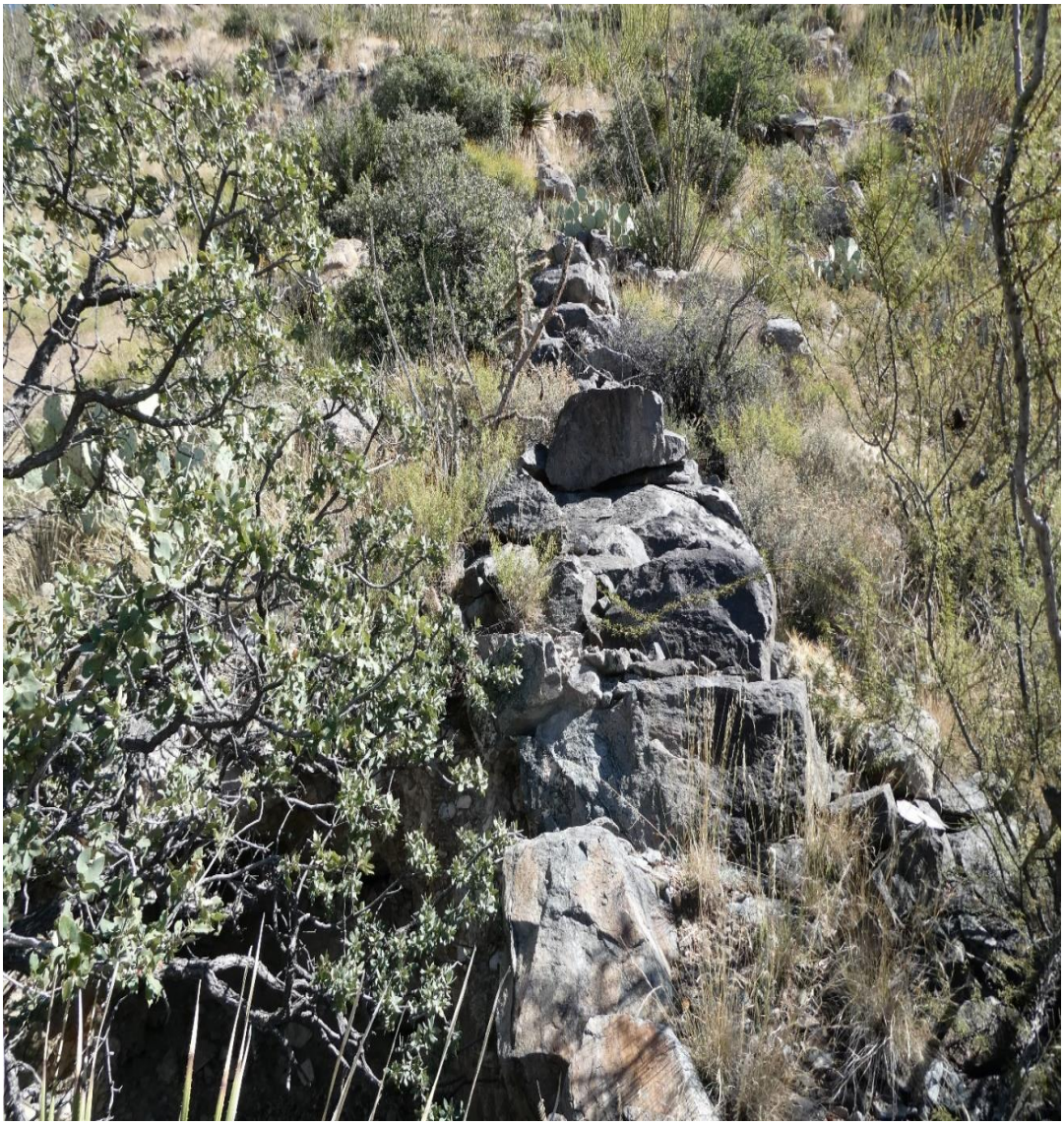

FIGURE 42. Nepheline syenite dike at the Llewellyn prospect, looking north (1.5 m wide and approximately 33 m long).

TABLE 9. Modal analyses of Chess Draw syenites.

Mineral	CORN150	CORN176	CORN177	CORN180	CORN181	CORN79
Lithology	syenite	syenite	Syenite	Syenite	Syenite	Syenite
K-feldspar	22	5		55		
Plagioclase		9	10			0.5
Perthite		24	40	2		
Quartz					2	12
Aegirine-augite	40	36	3		1	
Augite			7			
Hastingsite		1				
Aenigmatite			2		1	
Clinopyroxine	1					
Natrolite	1					
Analcime	18					6
Nepheline		6	1	3	2	9
Sodalite		1				
Biotite	2	1	2			
Titanite			1			
Cancrinite				6	49	
Phlogopite			2			
Calcite					7	39
Fluorite						13
Clay	13	6	8	6	7	
kaolinite						10
Zeolite				6		
Chlorite	1				1	
Hematite	1	11	20	12	30	5
Ilmenite			tr			
titanite			tr			
pyrite						0.5
Monazite			1			
muscovite						5
apatite			tr			
Zircon						
Calderite					tr	
Pyrolusite					tr	
Total			100		100	

Mineral	Chessdraw B12D121	Chessdraw B34D329	Chessdraw B8D84	Chessdraw B95D889
Lithology				
K-feldspar	39	28	55	20
Plagioclase	4		8	
Perthite	20	9	22	6
Quartz				
Aegirine-augite				
Augite				
Hastingsite				
Aenigmatite	2			
Clinopyroxine				
Natrolite		1		
Analcime				
Nepheline		1		

Mineral	Chessdraw B12D121	Chessdraw B34D329	Chessdraw B8D84	Chessdraw B95D889
Sodalite				4
Biotite	4			
Titanite				
Cancrinite				
Phlogopite				
Calcite	12	43	1	30
Fluorite				
Clay	10	15	2	30
kaolinite				
Zeolite				
Chlorite			1	4
Hematite		2	9	6
Ilmenite	1		1	
pyrite				
Monazite	1			
muscovite				
zircon		1		
Total	96	100	99	100

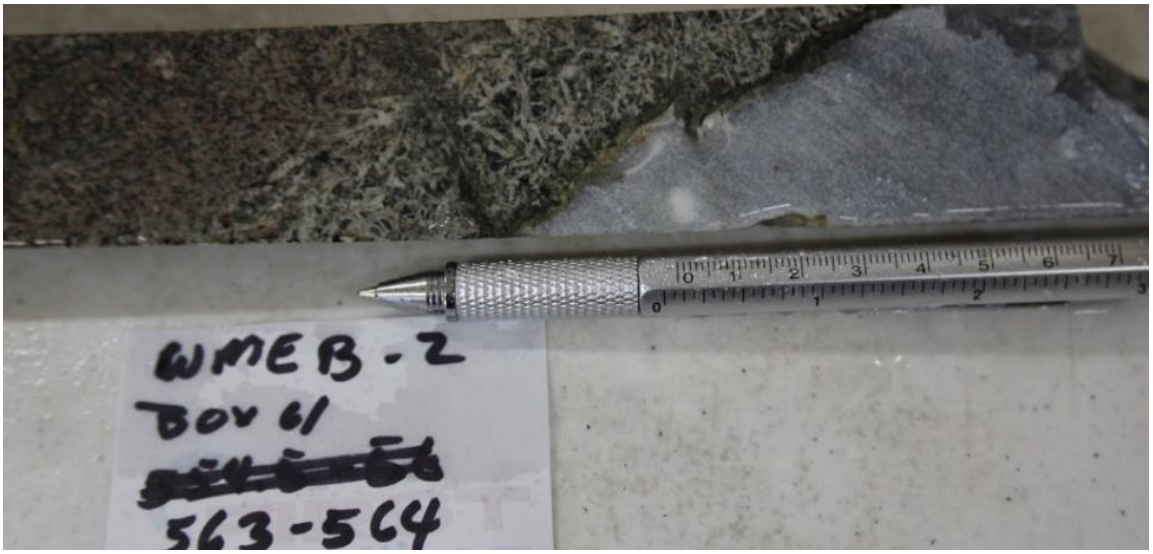

FIGURE 43. Nepheline syenite intruding unaltered limestone (Wind Mountain core, WMEB-2, depth 563-564 ft). Note thin layer of skarn at contact.

FIGURE 44. Contact between nepheline syenite and green skarn or tactite (metasomatized shale or siltstone; Wind Mountain core, WMEB-4, depth 229.1-229.7 ft).

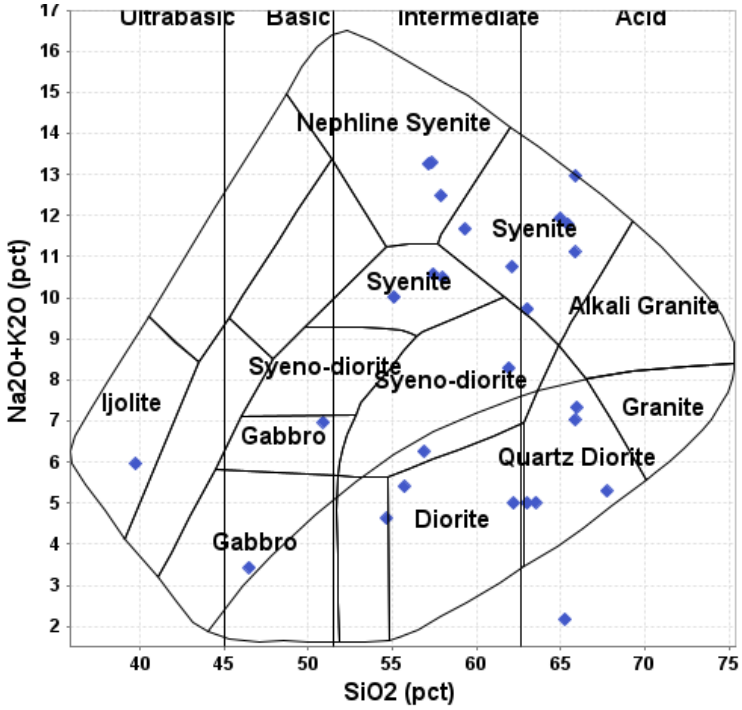

FIGURE 45. TAS plutonic classification plot for syenite and nepheline syenite dikes from Chess Draw (Cox et al. 1979 adapted by Wilson 1989). The curved line separates the alkaline (above the curve) from subalkaline (below the curve) rocks (Irvine and Baragar, 1971). Chemical analyses are in Appendix 4. Many of these dikes are altered, as shown by the scatter of the plotted samples.

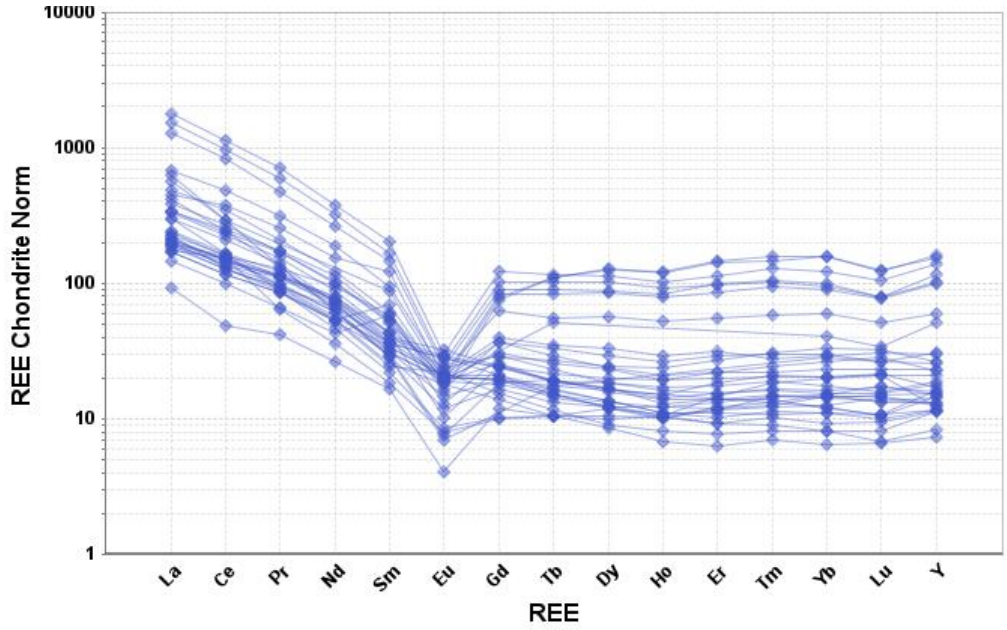

FIGURE 46. REE chondrite-normalized plot for syenite and nepheline syenite dikes from Chess Draw (chondrite values from Taylor and McLennan, 1985). Chemical analyses are in Appendix 4.

Trachyte dikes (PEt) are fine-grained, porphyritic dikes with phenocrysts of feldspar, locally forming a trachytic texture. Feldspars in dikes exposed at the surface are generally altered to white clay. The groundmass consists of feldspar, amphiboles, and quartz, and is typically altered to iron oxides and clay where exposed at the surface. Generally, the dikes are gray-green in color in drill core (Fig. 47, 48, 49) and orange to buff to yellow at the surface. They are found in Chess Draw (south of Mesquite Hills) and less altered dikes are found in drill core from the Chess Draw area. The dikes are 1 inch (2.5 cm; Fig. 49) to 50 ft (15 m) wide and as much as 500 ft (152 m) long. Although there are no age determinations, the dikes are older than the breccia dikes (PEbx), and younger than the nepheline syenite and syenite dikes (PEs, PEns; from cross cutting relationships in drill core; Fig. 48, 49).

Chemically the dikes plot as trachyandesite (Fig. 50). Chondrite-normalized REE patterns are light-REE enriched with a negative Eu anomaly (Fig. 51).

B.

FIGURE 47. A) Trachyte dike, Chess Draw, drill hole C-1, 121.2 ft depth. B) Gray trachyte dike intruding cream-colored nepheline syenite dike (Chess Draw, drill hole C-1, 188.5 ft depth).

FIGURE 48. Nepheline syenite fragment (approximately 1 in wide) in trachyte dike (Wind Mountain core, WMEB-1, depth 120 ft). Trachyte dike intrudes the nepheline syenite.

FIGURE 49. Nepheline syenite dike intruding a skarn or tactite (WMEB-6, 127.5 ft).

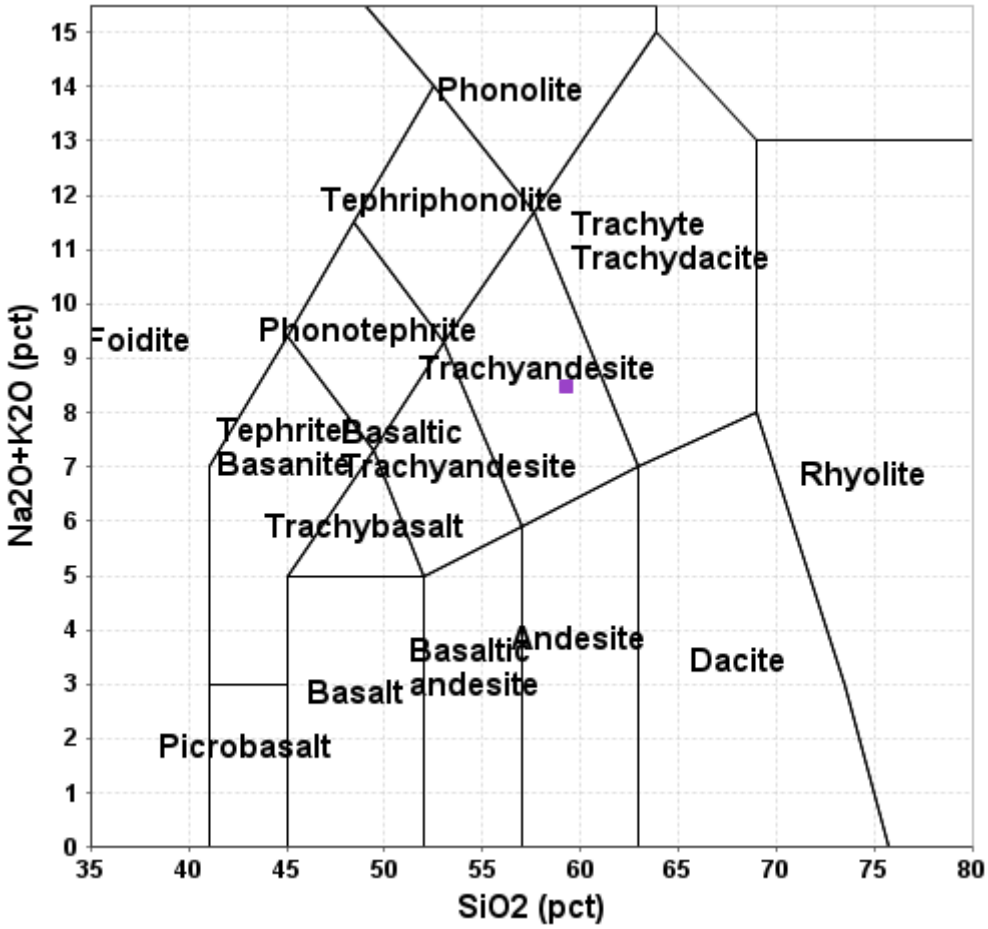

FIGURE 50. TAS (total alkali vs silica) plot of trachyte dikes from Chess Draw (La Maitre et al., 1989). Chemical analyses are in Appendix 4.

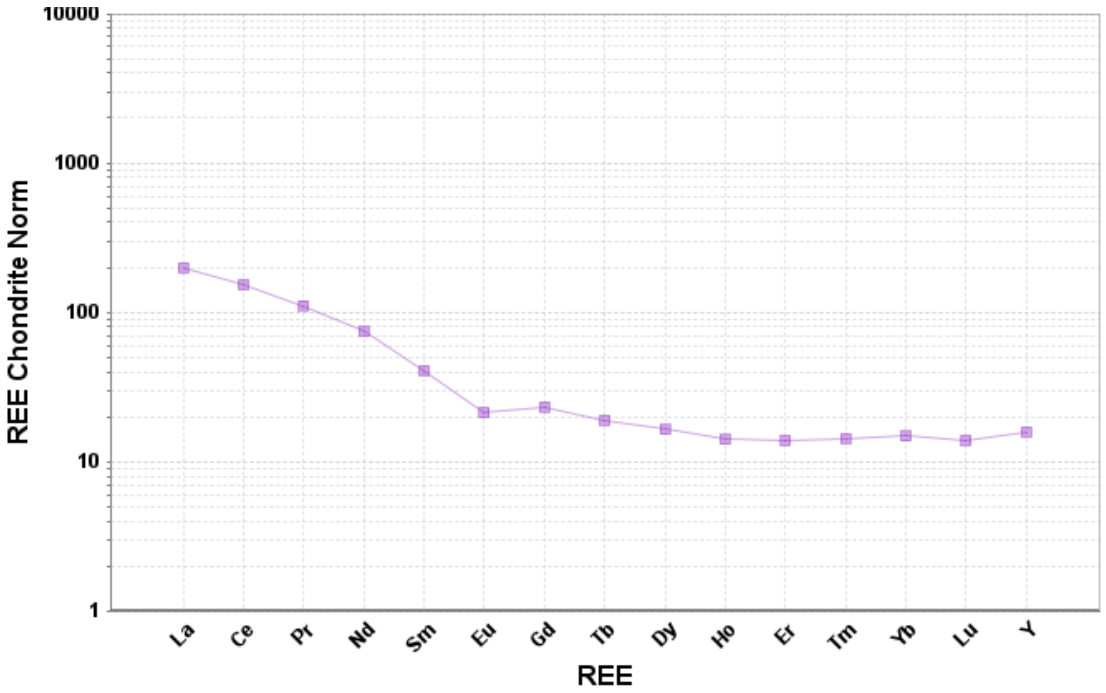

FIGURE 51. REE chondrite-normalized plot for trachyte dikes from Chess Draw (chondrite values from Taylor and McLennan, 1985). Chemical analyses are in Appendix 4.

Breccia dikes (PEbx) in Chess Draw are mostly altered where exposed at the surface and contain feldspar phenocrysts and rock fragments altered to clay. In drill core, they are black to gray matrix (feldspar, amphiboles) with small fragments (less than 3 cm) of phonolite, trachyte, nepheline syenite, syenite, sandstone, and limestone. The matrix locally has a trachytic texture. Although there are no age determinations, they are younger than the phonolite and trachyte dikes because the breccia dikes contain fragments of phonolite, trachyte, and syenite (Fig. 52, 53, 54, 55). Breccia dikes locally grade into syenite and trachyte dikes. The breccia dikes could actually be pipe like, but the contacts are not well exposed at the surface.

Chemically thebreccias plot as dacite to basalt to rhyolite, reflecting the alteration, including silicification, of many dikes (Fig. 56). Chondrite-normalized REE patterns are light-REE enriched with a negative Eu anomaly (Fig. 57).

B.

FIGURE 52. A) Breccia dike (black) cutting syenite dike, Chess Draw, Hole C-1, 217.5 ft depth. B) Breccia dike (black) cutting syenite dike, Chess Draw, Hole C-1, 139.2 ft depth. Note the round nepheline syenite rock fragment at the bottom of the core.

FIGURE 53. A) Thin black breccia dike intruding trachyte dike, Chess Draw (drill hole C-1, 177.0 ft depth). B) Volcanic breccia (Chess Draw Hole C1, depth 224.0 ft). Dark fragments are phonolite; light gray fragments are trachyte.

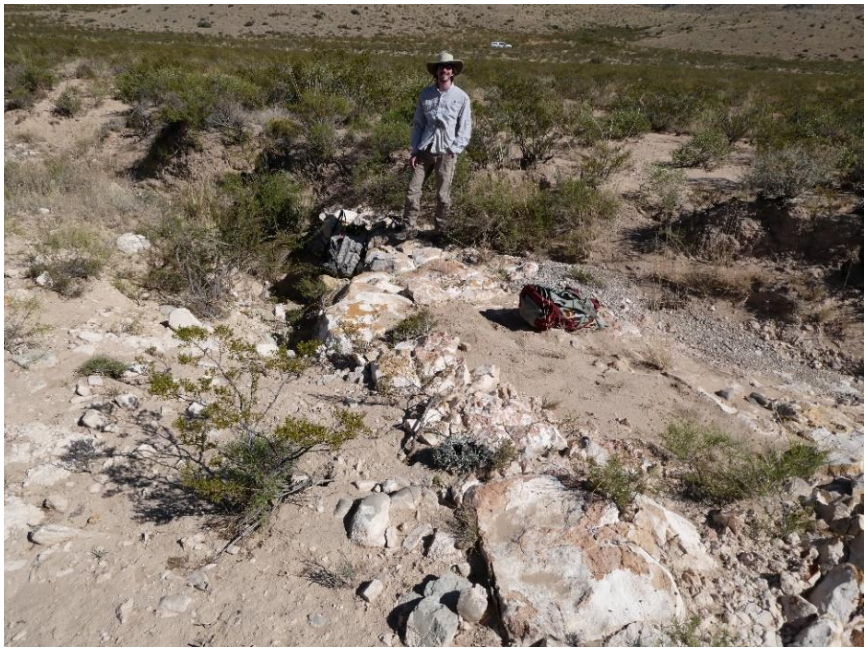

FIGURE 54. Altered breccia dike in Chess Draw.

FIGURE 55. Close-up of altered breccia dike in Figure 54.

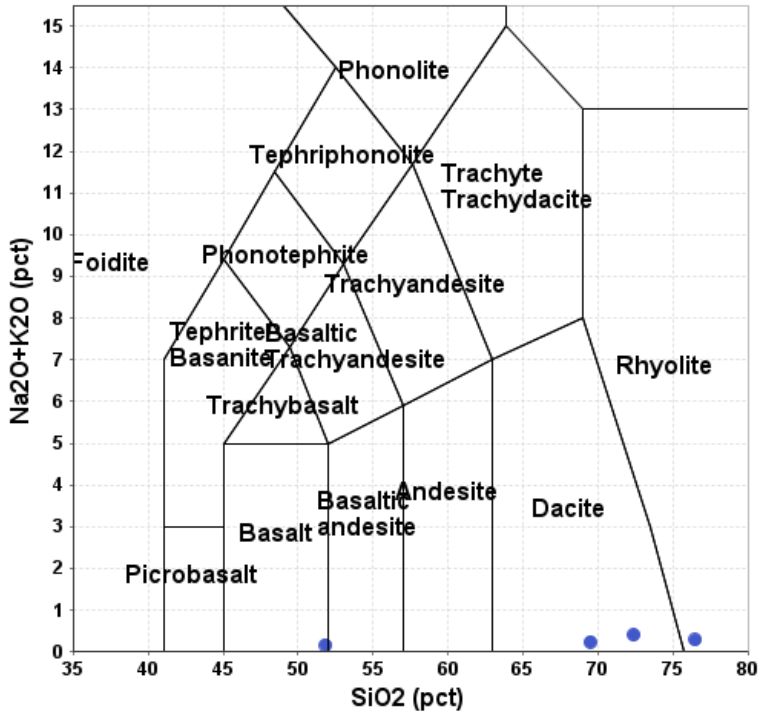

FIGURE 56. TAS (total alkali vs silica) plot of breccia dikes from Chess Draw (La Maitre et al., 1989). Chemical analyses are in Appendix 4.

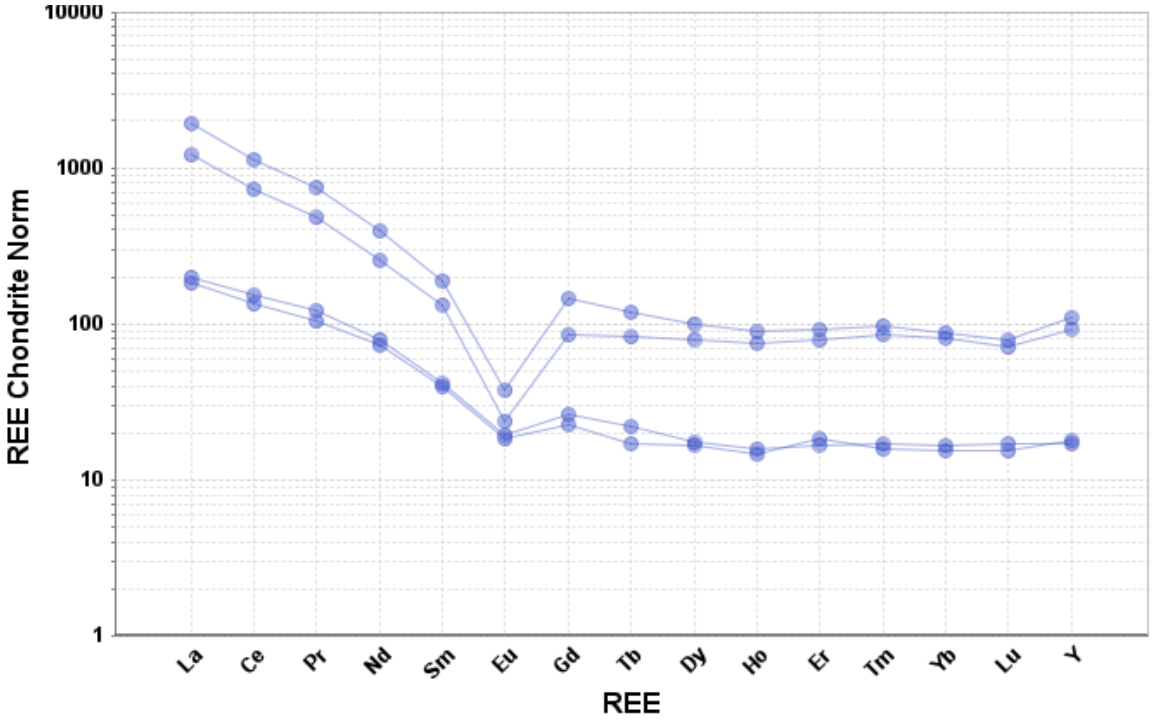

FIGURE 57. REE chondrite-normalized plot for breccia dikes from Chess Draw (chondrite values from Taylor and McLennan, 1985). Chemical analyses are in Appendix 4.

Cornudas Mountain (PEqs/PEs)

Cornudas Mountain (Fig. 58) is the northern-most of the intrusions in the Cornudas Mountains and is medium gray, weakly foliated, granoblastic to porphyrtic, fine- to medium-grained syenite (PEs) to quartz-syenite (PEqs). The rocks consist of tabular, euhdral anorthoclase, subhedral aegirine-augite, biotite, arfvedosonite, and local interstitial quartz, apatite, and anatase (Appendix 8, sample CORN4020). Cornudas Mountain is likely a laccolith (Plate 1). Limestone beds dip away from the laccolith at 10-20°. Elsewhere the intrusion rises above the plains with no visible contacts. Additional outcrops of quartz syenite are exposed east of the Cornudas Mountains (some are dikes) and are surrounded by limestone beds. A 50-ft-thick (15 m) sill intrudes the limestone west of Cornudas Mountain (Plate 1) and consists of augite, anorthoclase, and trace calderite (Table 10, Appendix 8, sample CORN4019).

Chemically, the samples plot as syenites (Fig. 59). Chondrite-normalized REE patterns are light-REE enriched with a slight negative Eu anomaly (Fig. 60).

FIGURE 58. Cornudas Mountains, looking north.

TABLE 10. Modal analyses of Cornudas syenite and quartz syenite.

Mineral	CORN210	CORN4016
Lithology	Quartz syenite	Syenite
K-feldspar	50	42
Hornblende	25	
Nepheline		24
zircon		1
Kaolinite	21	17
Hematite	4	10
sericite		3
Calcite		3
Total	100	100

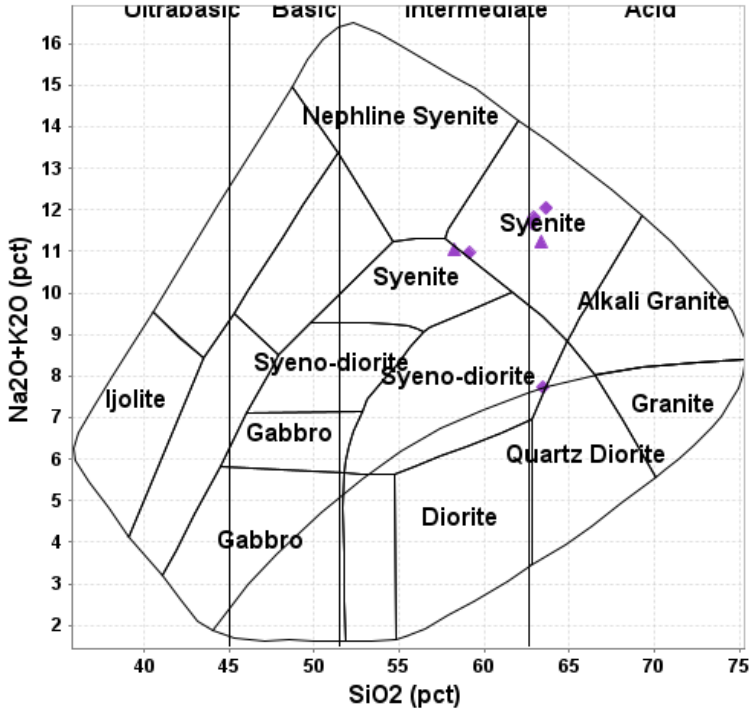

FIGURE 59. TAS plutonic classification plot for samples from Cornudas Mountain (Cox et al. 1979 adapted by Wilson 1989). The curved line separates the alkaline (above the curve) from subalkaline (below the curve) rocks (Irvine and Baragar, 1971). Chemical analyses are in Appendix 4. Triangles= quartz syenite (PEqs). Diamond=syenite (PEs).

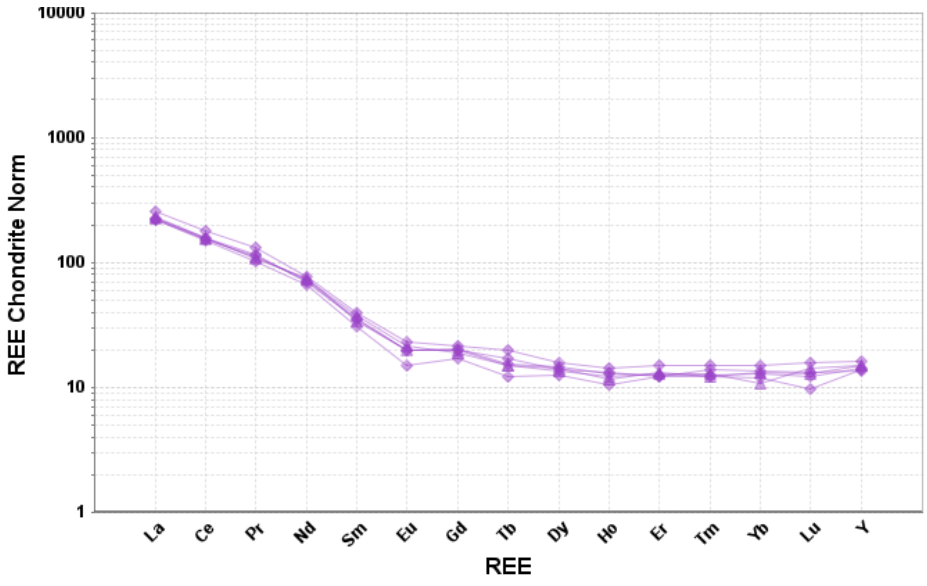

FIGURE 60. REE chondrite-normalized plot for samples from Cornudas Mountain (chondrite values from Taylor and McLennan, 1985). Chemical analyses are in Appendix 4. Triangles= quartz syenite (PEqs). Diamond=syenite (PEs).

McVeigh Hills (PEs, PEqs)

Previously unmapped, small syenite (PEs) to quartz syenite (PEqs) to nepheline syenite (PEns) intrusions were mapped in the McVeigh Hills north of the county road during this project. The syenite to quartz syenite to nepheline syenite is medium gray to orange, weakly foliated, granoblastic to porphyrtic, fine- to medium-grained (Fig. 61). The rocks consist of tabular, euhdral anorthoclase, subhedral clinopyroxene, biotite, and interstitial quartz (Table 11). Phonolite dikes intrude the syenite (Fig. 62, 63).

Chemically, the samples plot as syenite and nepheline syenite (Fig. 64). Chondrite-normalized REE patterns are light-REE enriched with a slight negative Eu anomaly (Fig. 65).

FIGURE 61. Syenite in the McVeigh Hills, looking northwest.

FIGURE 62. Phonolite dike in the McVeigh Hills intruding limestone.

FIGURE 63. Close-up of phonolite dike with fragments of syenite (sample CORN225).

TABLE 11. Modal analysis of McVeigh Hills trachyte and syenite.

Mineral	CORN208
Lithology	trachyte
K-feldspar	58
Hornblende	18
Actinolite	1
Arfedsonite	2
Nepheline	5
Biotite	9
Chlorite	2
Hematite	5
Total	100

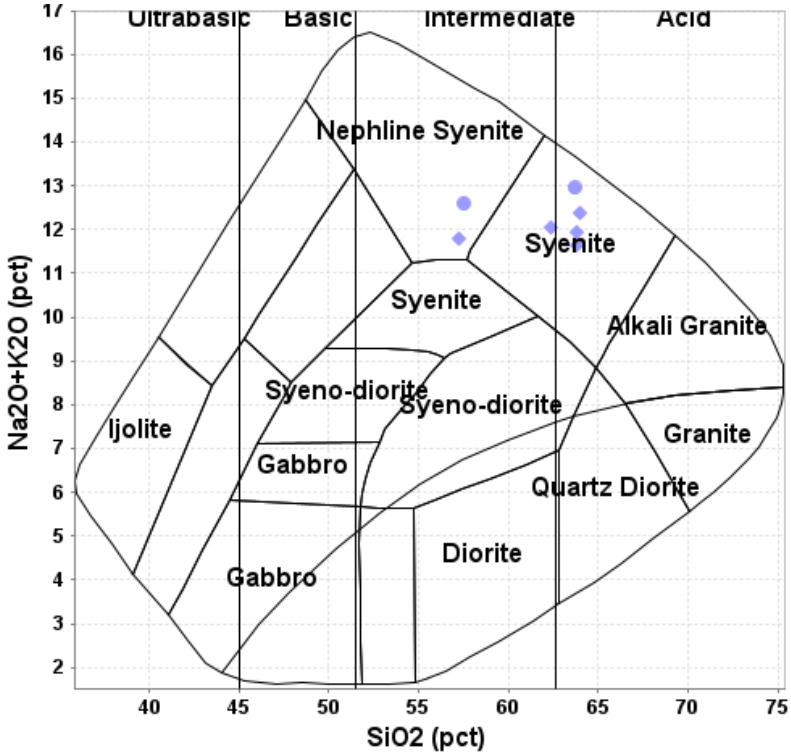

FIGURE 64. TAS plutonic (blue) classification plots for samples from McVeigh Hills (Cox et al. 1979 adapted by Wilson 1989). The curved line separates the alkaline (above the curve) from subalkaline (below the curve) rocks (Irvine and Baragar, 1971). Chemical analyses are in Appendix 4.

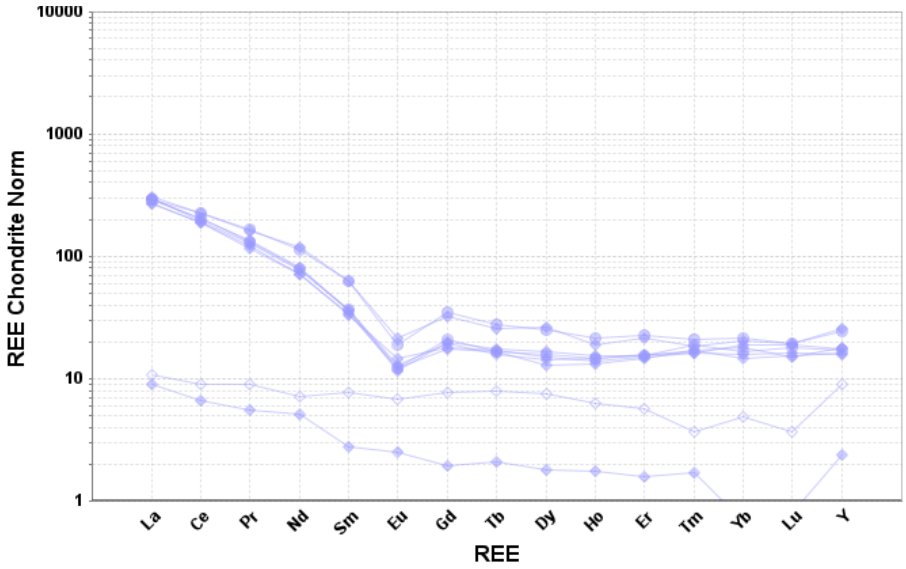

FIGURE 65. REE chondrite-normalized plot for samples from McVeigh Hills (chondrite values from Taylor and McLennan, 1985). Chemical analyses are in Appendix 4. Closed diamonds=syenite. Circles=phonolite dike. Open diamond=altered limestone (skarn).

Washburn Mountain (PEns)

The nepheline syenite sill that forms Washburn Mountain (Fig. 66) is dark gray, holocrystalline with an aphanitic groundmass and consists of anorthoclase, nepheline, aegirine-augite, and altered arfvedsonite. Locally a porphyritic texture is formed by large anorthoclase phenocrysts up to 2-3 cm long. Local cavities host calcite and analcime. The sill intruded Cretaceous rocks, but the contacts are mostly covered.

Chemically, one sample plots as nepheline syenite and another sample as syeno-diorite (Fig. 67). Chondrite-normalized REE patterns are light-REE enriched with a slight negative Eu anomaly (Fig. 68).

FIGURE 66. Washburn Mountain, looking southeast.

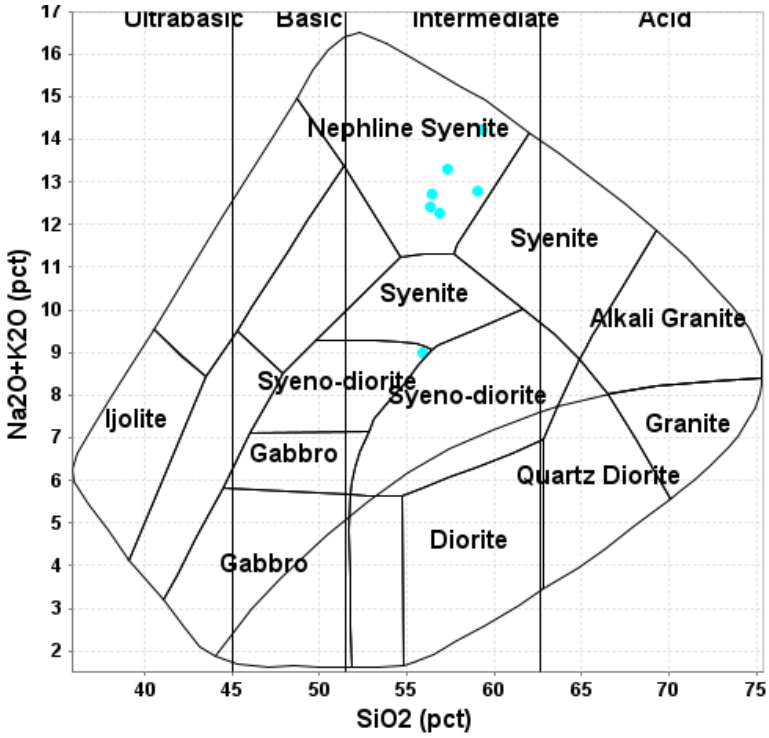

FIGURE 67. TAS plutonic (blue) classification plots for samples from Washburn Mountain (Cox et al. 1979 adapted by Wilson 1989). The curved line separates the alkaline (above the curve) from subalkaline (below the curve) rocks (Irvine and Baragar, 1971). Chemical analyses are in Appendix 4.

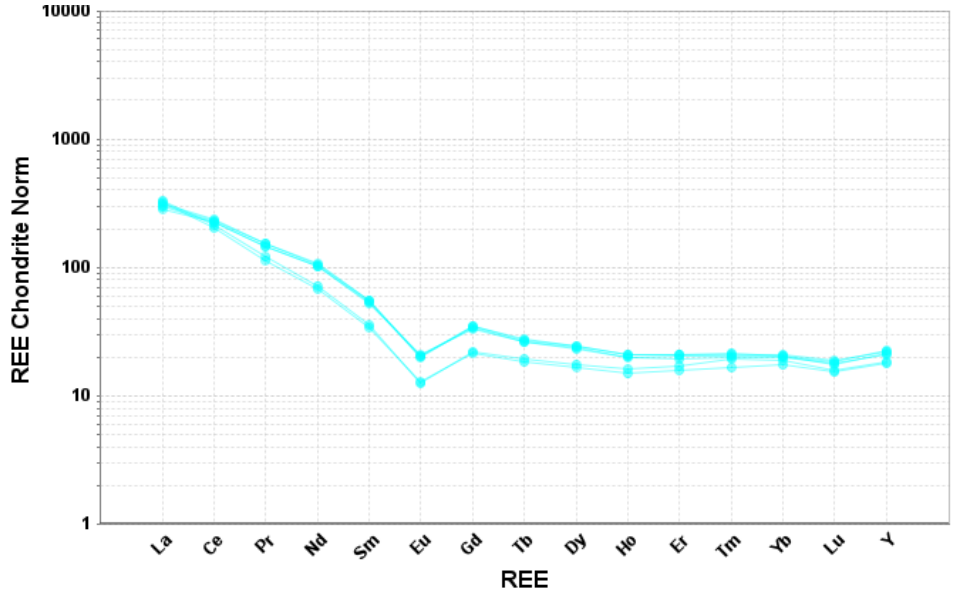

FIGURE 68. REE chondrite-normalized plot for samples from Washburn Mountain (chondrite values from Taylor and McLennan, 1985). Chemical analyses are in Appendix 4.

Alamo Mountain (PEp)

Alamo Mountain (Fig. 69) consists of a medium-gray to dark green, aphanitic, foliated phonolite sill that shows well-developed magmatic foliation, locally displaying trachytic texture. On western and southern Alamo Mountain (PEp), phonolite is platy with foliation dipping at a low angle to underlying sedimentary bedding. A more mafic phase is mapped separately (PEm). Modal analyses are in Table 12.

Chemically the samples plot as phonolite (Fig. 70). Chondrite-normalized REE patterns are light-REE enriched with a slight negative Eu anomaly (Fig. 71).

FIGURE 69. Alamo Mountain, looking west.

TABLE 12. Modal analyses of Alamo phonolite.

Mineral	CORN4001	CORN4002	CORN2102
Lithology	Phonolite	Phonolite	Phonolite
K-feldspar	20	45	55
Actinolite		2	
Aegirine-augite	17	12	
Hornblende			8
Nepheline	25	1	
Biotite	5	1	
Cancrinite	2		
Kaersutite	2		
Hematite	4	4	
Chlorite			37
Sericite (white phyllosilicate)	24	35	
Total			

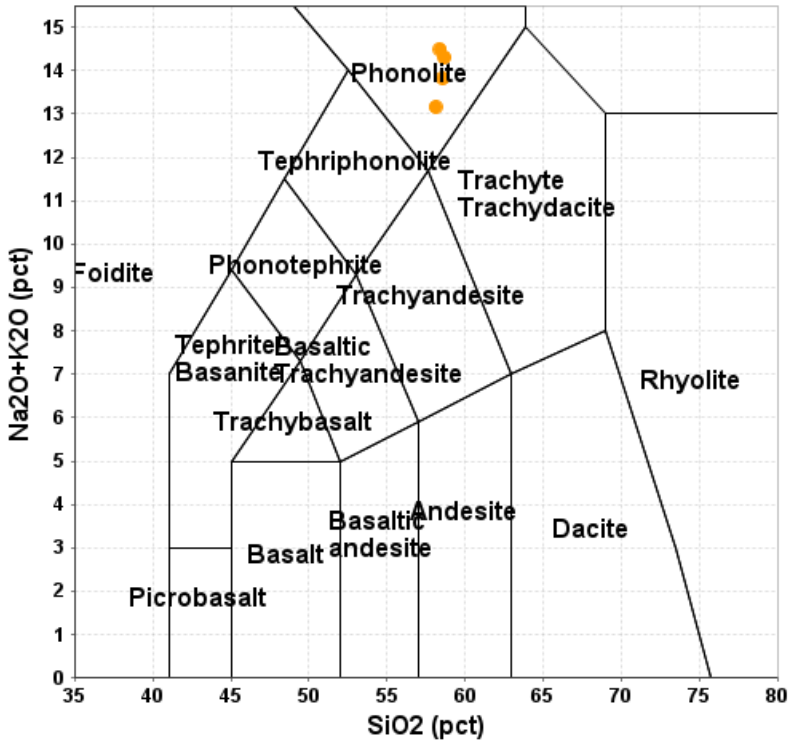

FIGURE 70. TAS plutonic (blue) classification plots for samples from Alamo Mountain (Cox et al. 1979 adapted by Wilson 1989). The curved line separates the alkaline (above the curve) from subalkaline (below the curve) rocks (Irvine and Baragar, 1971). Chemical analyses are in Appendix 4.

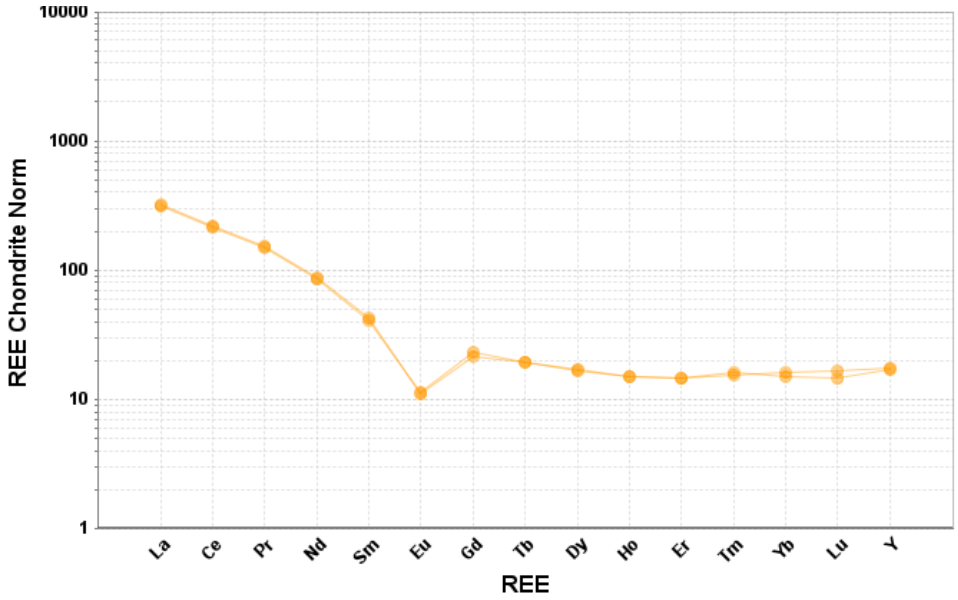

FIGURE 71. REE chondrite-normalized plot for samples from Alamo Mountain (chondrite values from Taylor and McLennan, 1985). Chemical analyses are in Appendix 4.

Flat Top Mountain (PEp)

Flat Top Mountain (Fig. 72) consists of a 50-75 ft (15-23 m) thick, near-horizontal, black to dark green, fine-grained phonolite sill (PEp) forming a cap on Flat Top Mountain. Modal analyses are in Table 13. Trachytic to porphyritic texture is locally found. The groundmass is generally feldspar, aegirine and analcime and exhibits well-developed magmatic foliation. Claubaugh (1941) describes the center of a nepheline phenocryst partially replaced by analcime and bordered by aegirine. Phonolite dikes intrude the limestone on the south, southeast, east, and north flanks (Plate 1). Some of these dikes could be feeder dikes.

Chemically, the sills plot as phonolite (Fig. 73). Chondrite-normalized REE patterns are light-REE enriched with a negative Eu anomaly (Fig. 74).

FIGURE 72. Flat Top Mountain, looking west.

TABLE 13. Modal analyses of Flat Top sill.

Mineral	CORN804	CORN4003	CORN4004	CORN2105
Lithology	phonolite	phonolite	phonolite	Phonolite, altered
K-feldspar	50	45	23	
Hornblende	15			
Actinolite	8		8	
Aegirine		35	22	
Nepheline	8	8	11	1
Biotite	2			
Apatite		1	1	
Titanite			1	
Cancrinite			3	
Kaolinite	17			30
Hematite		1	2	
Sericite		10	29	10
Chalcedony				15
Calcite				44
Total	100	100	97	

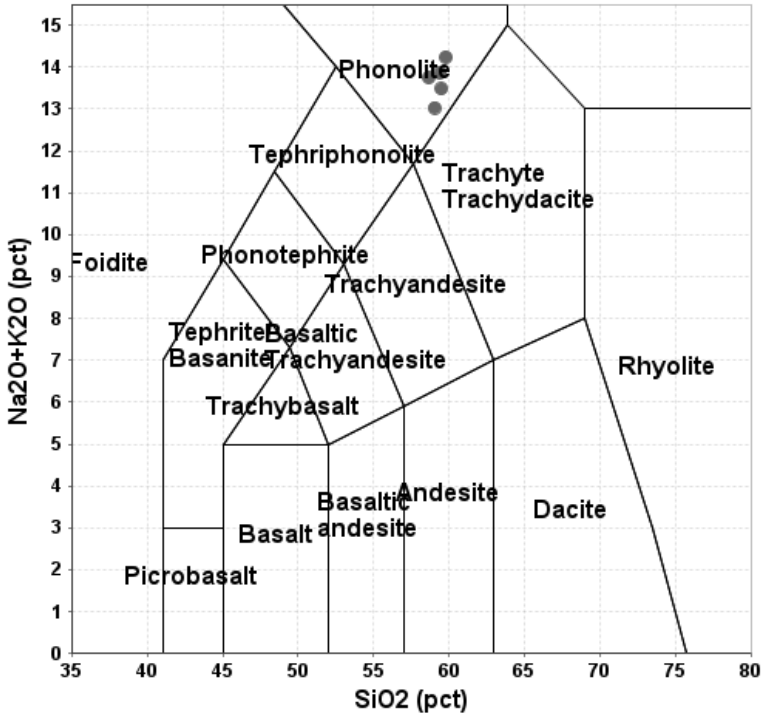

FIGURE 73. TAS classification diagram for samples from Flat Top Mountain (Le Maitre, 1989). Chemical analyses are in Appendix 4.

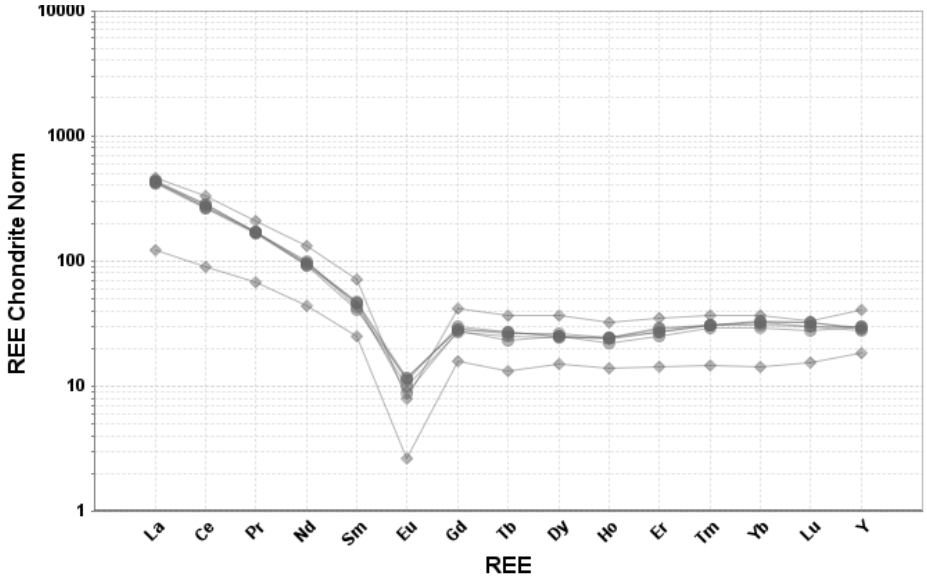

FIGURE 74. REE chondrite-normalized plot for samples from Flat Top Mountain (chondrite values from Taylor and McLennan, 1985). Chemical analyses are in Appendix 4. Circles=phonolite dike. Diamonds=phonolite.

San Antonio Mountain (PEns)

San Antonio Mountain (Fig. 75) is a prominent peak in the Cornudas Mountains (elevation 7023 ft) and consists of a gray, fine-grained, holocrystalline, porphyritic nepheline syenite, with local diabasic texture formed by laths of microcline or anorthoclase. Porphyritic texture is formed by large anorthoclase phenocrysts up to 2-3 cm long. The nepheline syenite consists of microcline or anorthoclase, nepheline, aegitine-augite, arfvedsonite, and hematite, with accessory aenigmatite, fayalite, titanomagnetite, and monazite (Table 14, Appendix 8, sample CORN4013).

Chemically, the samples plot as nepheline syenite to syenite (Fig. 76). Chondrite-normalized REE patterns are light-REE enriched with a negative Eu anomaly (Fig. 77).

FIGURE 75. San Antonio Mountain, looking south.

TABLE 14. Modal analysis of San Antonio nepheline syenite.

Mineral	CORN4013
Lithology	Nepheline syenite
Hornblende	18
Aegirine	12
Arfvedonsite	3
Nepheline	9
K-feldspar	16
natrolite	18
Kaersutite	3
Chlorite	1
Hematite	7
Zeolite	5
Sericite (white phyosilicate)	8
Total	100

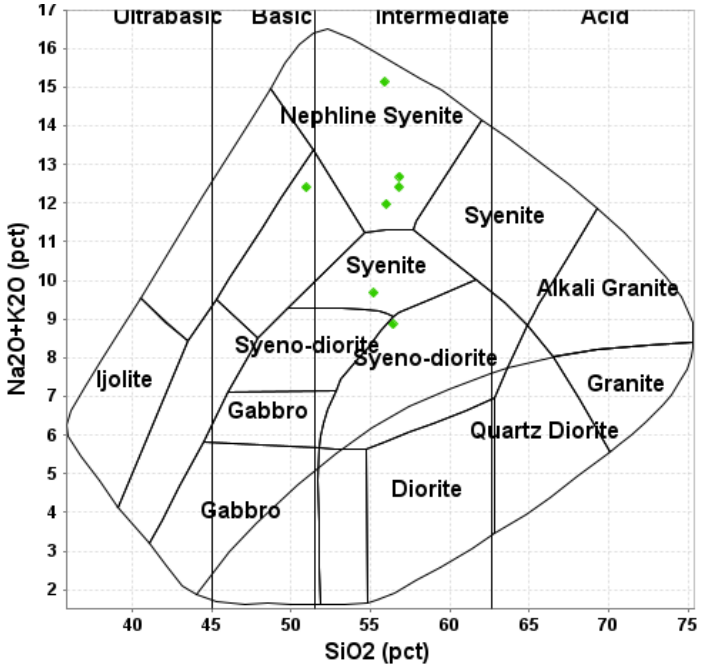

FIGURE 76. TAS plutonic (blue) classification plots for samples from San Antonio Mountain (Cox et al. 1979 adapted by Wilson 1989). The curved line separates the alkaline (above the curve) from subalkaline (below the curve) rocks (Irvine and Baragar, 1971). Chemical analyses are in Appendix 4.

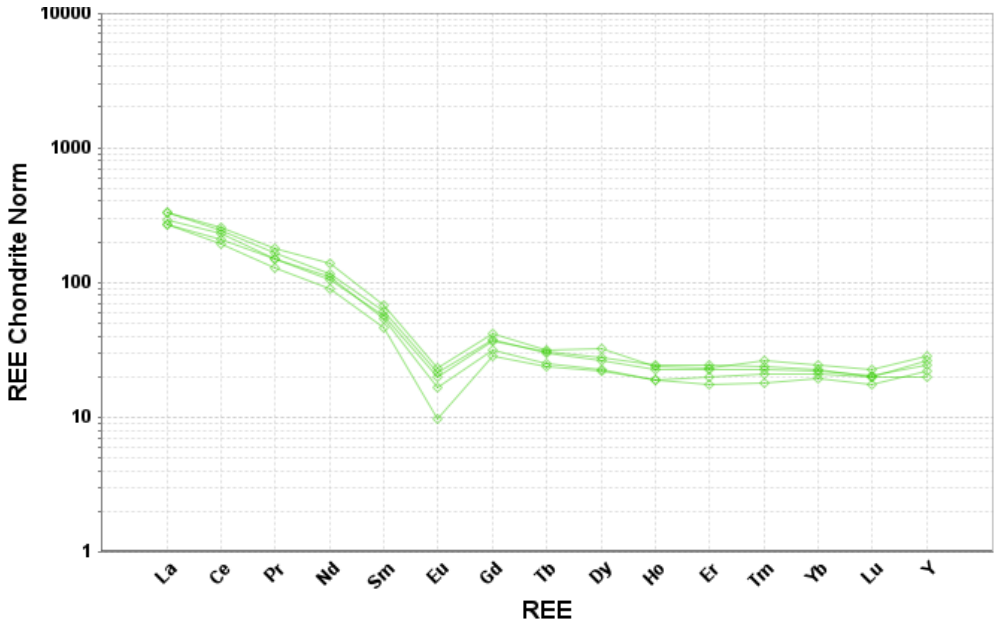

FIGURE 77. REE chondrite-normalized plot for samples from San Antonio Mountain (chondrite values from Taylor and McLennan, 1985). Chemical analyses are in Appendix 4.

Black Mountain (PEps)

Black Mountain (Fig. 78) is the youngest of the intrusions in the Cornudas Mountains and consists of dark gray to gray-green, porphyritic, foliated, fine- to medium-grained nepheline syenite sills (Fig. 79), with phenocrysts of anorthoclase up to 2-3 cm in length. Phenocrysts consist of euhdral anorthoclase up to 1 inch (0.025 m) long in groundmass of anorthoclase, clinopyroxene, biotite, nepheline, and analcime, with trace amounts of eudialyte locally (Table 15).

Samples plot as nepheline syenite (Fig. 80). Chondrite-normalized REE patterns are light-REE enriched with a negative Eu anomaly (Fig. 81).

FIGURE 78. Black Mountain, looking east.

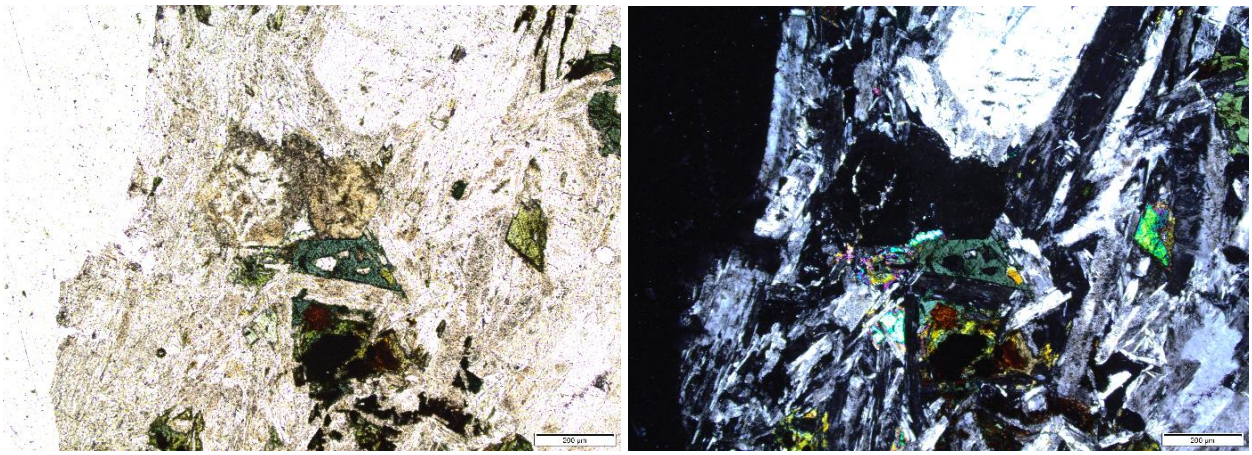

FIGURE 79. Photomicrograph of phonolite sill containing grossular garnet (center brown hexagonal crystals), aegirine-augite, arfvedsonite (green center), kaersutite (light green right),

hornblende (blades upper right), K-feldspar, and nepheline (CORN4011). Left is plane polarized light and right is crossed polarized light.

TABLE 15. Modal analyses of Black Mountain sill.

Mineral	CORN4011	CORN4012
Lithology	phonolite	Phonolite
K-feldspar	50	45
Hornblende	13	
Aegirine	9	10
Arfvedonsite	2	
enstatite	1	
Nepheline	1	7
sodalite	3	18
Kaersutite	1	
Hematite	7	5
Sericite (white phyosilicate)	13	15
Total		

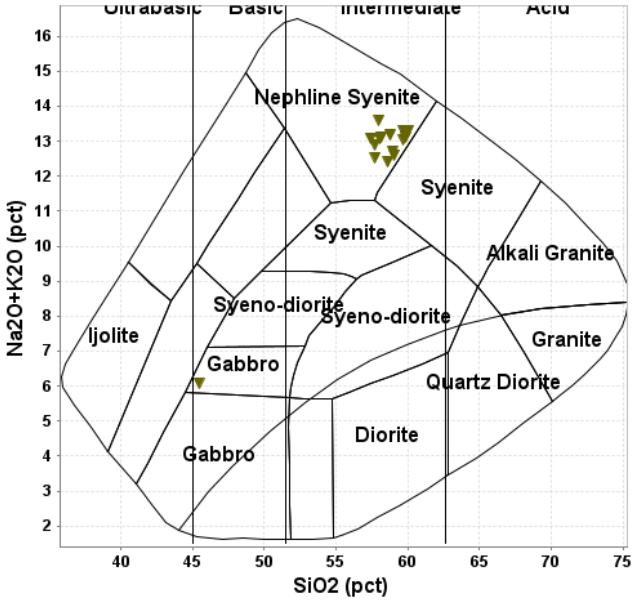

FIGURE 80. TAS plutonic classification plot for samples from Black Mountain (Cox et al. 1979 adapted by Wilson 1989). The curved line separates the alkaline (above the curve) from subalkaline (below the curve) rocks (Irvine and Baragar, 1971). Chemical analyses are in Appendix 4.

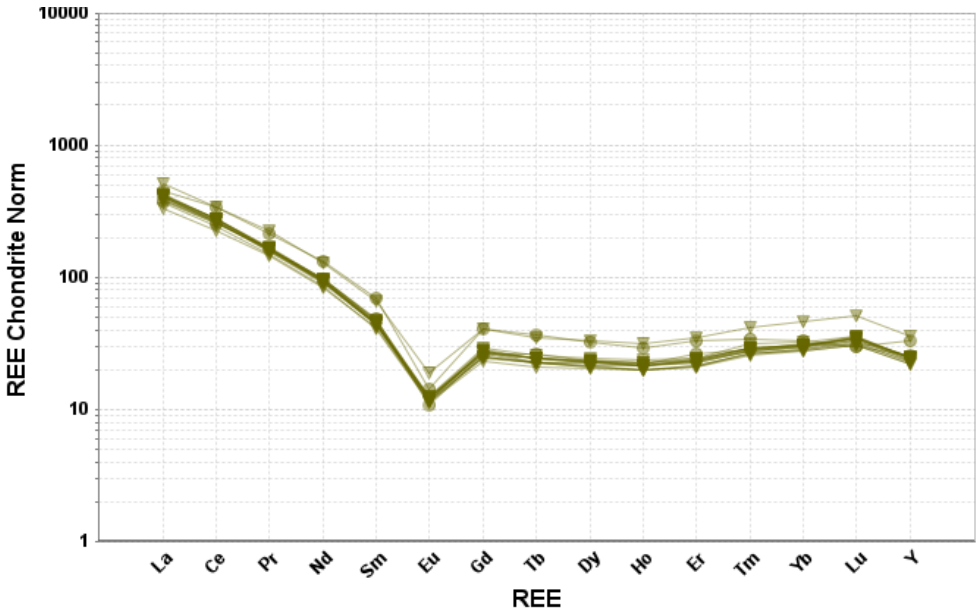

FIGURE 81. REE chondrite-normalized plot for samples from Black Mountain (chondrite values from Taylor and McLennan, 1985). Chemical analyses are in Appendix 4. Diamond (upside down)=nepheline syenite. Circle=phonolite.

PETROCHEMISTRY OF THE IGNEOUS ROCKS

Igneous rocks in the Cornudas Mountains are ferroan, alkali-calcic to alkali (according to diagrams by Frost et al., 2001). Geochemically, the rocks plot as WPG (within-plate granites) to VAG (volcanic arc granites, according to diagrams by Pearce et al., 1984), and active continental margins (according to diagrams by Schandl and Gordon, 2002). Most igneous rocks exhibit light-REE enriched chondrite normalize REE patterns with a strong negative Eu anomaly. The negative Eu anomaly indicates feldspar fractionation.

Potter (1996a, b) reports isotopic values for several samples in the Cornudas Mountains (Table 16). These data are consistent with magmatic evolution from the asthenosphere with possible contamination from the lithosphere or contamination by mafic intrusions. Collectively, the geochemical and isotopic data are consistent with the Cornudas Mountains having an asthenospheric source and the younger rocks having a source in the lower to middle crust (Potter, 1996a, b; McLemore, 2018).

TABLE 16. Isotopic values for intrusions in Cornudas Mountains (samples defined in Table 2; locations in Appendix 4).

Sample	$^{143}Nd/^{144}Nd$	ƐNd	$^{87}Rb/^{86}Sr$	$^{87}Sr/^{86}Sr$
AL-11	0.512781	2.8	9.38	0.7117
AL-11 (mafic)			5.45	0.7081
AS-5	0.512801	3.2	0.29	0.7032
AS-5 (biotite)			8.90	0.7080
Z-2			7.36	0.7090
DE-1			0.79	0.7041
DE-1			0.79	0.7048
DE-5			0.85	0.7045
DE-5 (biotite)			7.43	0.7074
SA-1			1.80	0.7094
DM-5	0.512884	4.8		
CD-7	0.512772	2.6	7.24	0.7124

STRUCTURE

Gentle folds and minor faults form the Otero and Diablo platforms (Black, 1975; Woodward et al., 1975). However, deformation changes in the vicinity of the intrusions in the Cornudas Mountains, where folding is associated with the intrusions. The major deformation of sedimentary strata in the Cornudas Mountains are broad domes and asymmetrical folds (Collins, 1958; Nutt and O'Neill, 1998). There are some faults with significant displacement (Plate 1). Permian units dip away from the laccoliths and exhibit little deformation where sills intrude them. Minor faults with iron-staining, no mineralization, and little displacement are found locally in the limestones surrounding Chess Draw (Plate 1).

GEOPHYSICAL INTERPRETATIONS

A detailed aeromagnetic and radiometric survey was funded by the USGS Earth MRI program, which was flown in January and February 2021 (Fig. 82). This purpose of this survey is to compliment geologic mapping by the NMBGMR and Texas Bureau of Economic Geology. The northern survey, the Cornudas block, was flown by helicopter at 200 m spaced N-S flights and 2000 m spaced E-W tie lines, at 125 m draped altitude. All data are online (Bultman, 2021a). This survey replaced the NURE (National Uranium Resource Evaluation program) 5- to-10-km flight line spacing.

The laccoliths and plugs are defined by distinct red aeromagnetic anomalies (Fig. 82) that project into the subsurface as vertical, cylindrical features (Bultman, 2021b, 2022). The laccoliths and sills are more magnetic and radiometric than the sedimentary rocks they intruded. Most of the sills and dikes have little or no magnetic or radiometric anomalies. The survey also indicates that magnetic sources underlie south Chess Draw and McVeigh Hills at 40 or more meters (Bultman, 2022). This geophysical survey aided focused detailed mapping in the Chess Draw and McVeigh Hills.

In the northern Chess Draw, the exposed intrusions and dikes probably represent the top of a larger, concealed intrusion, possibly a laccolith. Breccia dikes are particularly suggestive of a concealed intrusion in the area. The high REE concentrations in the nepheline syenite sill and breccia and phonolite dikes are consistent with potential higher concentrations of REE in the subsurface. There is no indication of intrusions at the surface above the magnetic anomaly in the southern Chess Draw. In the McVeigh Hills, new mapping revealed small intrusions with moderate to low REE in that area (Fig. 65).

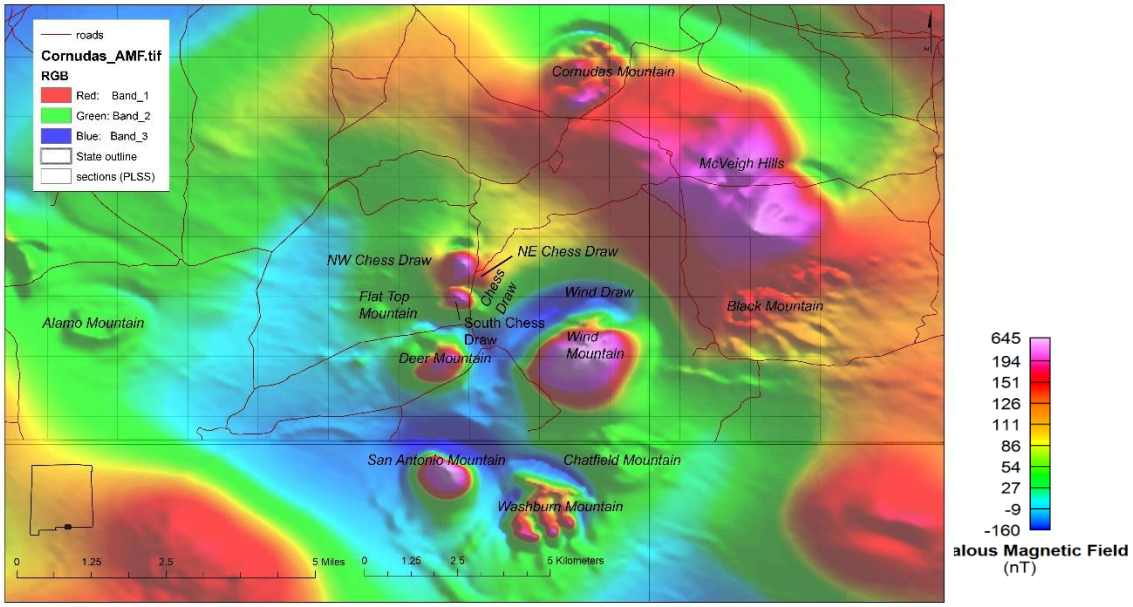

FIGURE 82. Map of the anomalous magnetic field (AMF) of the Cornudas Mountains (Bultman, 2021, 2022) showing intrusive laccoliths and plugs (red anomalies) that extend deep into the subsurface, with additional intrusions potentially buried in the subsurface. New mapping in Chess Draw and McVeigh Hills indicates the anomalies are the top of syenite and phonolite intrusions, possibly as sills, laccoliths, or plugs.

DESCRIPTION OF MINERAL DEPOSITS AND ALTERATION

There are three types of REE mineral deposits in the Cornudas Mountains: 1) REE-bearing nepheline syenite intrusions and phonolite dikes, 2) volcanic breccia dikes, and 3) REE-bearing skarns and carbonate-replacement deposits. Mines, prospects and mineralized zones are scattered throughout the Cornudas Mountains, exposing some of these mineralized and altered areas, and are more abundant in the Chess Draw and Wind Mountain areas (Fig. 83, Appendix 1). The Wind Mountain nepheline syenite adit (NMOt0014) is the largest of the workings. Most of these mines and prospects are described in this section and summarized in Appendix 1. The mineral-resource potential is described in a different section.

Calcite veins are common in limestones near the mineralized skarns and intrusions, and could be an exploration guide to mineralized zones. Contact metamorphism (skarns, carbonate-replacement deposits) is found throughout the Cornudas Mountains, but is not extensive and mostly concealed beneath boulders and alluvium eroding from the laccoliths and sills. Even in drill core, alteration zones are typically less than 1 meter thick (Fig. 84). The limestones west of Cornudas Mountain and along the contact with the Wind Mountain nepheline syenite are locally recrystallized to marble or altered to green skarn or unmineralized tactite (metasomatized shale or siltstone, Fig. 44, 49). Skarns containing calc-silicate minerals are rare, but local narrow bands of aegirine, riebeckite, analcime, calcite, dolomite, and local eudialyte border many dikes and form small skarns. Small fine-grained green skarns, consisting of epidote, calcite, garnet, and locally eudialyte, are found along the contact between the limestone and Wind Mountain nepheline syenite. Carbonate-replacement deposits consist of predominantly calcite with few additional minerals. Locally, the skarns and contact-replacement deposits contain eudialyte and are of economic interest. More details are described below.

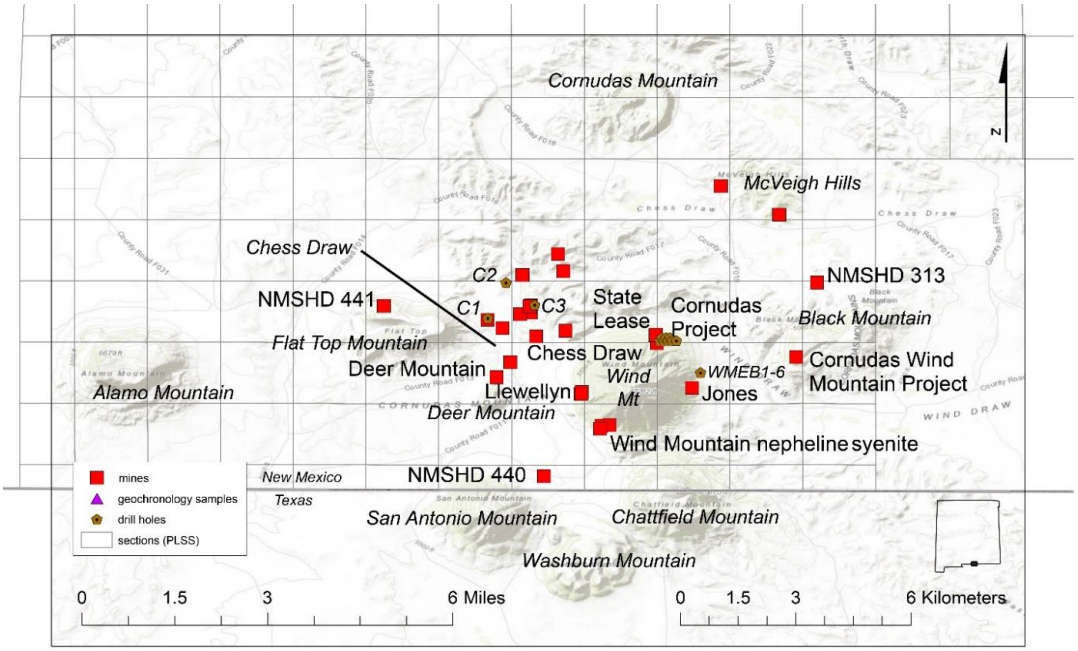

FIGURE 83. Mines and prospects in the Cornudas Mountains showing locations of intrusive bodies and drill holes. Intrusions are summarized in Table 1.

FIGURE 84. Nepheline syenite in contact with green skarn (tactite) and black and white recrystallized limestone (east side wind Mountain, Hole WMEB-1, 102 ft).

Wind Mountain nepheline syenite adit

The Wind Mountain nepheline syenite adit (NMot0013) was constructed by AddWest, Inc. in 1993 on the south side of Wind Mountain to produce a test shipment of nepheline syenite for ceramic, glass, and other industrial use (Fig. 85, 86). The adit is approximately 300 ft (91 m) long (Fig. 87, 88). Flooding of the adit occurs after heavy rain storms. The potential for nepheline syenite for industrial purposes is discussed by McLemore and Guilinger (1993, 1996) and McLemore et al. (1994, 1996a, b).

Moderate REE potential is found in the nepheline syenite, phonolite dikes, skarns, and carbonate-replacement deposits from the vicinity of the adit, eastward for approximately 3000 ft (Fig. 91; 914 m). The carbonate-replacement deposits are adjacent to the phonolite dikes and/or nepheline syenite, but are typically small (less than 1 m wide and 50 m long) and exposed mostly in the arroyos. Marbles and recrystallized limestone are characteristic of these deposits.

Chondrite-normalized REE patterns are light-REE enriched with a negative Eu anomaly (Fig. 89, 40-2274 ppm total REE). Total REE shows a strong correlation with Zr (Fig. 90), which is consistent with eudialyte minerals hosting the REE and Zr.

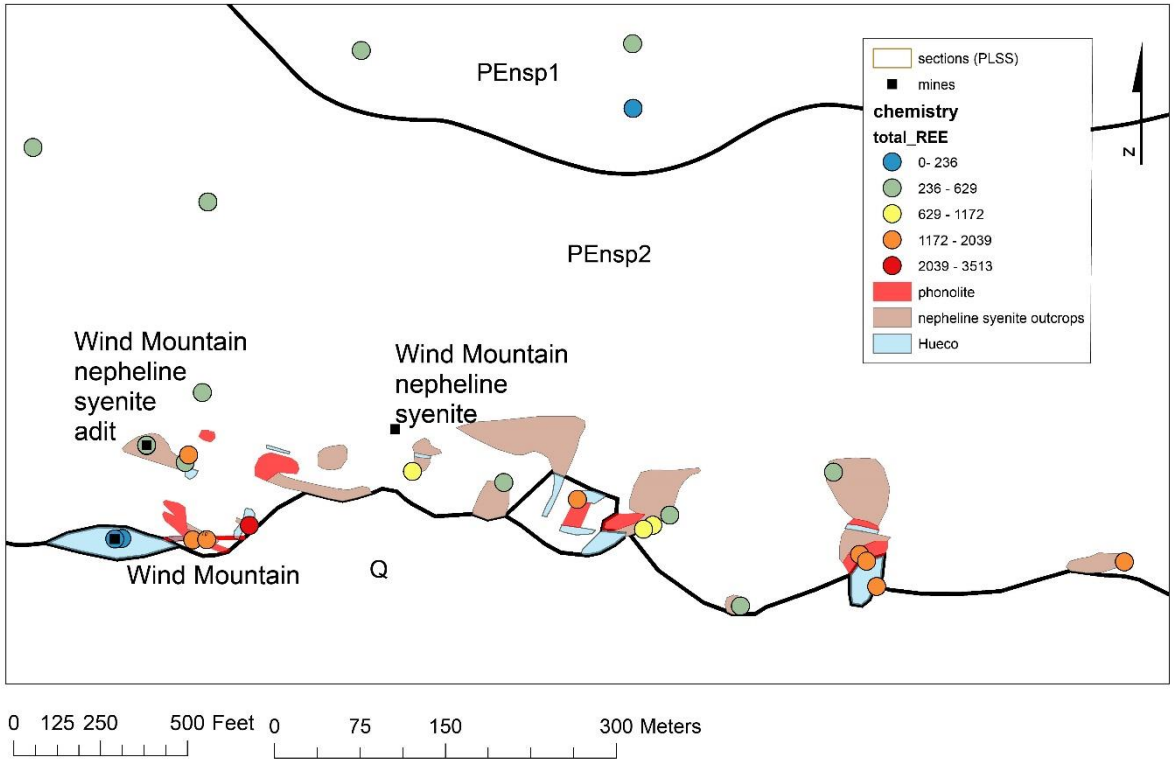

FIGURE 85. Geologic map of the south side of Wind Mountain, including the Wind Mountain nepheline syenite adit. See Table 4 for description of igneous units. Location in Fig. 83.

FIGURE 86. Portal (entrance) to the Wind Mountain nepheline syenite adit (NMOt0013).

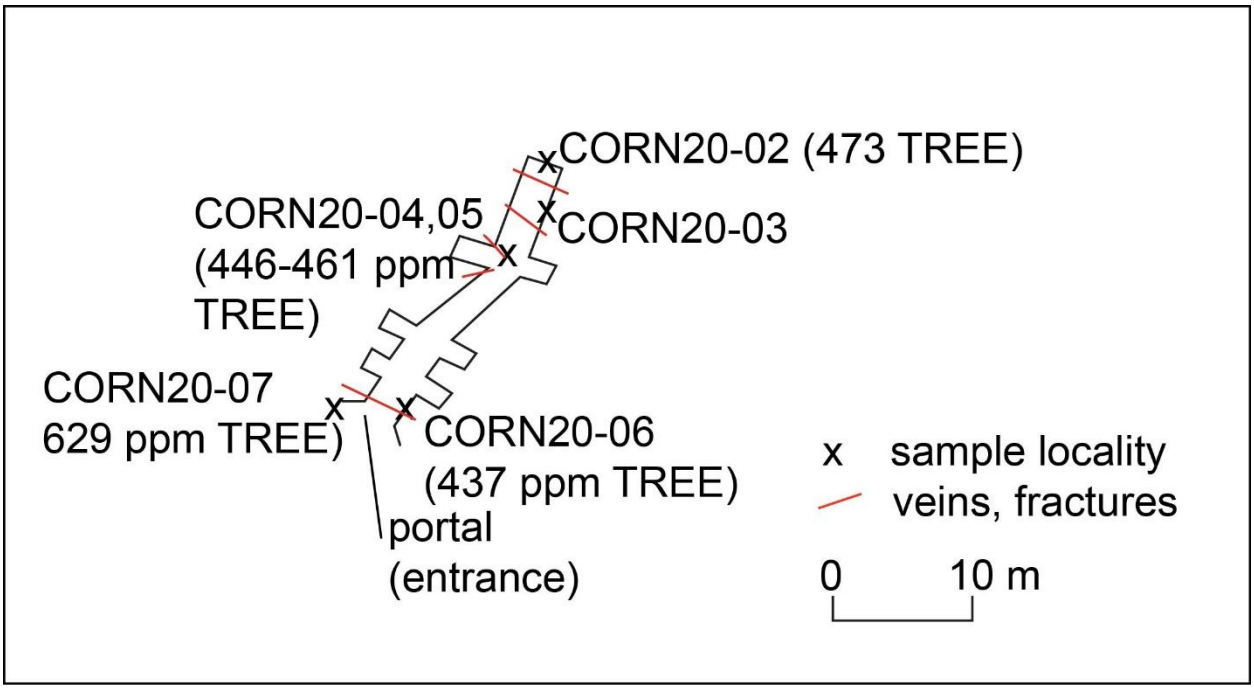

FIGURE 87. Plan map of the Wind Mountain nepheline syenite adit, showing sample locations and total REE concentrations (NMOt0013).

FIGURE 88. Looking north down the Wind Mountain nepheline syenite adit. The back (top) is approximately 10-15 ft high.

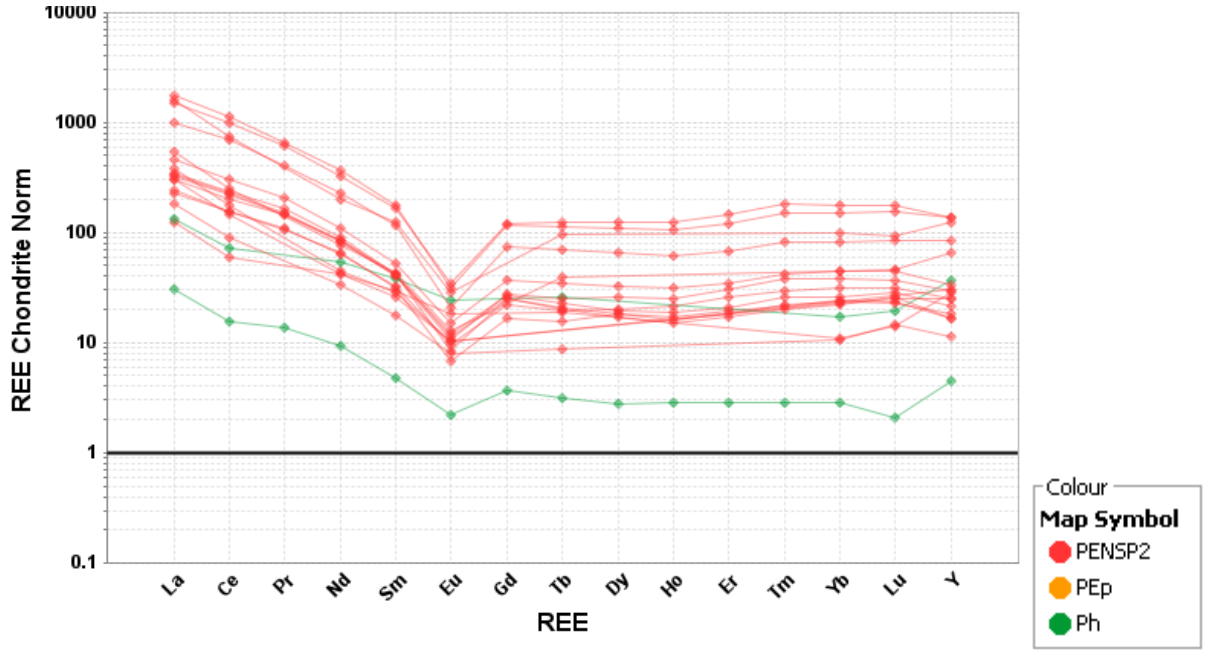

FIGURE 89. REE chondrite-normalized plot for samples from Wind Mountain nepheline syenite adit area, south side of Wind Mountain (chondrite values from Taylor and McLennan, 1985). Chemical analyses are in Appendix 4. Geologic map showing sample locations is in Figure 85.

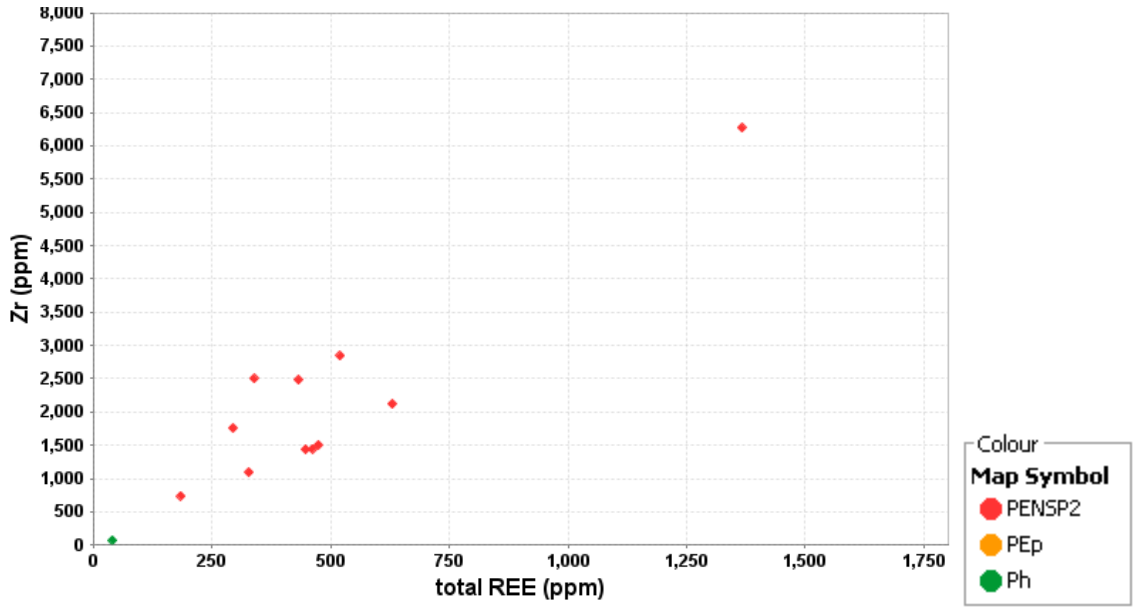

FIGURE 90. Zr vs total REE plot for samples from Wind Mountain nepheline syenite adit area.

Llewellyn prospect

The Llewellyn prospects (NMOt0012, NMOt0422, NMOt0423, NMOt0435) are on the west flank of Wind Mountain and consist of a 25 ft (7.6 m) adit and 4 prospect pits (3-5 ft, 1-1.5 m deep), exposing steeply dipping altered limestones and shales of the Hueco Formation (Fig. 91). F.P. Llewellyn first claimed the deposit (Collins, 1958) at the site of a small spring where caliche is abundant. A geologic map of the area is in Figure 91, a plan of the adit is in Figure 92, and a view of the portal is in Figure 93. Thin veins of eudialyte and thin dikelets of phonolite and nepheline syenite (<5 cm thick) intruded along steeply dipping, altered limestones and shales within the adit (Fig. 94, 95, 96). The contact between the nepheline syenite and skarns is sharp (Fig. 97). At least two nepheline syenite dikelets intruded along the bedding planes within the adit and range from 5-10 cm in thickness (Fig. 94). A phonolite dike is exposed in the prospect pits (Fig. 98) that pinches out in the adit (Fig. 91) and contains as much as 1398 ppm total REE (CORN20-34). Radioactivity associated with the phonolite dikes is as much as three times background. Pyrite is found as fracture coatings surrounded by hematite and limonite. Quartz crystals and minor silicification is locally present. Eudialyte, zircon, monazite, bastnäsite, calcio-catapleiite, vitusite, xenotime, fluorite, and rutile are found in the eudialyte veins, nepheline syenite, and phonolite dikelets. Roumaite, a Nb-REE (~14 wt. % Nb and 7-10 wt. % REE) silicate mineral, along with molybdenite and galena are found in the selvages adjacent to the eudialyte vein. Tremolite and amphiboles are found in the dark green skarns (Fig. 97) and disseminated throughout the recrystallized limestones (Fig. 95). Schreiner (1993) reports galena and sphalerite present in the fractures. Warner et al. (1959) report Be analyses in the area. A second phonolite dike is uphill (east) from the adit and contains as much as 3313 total REE (Fig. 91; CORN123). Samples surrounding the mineralized area defined by the phonolite dikes are low in total REE (Fig. 91).

Chondrite-normalized REE patterns are light-REE enriched with a negative Eu anomaly (Fig. 99). Total REE shows a strong correlation with Zr (Fig. 100), which is consistent with eudialyte minerals hosting the REE and Zr.

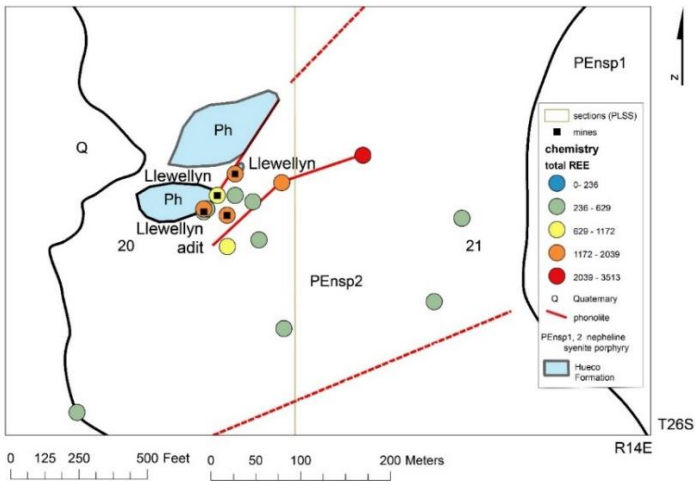

FIGURE 91. Geologic map of the Llewellyn prospect area, showing sample locations. Location in Fig. 83.

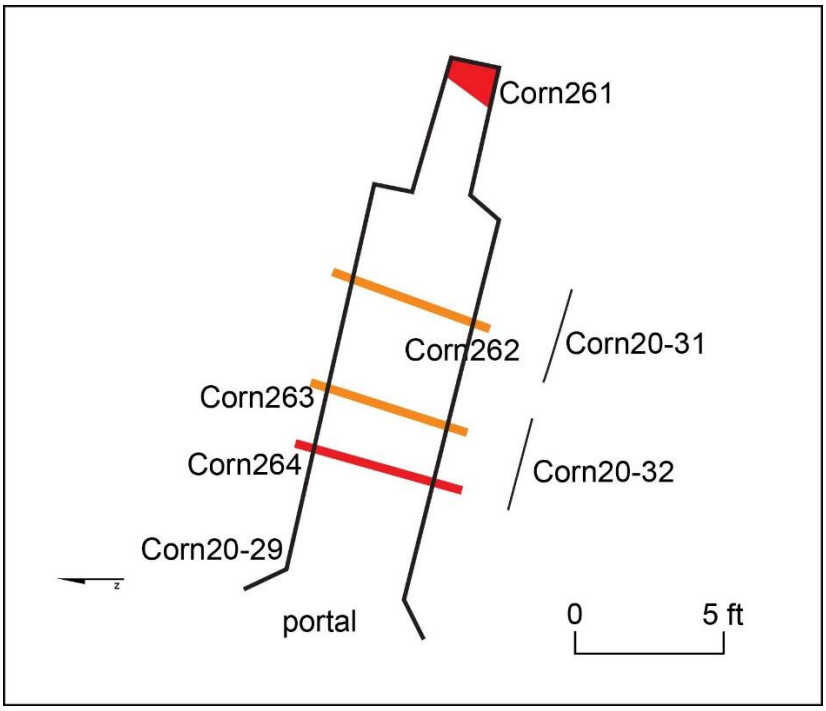

FIGURE 92. Plan map of the Llewellyn adit, showing sample locations (NMOt0012).

FIGURE 93. Portal (entrance) to the Llewellyn adit, constructed in altered limestone and shale from the Hueco Formation, looking east (NMOt0012).

FIGURE 94. Eudialyte vein cutting altered limestone and shale in Hueco Formation at the Llewellyn adit.

FIGURE 95. South wall of the Llewellyn adit showing altered layers of the Hueco Formation. Note the steep dips to the west.

FIGURE 96. Thin phonolite dikelet intruding the altered limestone and shale in Hueco Formation on south wall of the Llewellyn adit. Note the steep dip to the west.

FIGURE 97. Lens of nepheline syenite intruding altered limestone in Hueco Formation at the Llewellyn adit.

FIGURE 98. Altered limestone in one of the prospect pits in Hueco Formation at the Llewellyn prospect. Note the steep dips to the west.

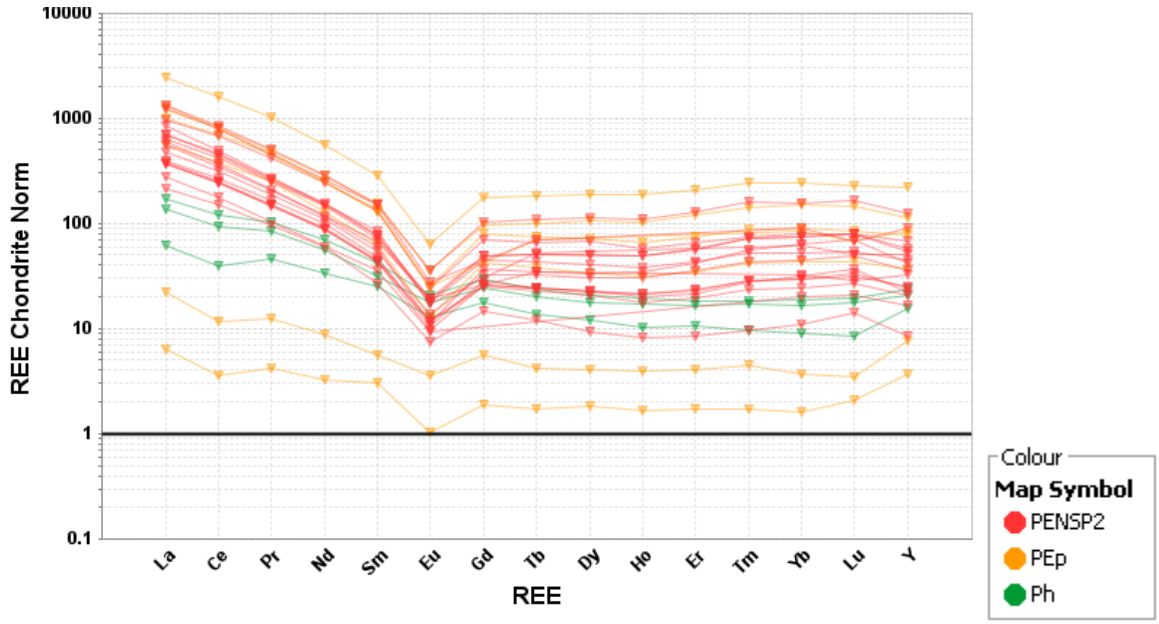

FIGURE 99. REE chondrite-normalized plot for samples from Llewellyn area, western flank Wind Mountain (chondrite values from Taylor and McLennan, 1985). Chemical analyses are in Appendix 4. Geologic map showing sample locations is in Figure 91.

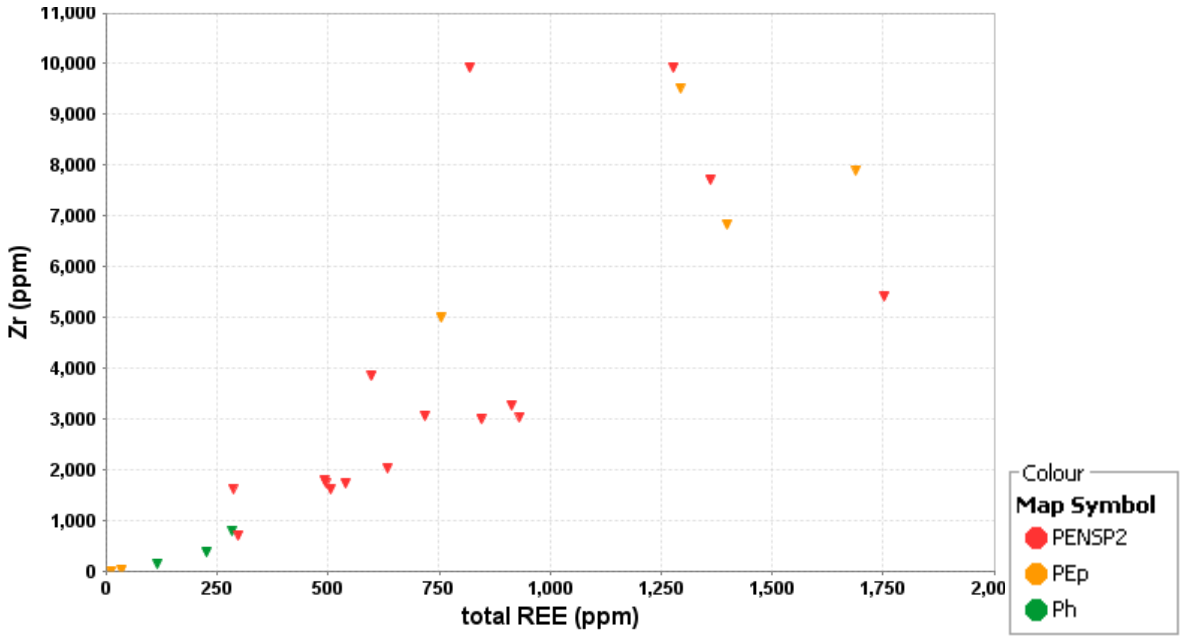

FIGURE 100. Zr vs total REE plot for samples from Llewellyn area, western flank Wind Mountain.

State Lease

State Lease (NMOt043, NMOt0437) is on state land on the northern flanks of Wind Mountain and consists of two shallow shafts (Fig. 101). The shafts have exposed portions of a skarn formed in Hueco limestone (Fig. 102, 103), adjacent to a phonolite dike. The skarn is approximately 150 ft (45 m) long and 60 ft (18 m) wide and is characterized by medium beds (1-3 ft, 0.3-1 m thick) of alternating unaltered limestone, green tactite or skarn (chlorite and possibly epidote?), recrystallized limestone, and hematite-replaced limestone (Fig. 104). The Hueco limestone is mostly unaltered and medium bedded (Fig. 102). A composite sample across the skarn (3 ft) in shaft NMOt043 contains 1599.55 ppm total REE (CORN239). Samples of phonolite contain the highest total REE concentrations (Fig. 104, 3513.08 ppm total REE, CORN242). The samples exhibit light REE-enriched chondrite-normalized patterns, similar to other REE-bearing zones in Wind Mountain (Fig. 106).

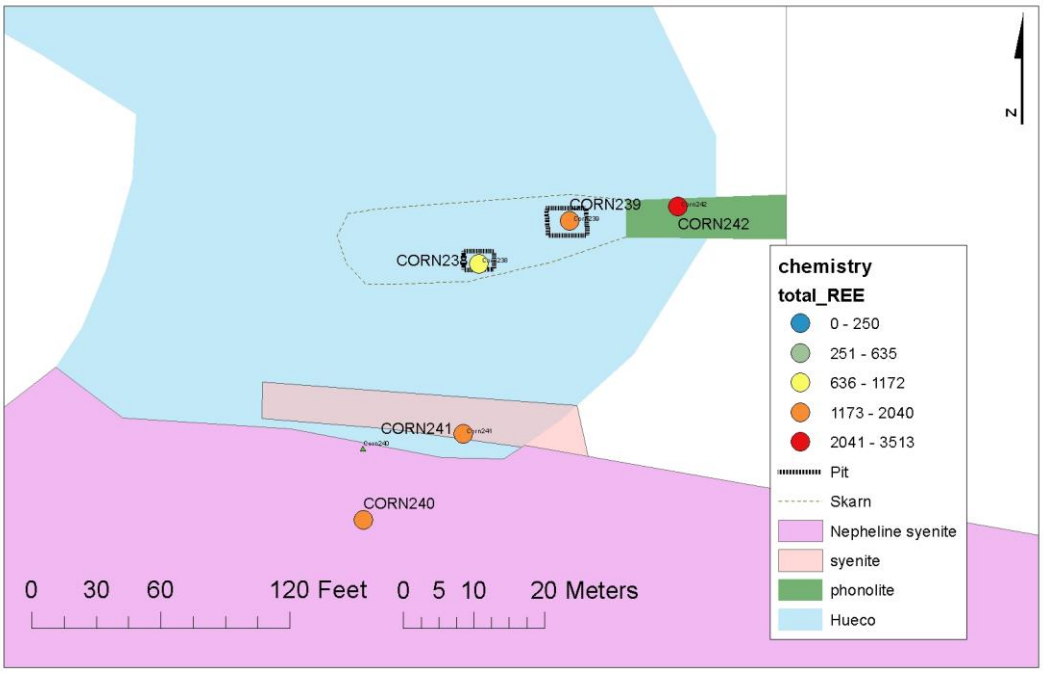

FIGURE 101. Geologic map of State Lease area, in section 16, T26S, R14E, near State Lease prospects (NMOt043, NMOt0437), northern flank Wind Mountain. Location in Figure 83.

FIGURE 102. Unaltered, thinly bedded Hueco limestone dipping approximately 40°N along the northern flanks of Wind Mountain in section 16, T26S, R14E, near State Lease prospects (NMOt043, NMOt0437).

FIGURE 103. Skarn in Hueco limestone near phonolite dike (NMOt043). Pit is approximately 4 ft deep. Composite sample across the skarn (3 ft) contained 1599.55 ppm total REE (CORN239).

FIGURE 104. State lease skarn made up of beds of hematite-replaced limestone and recrystallized limestone, northern flanks of Wind Mountain in section 16, T26S, R14E, near State Lease prospects (NMOt043, NMOt0437).

FIGURE 105. Phonolite dike intruding Hueco limestone near the contact with the skarn. Samples of phonolite contained 3513.08 ppm total REE (CORN242). Note limestone outcrops in upper left of photograph.

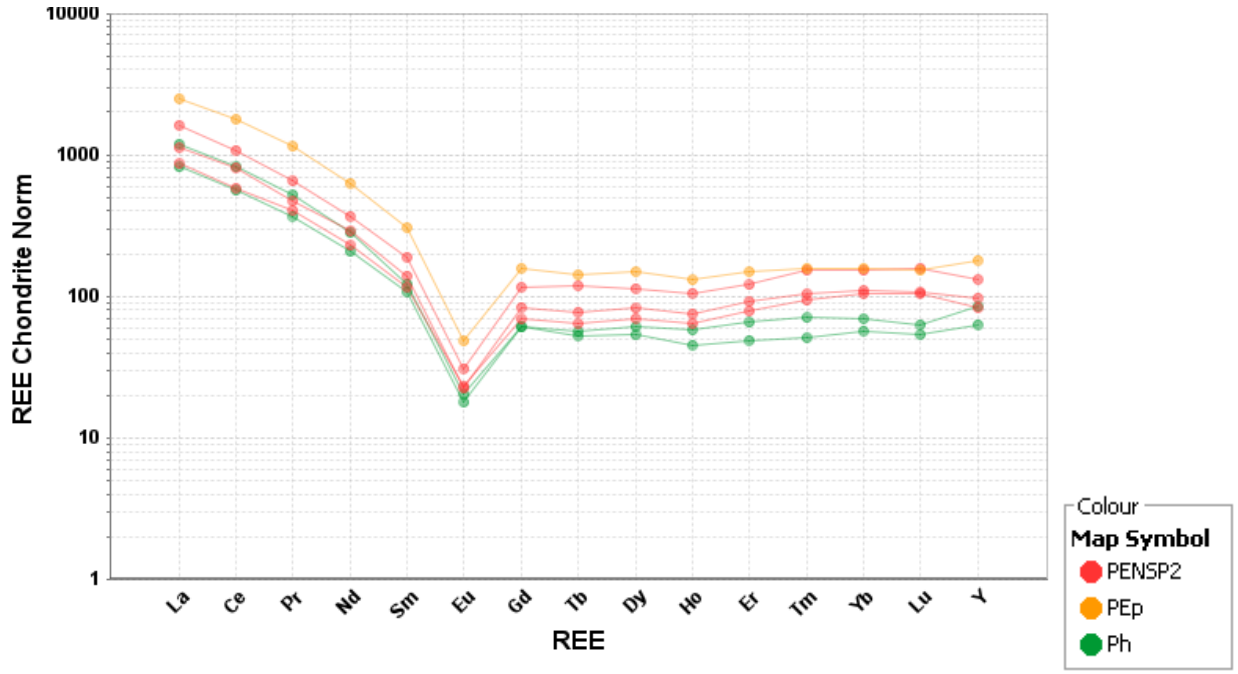

FIGURE 106. REE chondrite-normalized plot for samples from State Lease area, in section 16, T26S, R14E, near State Lease prospects **(**NMOt043**,** NMOt0437), northern flank Wind Mountain (chondrite values from Taylor and McLennan, 1985). Chemical analyses are in Appendix 4. Geologic map showing sample locations is in Figure 101.

North Wind Mountain Skarn

The north Wind Mountain skarn (CORN104) is a small outcrop on the edge of Wind Mountain near Wind Mountain Draw (Fig. 107). It is a small green skarn layer in Hueco limestone that contains eudialyte (aqualite) and pyrochlore (Appendix 8); modal analysis is in Table 17.

TABLE 17. Modal analysis of skarn (CORN104).

Mineral	CORN104
Lithology	skarn
Aegirine-augite	58
Clinopyroxene	3
Nepheline	7
Clay	28
Analcime	2
Aqualite	1
Pyrochlore	tr
Total	99

FIGURE 107. Close-up of the nepheline syenite (cream-orange)-skarn (green) contact, north Wind Mountain skarn (photo CORN104c). Eudialyte is found in both the nepheline syenite and the skarn.

Geovic Winkie Drill Data (Northeastern Wind Mountain)

In 2011-2012, Geovic Mining Co. drilled 10 winkie drill holes on the northeastern edge of Wind Mountain, east of the state lease (Fig. 4, Table 3). Winkie drill holes are developed by a portable drill and are used in environmentally sensitive areas where there are no roads and the drilling equipment is carried by hand, mules, or low-impact 4-wheelers. The drill core is generally less than 1-inch in diameter. Winkie drill data are typically interpreted separately from

normal dill core data because it is considered a small sample size that is not representative of the deposit. The archived drill core was not examined by the authors.

The lithology ranges from nepheline syenite to syenite to syeno-diorite (Fig. 108). The geochemical analyses indicate high correlations between total REE, Nb, Be, Th, and Zr (Table 18, 19, Fig. 109, 110, 111), similar to surface samples. The samples exhibit similar light-REE enriched chondrite-normalized plots as other samples in the Cornudas Mountains (Fig. 109). Downhole profiles indicate no increase in trace elements with depth (Fig. 112), but suggest certain zones are more enriched in these elements than others. These correlations are similar to correlations found in other data sets from the Cornudas Mountains. These correlations are a result of similar minerals containing total REE, Nb, Be, Th, and Zr.

TABLE 18. Summary statistics of chemical analyses from Wind Mountain winkie drill holes.

	TiO_2	Be	Hf	Nb	Sc	Th	U	Y	Zr	Total REE
Count	51	51	51	51	33	51	51	51	51	51
Minimum	0.05	9	25.6	138	1.0	22	5	29	1204	277
Maximum	0.232	64	204.0	1120	2.0	533	133	252	12680	1913
Mean	0.13	22	54	319	1	54	14	70	2690	666
Median	0.137	19	42.2	267	1.0	41	10	51	2057	540
Standard Deviation	0.04	9	36	167	0.4	69	17	52	1988	362

TABLE 19. Selected Pearson correlation coefficients of chemical analyses from Wind Mountain winkie drill holes. Number of samples=51 (Table). Highlighted values indicate significant correlations.

	TiO_2	P_2O_5	Be	Hf	Nb	Pb	Sc	Th	U	Y	Zn	Zr	Total REE
TiO_2	1.0												
P_2O_5	0.7	1.0											
Be	-0.53	-0.25	1.0										
Hf	-0.4	-0.35	0.79	1.0									
Nb	-0.39	-0.24	0.88	0.97	1.0								
Pb	-0.17	-0.03	0.77	0.69	0.79	1.0							
Sc	0.65	0.31	-0.34	-0.26	-0.24	-0.11	1.0						
Th	-0.16	-0.01	0.78	0.67	0.78	1.0	-0.19	1.0					
U	-0.19	-0.05	0.81	0.73	0.83	0.98	-0.07	0.98	1.0				
Y	-0.32	-0.28	0.61	0.93	0.87	0.47	-0.08	0.45	0.52	1.0			
Zn	-0.26	-0.04	0.9	0.74	0.85	0.94	-0.14	0.95	0.95	0.53	1.0		
Zr	-0.37	-0.29	0.83	0.98	0.98	0.81	-0.22	0.79	0.84	0.88	0.83	1.0	
Total REE	-0.35	-0.24	0.67	0.94	0.9	0.52	-0.07	0.51	0.57	0.98	0.59	0.9	1.0

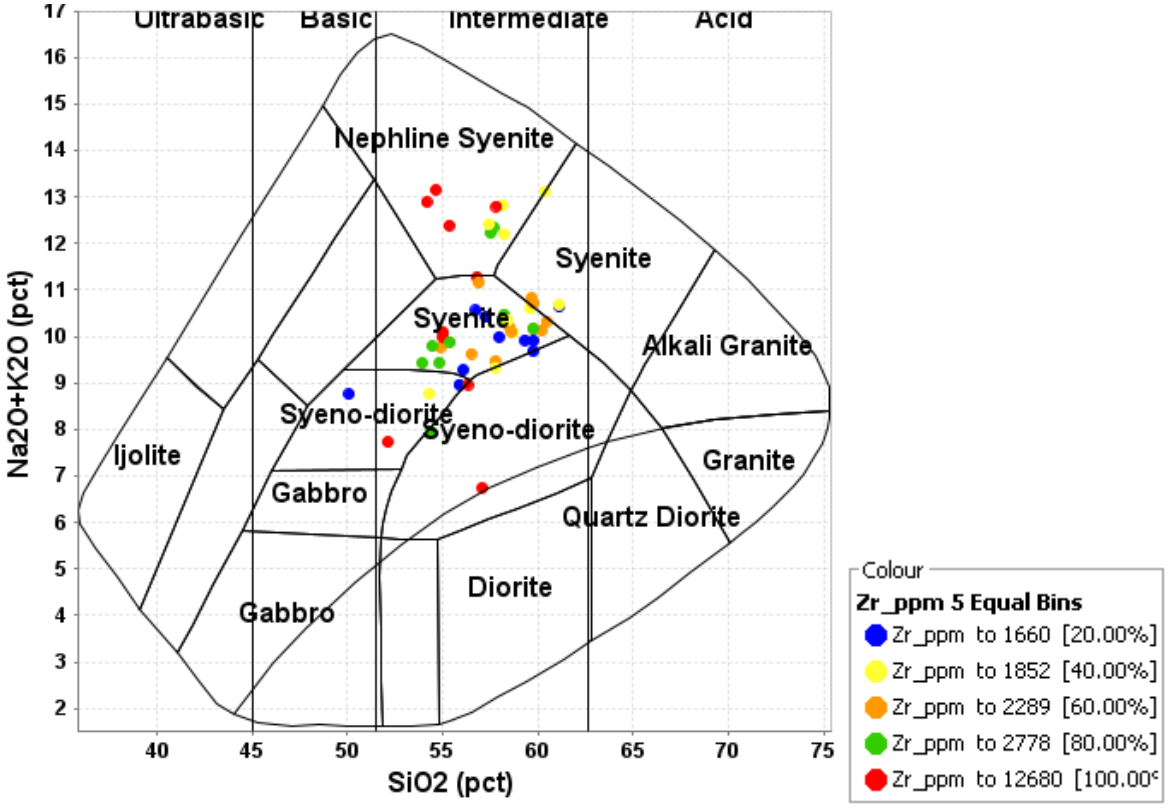

FIGURE 108. TAS plutonic classification plot for Wind Mountain winkie drill hole samples (Cox et al. 1979 adapted by Wilson 1989). The curved line separates the alkaline (above the curve) from subalkaline (below the curve) rocks (Irvine and Baragar, 1971). The colors reflect concentrations of Zr (ppm). Note that the higher REE samples also have higher Zr.

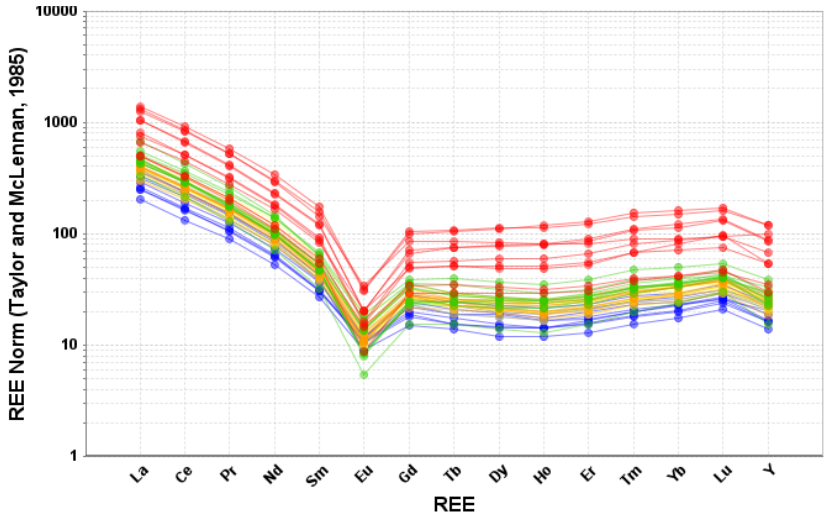

FIGURE 109. REE chondrite normalized plot of Wind Mountain winkie drill hole samples (chondrite values from Taylor and McLennan, 1985). The colors reflect concentrations of Zr (ppm; legend in Fig. 108). Note that the higher REE samples also have higher Zr.

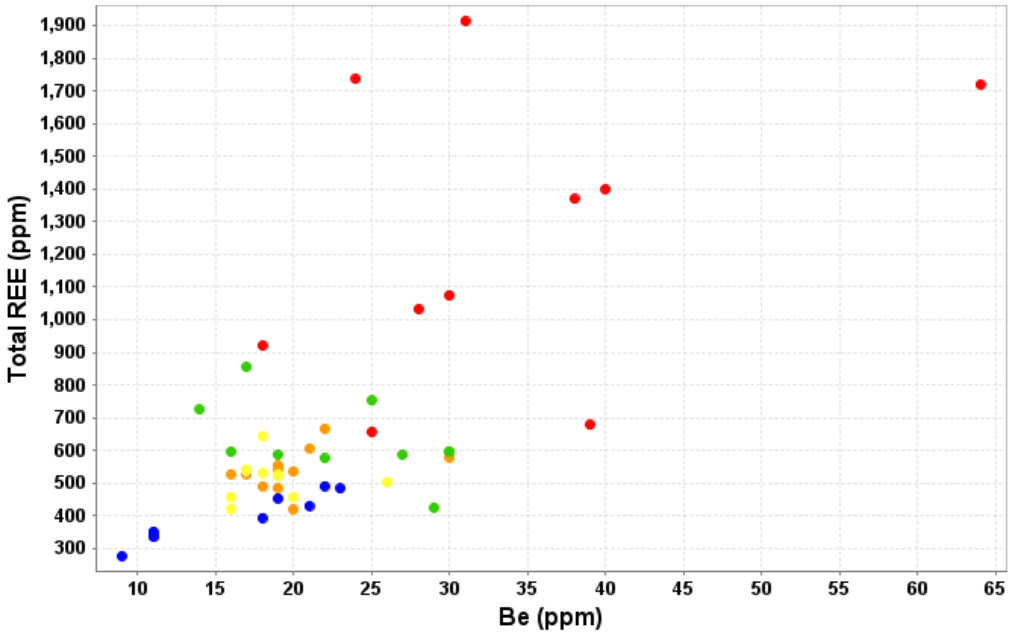

FIGURE 110. Total REE vs. Be plot of Wind Mountain winkie drill hole samples. The colors reflect concentrations of Zr (ppm) (legend in Fig. 108). Note that the higher REE and Be samples also have higher Zr.

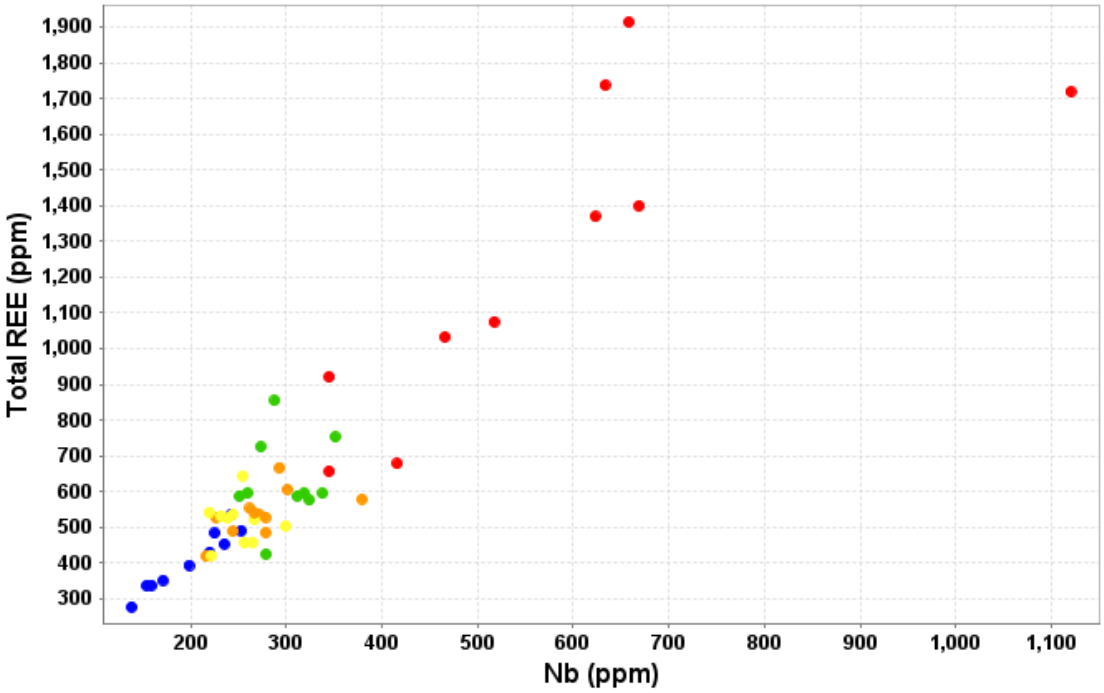

FIGURE 111. Total REE vs. Nb plot of Wind Mountain winkie drill hole samples. The colors reflect concentrations of Zr (ppm) (legend in Fig. 108). Note that the higher REE and Nb samples also have higher Zr.

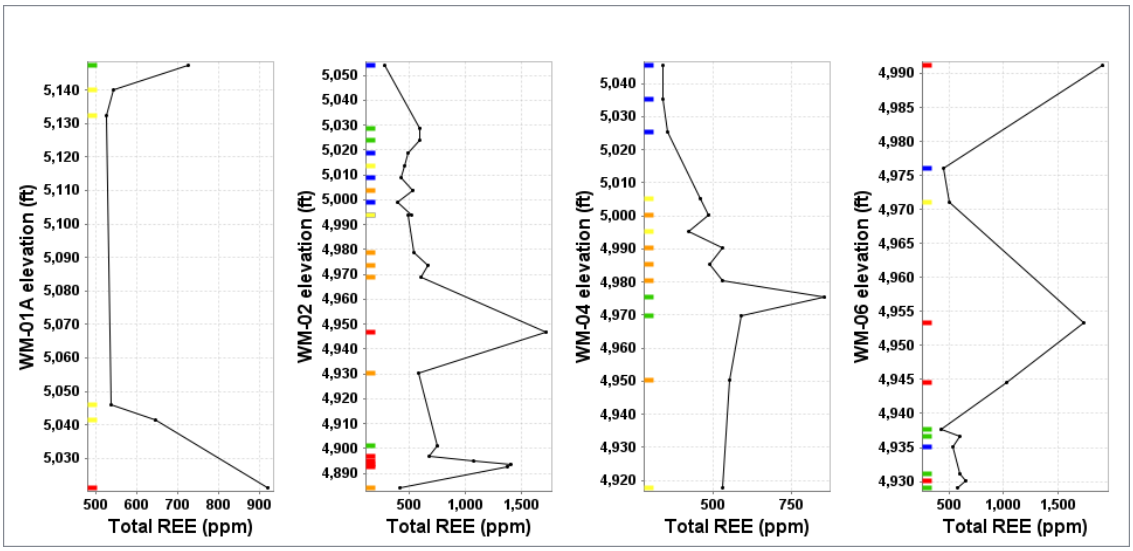

FIGURE 112. Downhole profile showing concentrations of total REE for Wind Mountain winkie drill holes. The colored bars reflect concentrations of Zr (ppm) (legend in Fig. 108).

Jones Prospect (eastern Wind Mountain)

There are no workings on the Jones claims (NMOt0011), but Collins (1959) indicates the area was prospected in the 1950s. The contact between the limestone and nepheline syenite is partially intruded by a phonolite dike, 1-15 ft wide (0.3-4.5 m) and over 600 ft (183 m) long (Fig. 113). A geologic map of the area is in Figure 113. This is one of the few areas in the Cornudas Mountains where the stratigraphic relationships between the Hueco, Yeso, and San Andres formations are well exposed. Minor recrystallization of the limestones has occurred along the intrusive contacts and the fault, but no major skarns were found at the surface. However, in drill core, thin zones (less than 10 cm wide) of skarns and recrystallized limestone are found (Fig. 43, 44, 49, 84), but there are no indications of eudialyte mineralization in the altered limestones. REE and Zr are elevated (Fig.114, 115). Geovic constructed a drill pad in the northern portion of the area (see description of drill core below).

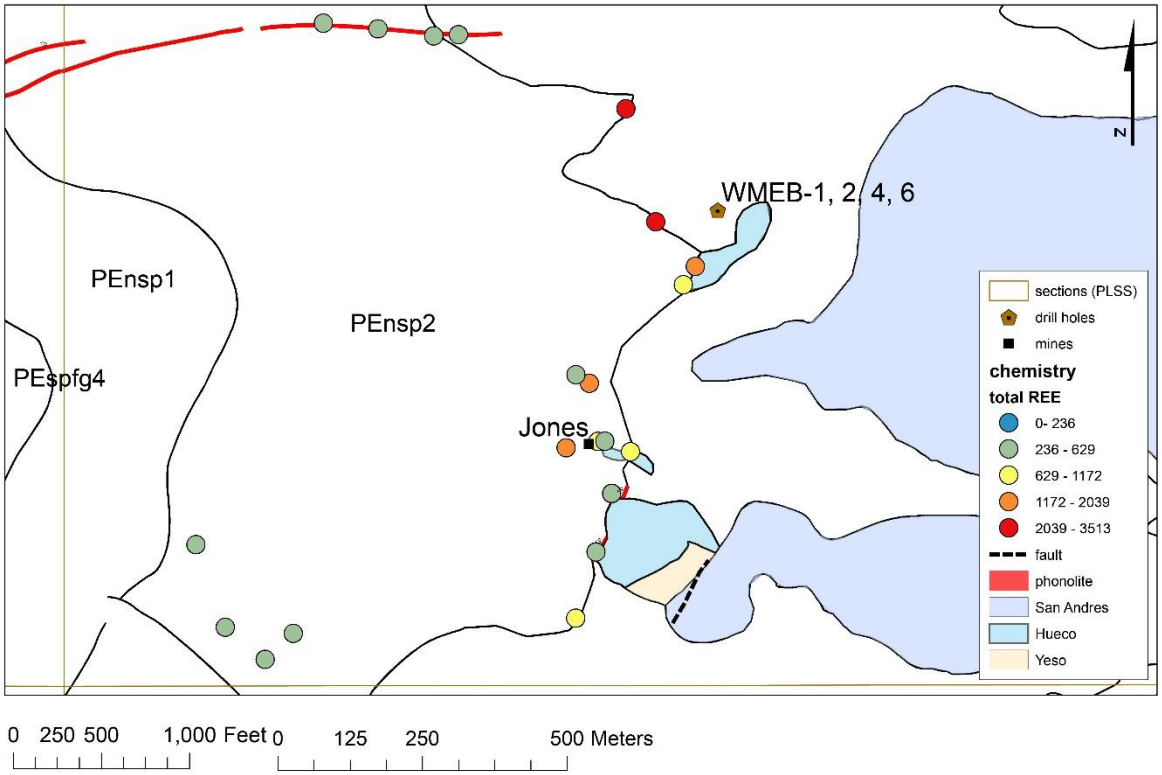

FIGURE 113. Geologic map of Jones prospect area. Location in Fig. 83.

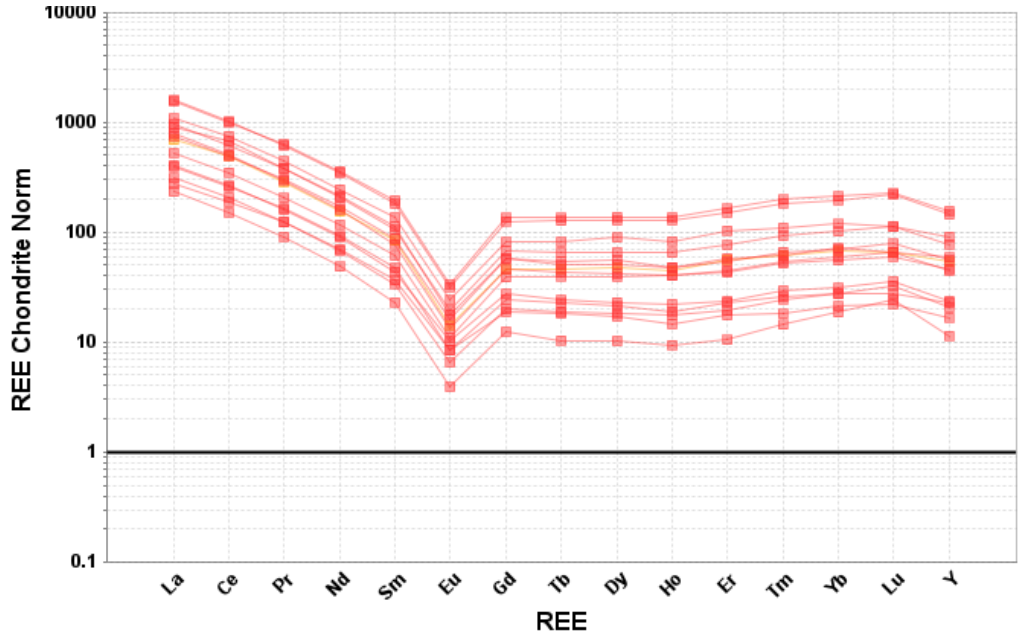

FIGURE 114. REE chondrite-normalized plot for samples from the Jones prospect (chondrite values from Taylor and McLennan, 1985). Chemical analyses are in Appendix 4.

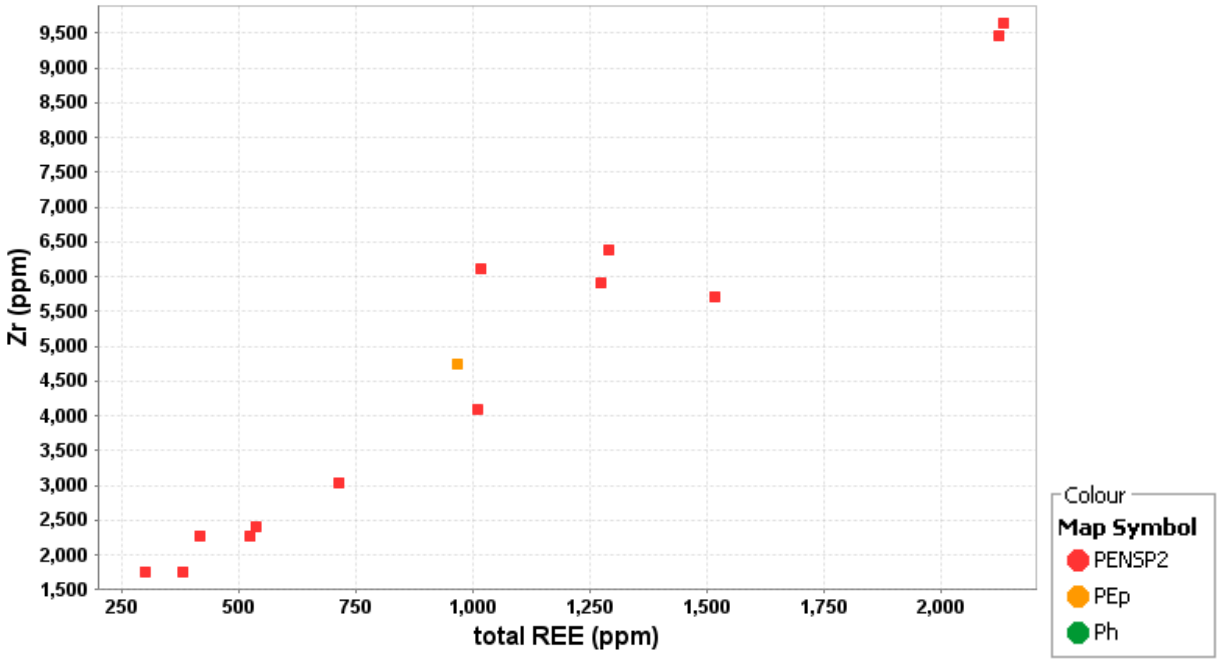

FIGURE 115. Zr vs Total REE plot for samples from Llewellyn area, western flank Wind Mountain.

Geovic drill holes (Eastern Wind Mountain)

Geovic Mining Co. constructed a drill pad north of the Jones claims on the eastern flank of Wind Mountain and drilled 4 drill holes at different inclinations (Table 3, Fig. 4, 113). A helicopter was used to avoid constructing roads to the site. Eudialyte in nepheline syenite is found throughout the drill holes (Fig. 116, 117, 118, 119). Most samples plot as nepheline syenite on a TAS diagram (Fig. 120). Both Zr and total REE are higher in these samples than in the winkie holes (Tables 20, 21). The samples exhibit similar light-REE enriched chondrite-normalized patterns as other samples in the Cornudas Mountains (Fig. 121). The geochemical analyses indicate similar high correlations between total REE, Nb, Be, Th, and Zr (Tables 20, 21, Fig. 122, 123). Downhole profiles indicate trace elements are sporadic with depth (Fig. 124), but suggest certain zones are more enriched in these elements than others. These correlations are similar to correlations found in other data sets from the Cornudas Mountains and are a result of similar minerals containing total REE, Nb, Be, Th, and Zr.

TABLE 20. Summary statistics of chemical analyses from Wind Mountain drill holes.

	TiO_2	P_2O_5	Be	Hf	Nb	Pb	Sc	Th	U	Y	Zr	Total REE
Count	184	182	184	184	183	184	54	184	184	184	184	184
Minimum	0.04	0.01	2.0	3.2	9.0	15.0	1.0	7.4	2.2	21.0	150.0	138
Maximum	0.38	0.25	71.0	193.0	1230	260.0	5.0	297.0	111.0	299.0	10070	2611
Mean	0.10	0.06	25	68	380	50	1.3	60	20	94	3673	872
Median	0.10	0.05	24.0	52	330	39	1.0	48.3	16.25	70.5	2850	679
Standard Deviation	0.04	0.04	9.3	40.0	194	36	0.66	40	16	60	2156	484

TABLE 21. Selected Pearson correlation coefficients of chemical analyses from Wind Mountain drill holes. Number of samples=51 (Table). Highlighted values indicate significant correlations.

	TiO_2	P_2O_5	Be	Hf	Nb	Pb	Sc	Th	U	Y	Zr	Total REE
TiO_2	1.0											
P_2O_5	0.57	1.0										
Be	-0.25	0.034	1.0									
Hf	-0.25	-0.11	0.79	1.0								
Nb	-0.17	-0.06	0.85	0.91	1.0							
Pb	-0.05	-0.02	0.75	0.73	0.84	1.0						
Sc	0.83	0.46	-0.34	-0.36	-0.2	-0.19	1.0					
Th	-0.06	0.041	0.82	0.73	0.89	0.94	-0.12	1.0				
U	-0.05	0.029	0.77	0.76	0.88	0.94	-0.07	0.97	1.0			
Y	-0.24	-0.1	0.74	0.95	0.85	0.62	-0.27	0.63	0.66	1.0		
Zr	-0.23	-0.1	0.81	0.98	0.9	0.75	-0.33	0.75	0.78	0.96	1.0	0
Total REE	-0.17	-0.04	0.8	0.97	0.92	0.76	-0.28	0.78	0.8	0.96	0.96	1.0

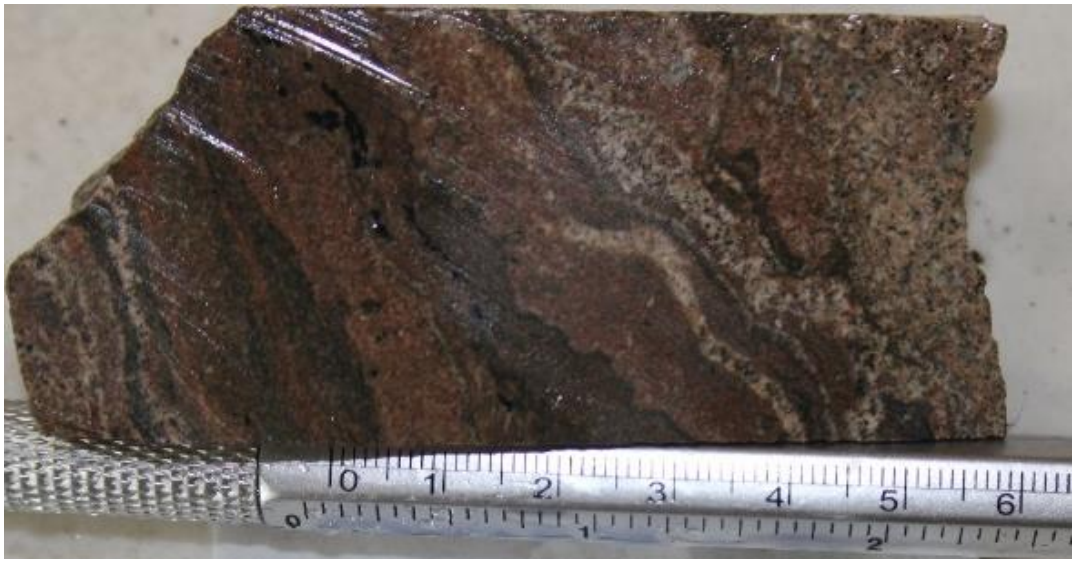

FIGURE 116. Mineralized nepheline syenite containing 1124.23 ppm total REE, 5650 ppm Zr, 362 ppm Nb (drill hole WMEB-4, 278 ft depth).

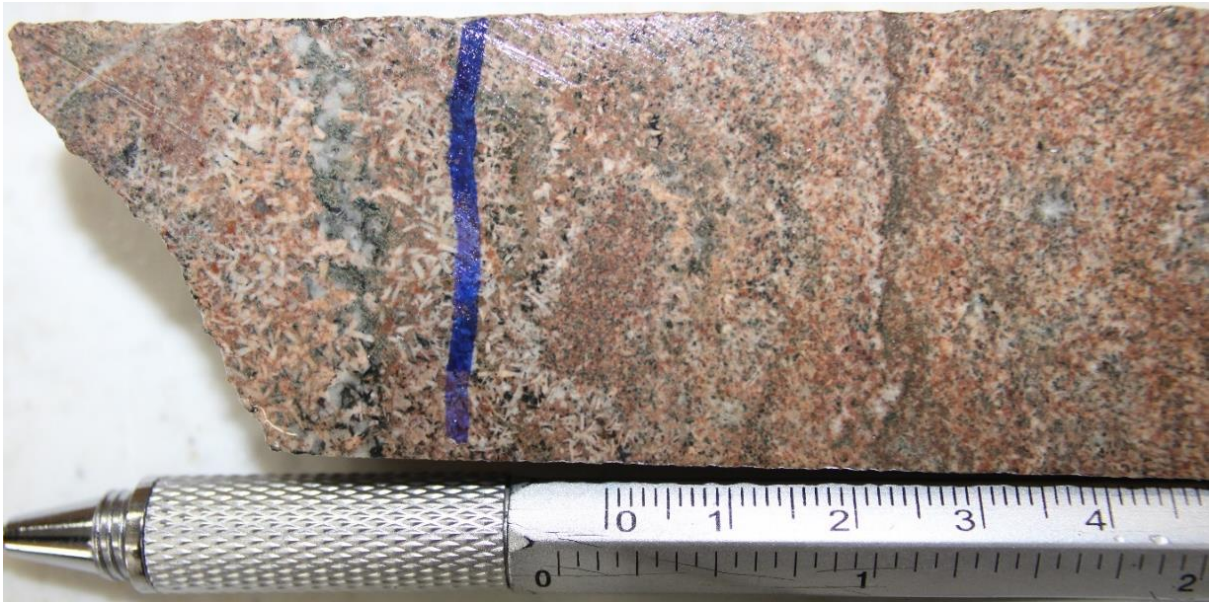

FIGURE 117. Nepheline surrounding fine grained nepheline syenite fragment, 886.13 ppm total REE, 4139 ppm Zr, 433 ppm Nb Hole WMEB-1, depth 244 ft).

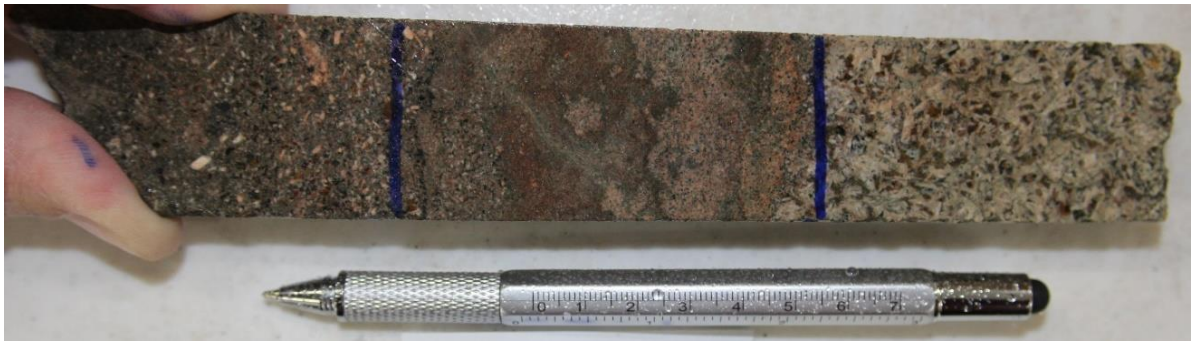

FIGURE 118. Trachytic syenite dike intruding nepheline syenite, 819.13 ppm total REE, 3627 ppm Zr (Hole WMEB-1, 223 ft).

FIGURE 119. Eudialyte in nepheline syenite, 1473.35 ppm total REE, 8826 ppm Zr (WMEB-2, 541.5 ft).

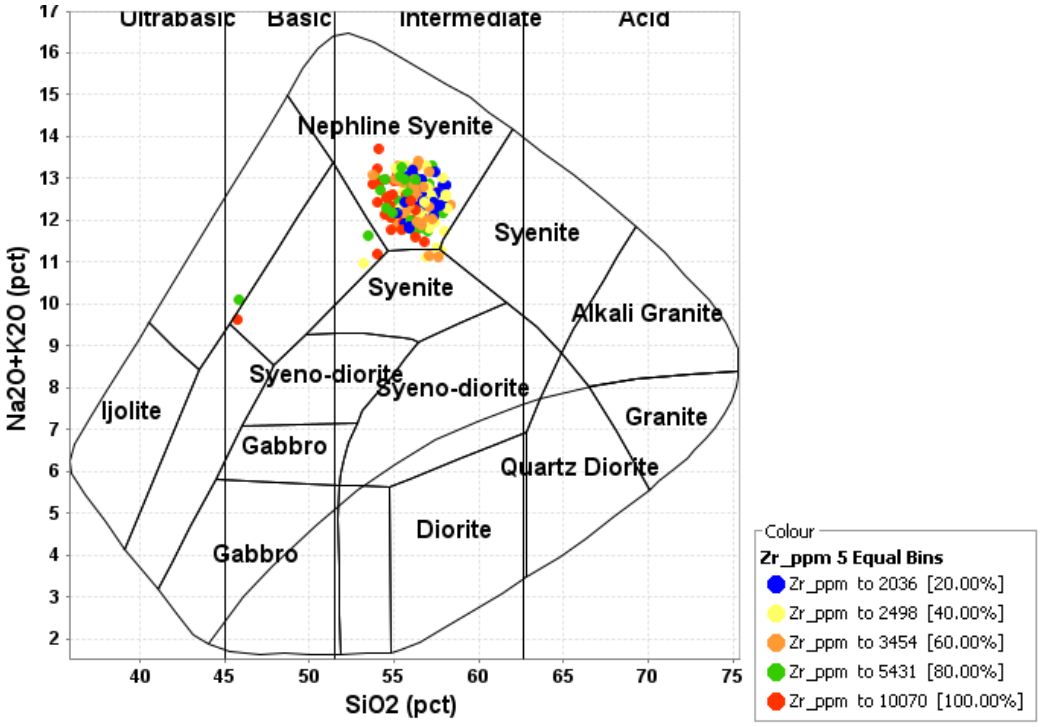

FIGURE 120. TAS plutonic classification plot for Wind Mountain drill hole samples (Cox et al. 1979 adapted by Wilson 1989). The curved line separates the alkaline (above the curve) from

subalkaline (below the curve) rocks (Irvine and Baragar, 1971). The colors reflect concentrations of Zr (ppm). Note that the higher REE samples also have higher Zr.

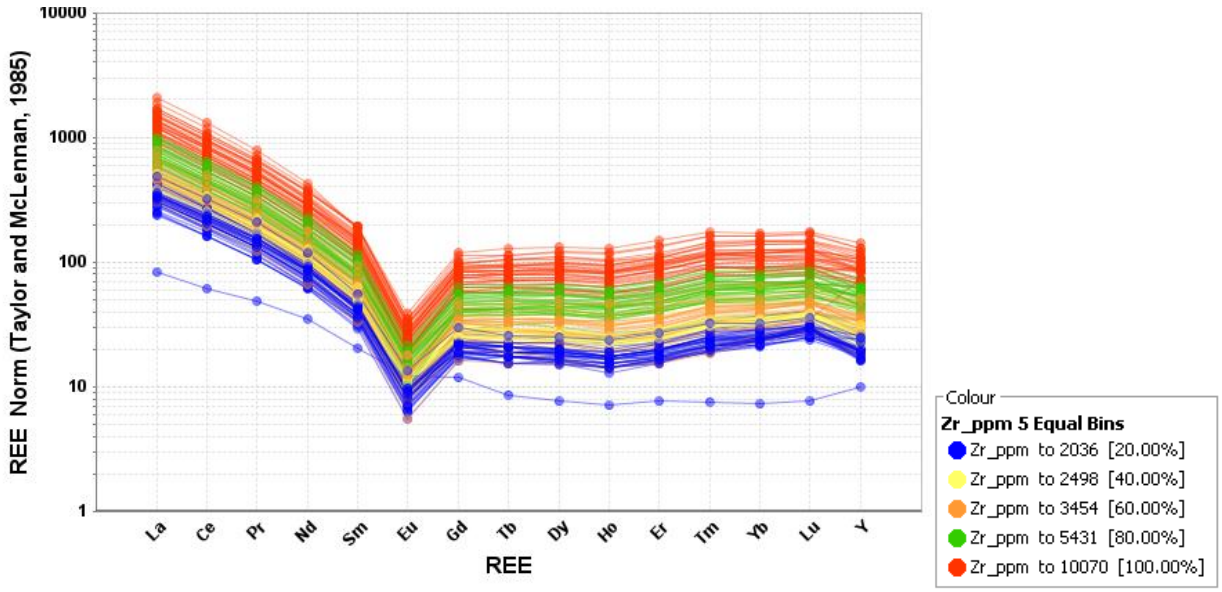

FIGURE 121. REE chondrite normalized plot of Wind Mountain drill hole samples (chondrite values from Taylor and McLennan, 1985). The colors reflect concentrations of Zr (ppm). Note that the higher REE samples also have higher Zr.

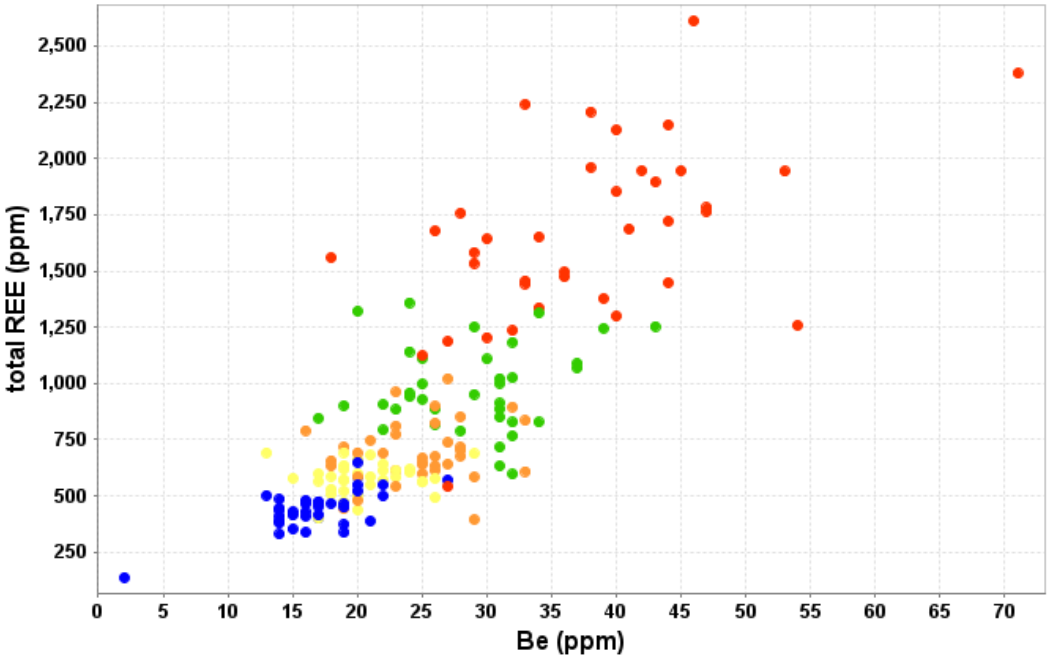

FIGURE 122. Total REE vs. Be plot of Wind Mountain drill hole samples. The colors reflect concentrations of Zr (ppm) (legend in Fig. 120). Note that the higher REE and Be samples also have higher Zr.

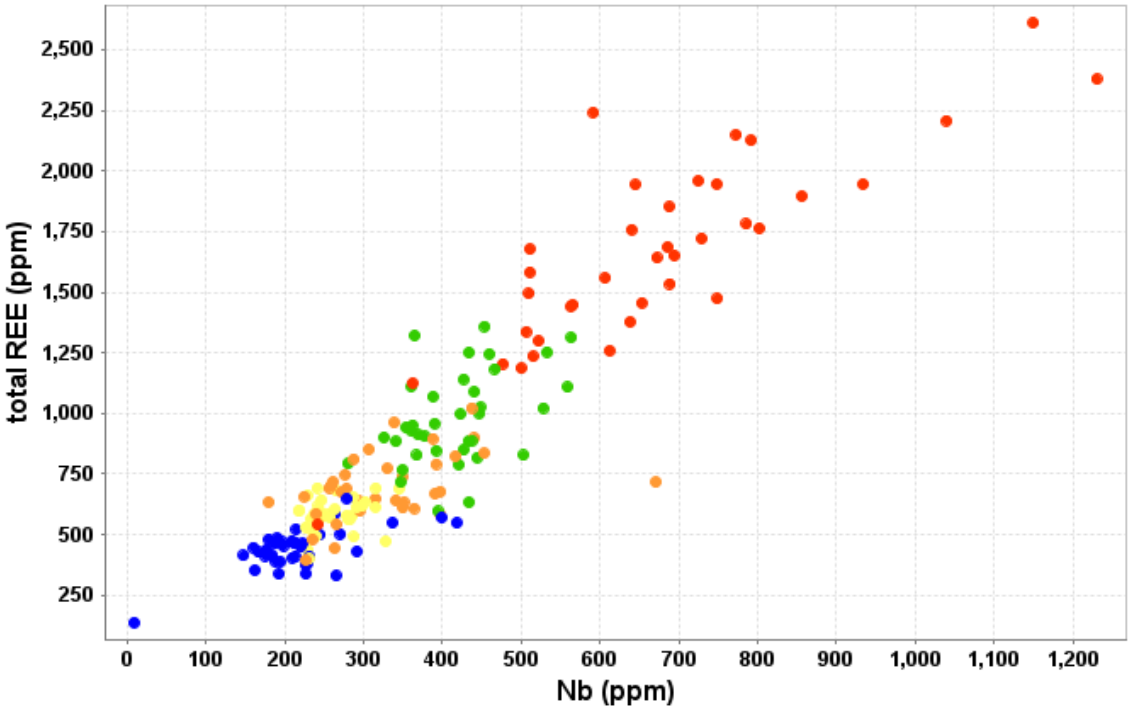

FIGURE 123. Total REE vs. Nb plot of Wind Mountain drill hole samples. The colors reflect concentrations of Zr (ppm) (legend in Fig. 120). Note that the higher REE and Nb samples also have higher Zr.

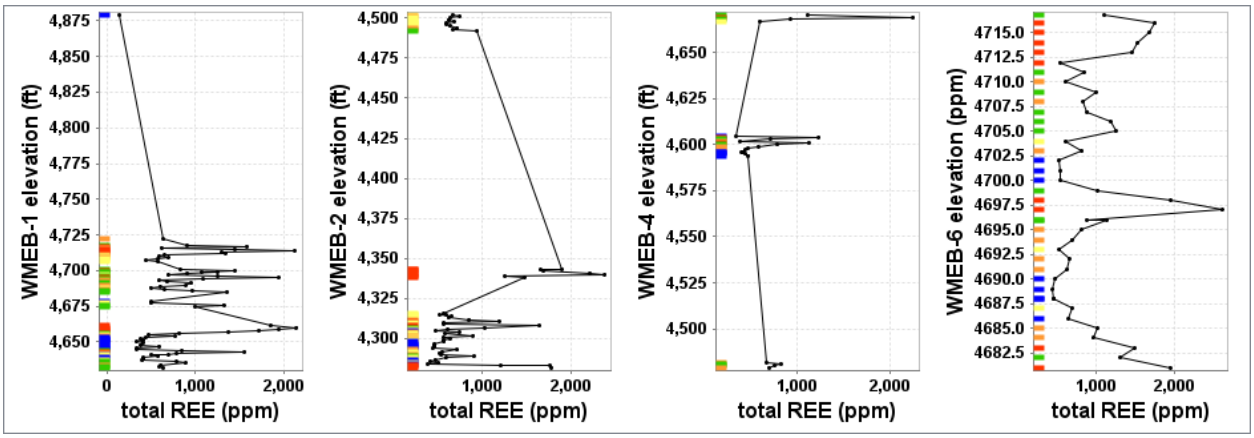

FIGURE 124. Downhole profile showing concentrations of total REE for Wind Mountain drill holes. The colored bars reflect concentrations of Zr (ppm) (legend in Fig. 120). Note that these are actually angled holes not vertical. The REE are in discrete zones.

Chess Draw area

Shallow shafts and prospect pits expose altered syenite, nepheline syenite, phonolite, and breccia dikes, skarns, and altered zones in limestone throughout the Chess Draw area. All three types of REE deposits are found in Chess Draw: 1) REE-bearing nepheline syenite sill and

phonolite dikes, 2) volcanic breccia dikes, and 3) REE-bearing skarns and carbonate-replacement deposits. The igneous intrusions are described above. Not all phonolite or volcanic breccia dikes exhibit elevated REE. The skarns and altered limestone are characterized by iron oxides, calcite, and clays, but only a few skarns contain local fluorite, eudialyte, and pyrite.

The Chess Draw samples exhibit light REE-enriched chondrite-normalized patterns, similar to other REE-bearing zones in Wind Mountain. Skarns and altered limestones contain variable total REE (21-2540 ppm), whereas the breccia dikes contain 296-2362 ppm total REE (Table 22, 23). Two geophysical magnetic anomalies are found in the Chess Draw area (Fig. 82). Additional deep drilling is recommended to identify the source of the magnetic anomalies, which could be intrusions elevated in REE.

TABLE 22. Summary statistics of chemical analyses from Chess Draw (Appendix 4).

	TiO_2	F	Be	Nb	Sc	Th	U	Zr	Total REE
Count	73	82	27	80	84	85	85	84	84
Minimum	0.01	110	5	4	0.1	0.8	3	31	12.6
Maximum	1.81	5550	28	2332	16	453	136	6670	2540
Mean	0.48	842	11	423	1.8	76	18	1822	584
Median	0.25	645	8	227	0.85	33	10	1273	464
Standard Deviation	0.46	788	7	540	2.4	114	25	1400	513

TABLE 23. Pearson correlation coefficients of chemical analyses from Chess Draw (Appendix 4). Number of samples=71 (Table). Highlighted values indicate significant correlations.

	TiO_2	F	Be	Nb	Sc	Th	U	Zr	Total REE
TiO_2	1								
F	-0.06	1							
Be	-0.49	0.46	1						
Nb	-0.34	0.18	0.11	1					
Sc	0.3	-0.17	-0.48	0.04	1				
Th	-0.31	0.2	0.07	0.94	0.09	1			
U	-0.34	0.2	0.22	0.89	0.11	0.88	1		
Zr	-0.49	0.22	0.38	0.86	-0.11	0.82	0.71	1	
Total REE	-0.33	0.23	0.21	0.62	-0.07	0.72	0.67	0.6	1

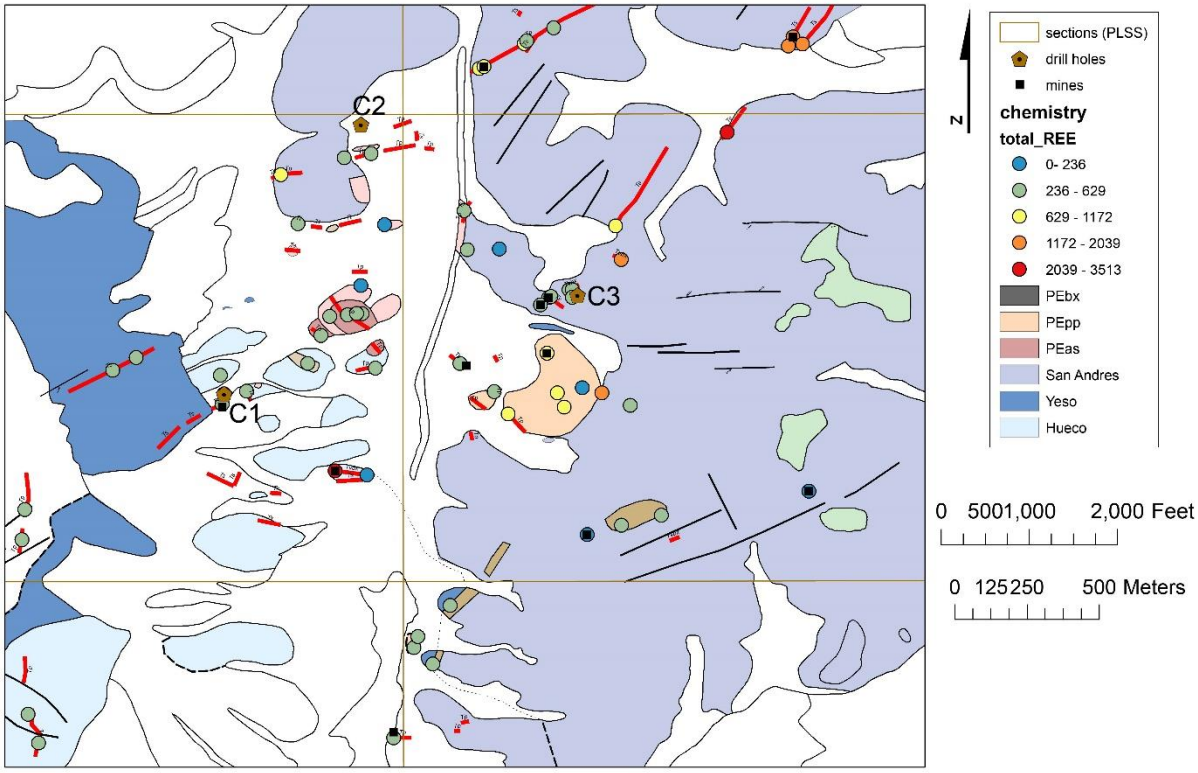

FIGURE 125. Geologic map of Chess Draw area. Location in Fig. 83. Uncolored units are Quaternary units. See Plate 1 for more details.

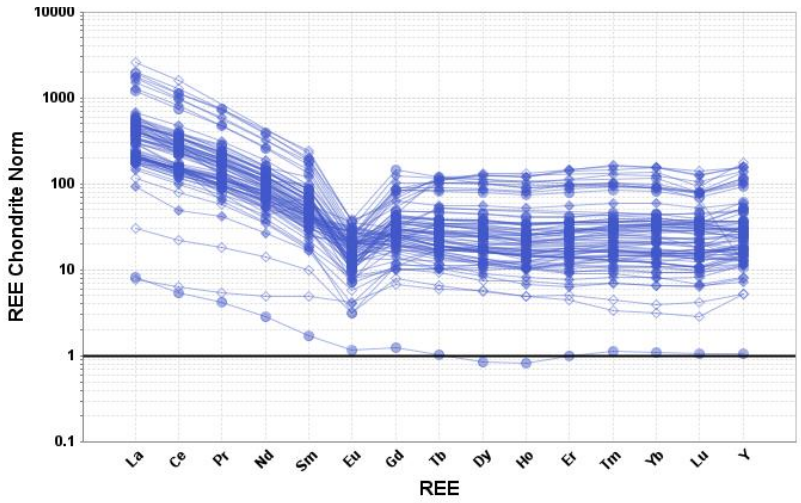

FIGURE 126. REE chondrite-normalized plot for samples from Chess Draw (chondrite values from Taylor and McLennan, 1985). Chemical analyses are in Appendix 4. Closed diamonds=syenite, nepheline syenite, and syenite quartz dikes. Closed circles=phonolite dikes. Open diamonds=altered limestone/skarn.

Chess Draw Drill Data

Three holes were drilled in Chess Draw by U.S. Borax during May and June, 1985 in order to obtain geological information and determine the potential for REE, Nb, Be, Ti, and other selected elements (Fig. 4; Table 2; Appendix 3). Joy Manufacturing used a Joy truck-mounted core rig to drill NX (2-1/8-inch diameter) holes, except the lower portion of C-3 was reduced to BX (1-5/8 inch diameter) at 455 ft due to drilling difficulties. The remaining drill core is arcived at the NMBGMR core facility.

Drill hole C-1 was located near a syenite dike near the augite-bearing syenite intrusion (PEas). Drill hole C-2 was located to intercept a series of northeast-trending altered syenite dikes. Drill hole C-3 was located near the phonolite plug. Chemical analyses and core logging confirmed U.S. Borax's conclusions that there is little or no economic potential indicated in these drill holes for REE, Nb, Be, Ti, and other selected elements. Much of the drill core is altered (Appendix 2). However, some of the best preserved unaltered samples of the volcanic breccia dikes are exposed in the drill core. But the Chess Draw economic potential is deeper than their holes were drilled to as discussed in another section.

The geochemical analyses indicate high correlations between total REE, Nb, Be, Th, and Zr (Table 24, 25), similar to surface samples. Note the lack of correlation of these elements with F (Table 24, 25; Fig. 127, 128). The samples exhibit similar light-REE enriched chondrite normalized plots as other samples in the Cornudas Mountains (Fig. 128). Downhole profiles indicate no increase in trace elements with depth (Fig. 129), but suggest certain zones are more enriched in these elements than others, typically in dikes and altered areas.

These correlations are similar to correlations found in other data sets from the Cornudas Mountains and are a result of similar minerals containing total REE, Nb, Be, Th, and Zr. The lack of correlation with F is consistent with these minerals being magmatic in origin and not hydrothermal.

TABLE 24. Summary statistics of chemical analyses from Chess Draw drill holes (C-1, C-2, C-3).

	Ti	F	Be	Nb	Sc	Th	U	Zr	Total REE
Count	68	68	66	68	68	68	68	68	68
Minimum	100	100	1	6	0.22	0.25	0.1	23	2.5
Maximum	9200	20000	14	430	13.5	64.1	19	2000	537
Mean	2325	1276	3.7	108	4.4	14.2	2.1	529	224
Median	2300	670	4.0	100.0	3.5	12.0	0.9	510.0	257.1
Standard Deviation	1495	2982	2.9	103	3.4	13.6	3.4	449	143

TABLE 25. Pearson correlation coefficients of chemical analyses from Chess Draw drill holes (C-1, C-2, C-3). Number of samples=68 (Table). Highlighted values indicate significant correlations.

	Ti	F	Be	Nb	Sc	Th	U	Zr	Total REE
Ti	1.0								
F	-0.0031	1.0							
Be	0.098	-0.13	1.0						
Nb	0.26	-0.13	0.8	1.0					
Sc	0.26	0.074	-0.31	-0.43	1.0				
Th	0.1	-0.093	0.84	0.91	-0.29	1.0			
U	-0.093	0.18	-0.19	-0.12	-0.0015	-0.071	1.0		
Zr	0.22	-0.13	0.82	0.97	-0.4	0.91	-0.11	1.0	
Total REE	0.51	-0.16	0.73	0.92	-0.21	0.81	-0.18	0.9	1.0

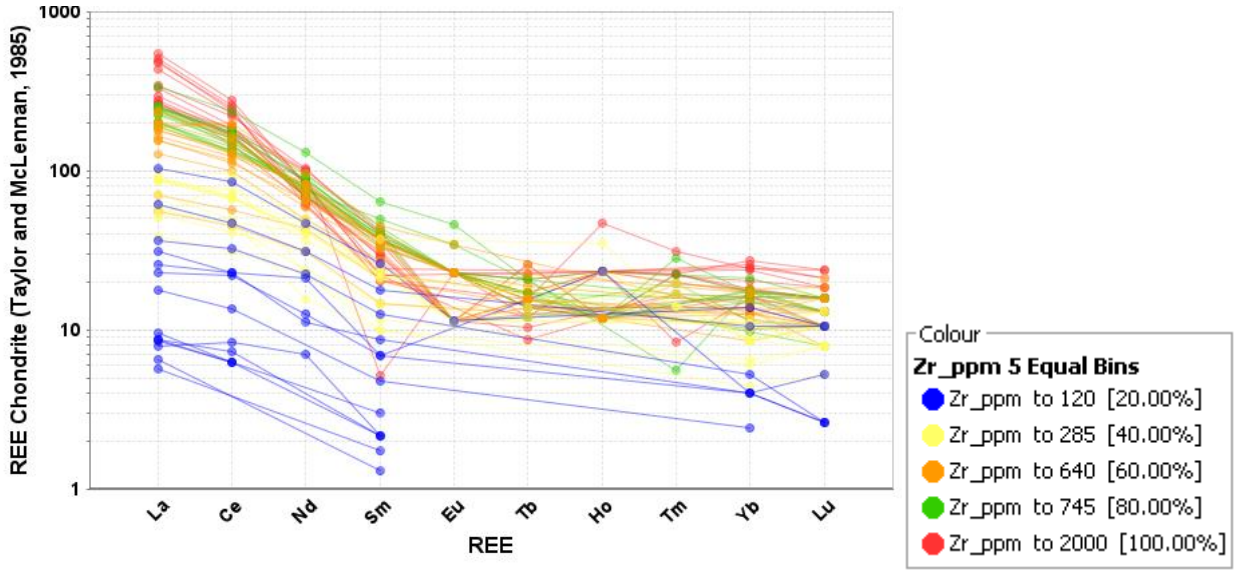

FIGURE 127. REE chondrite normalized plot of Chess Draw drill hole samples (C-1, C-2, C-3; chondrite values from Taylor and McLennan, 1985). The colors reflect concentrations of Zr (ppm). Note that the higher REE samples also have higher Zr.

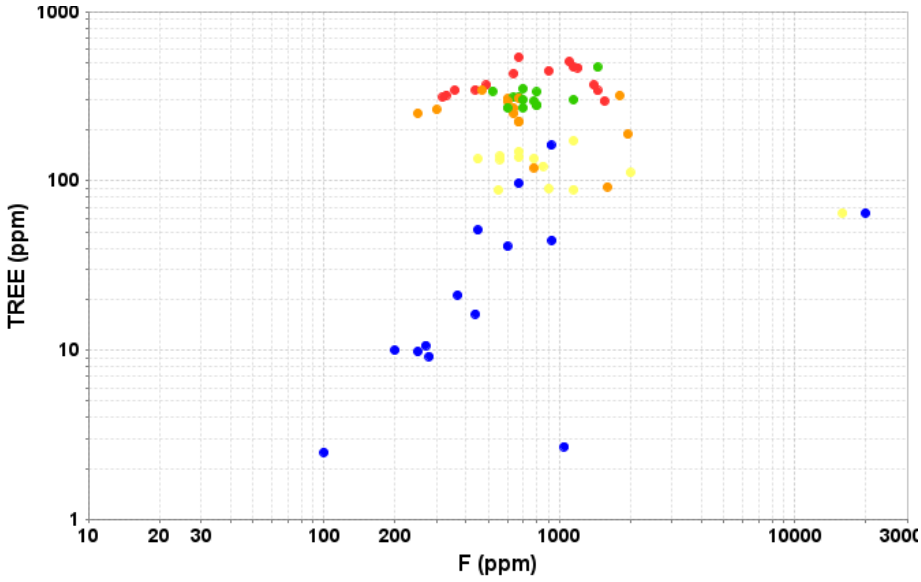

FIGURE 128. Total REE vs. F plot of Chess Draw drill hole samples (C-1, C-2, C-3). The colors reflect concentrations of Zr (ppm) (legend in Fig. 127). Note that the higher REE samples also have higher Zr.

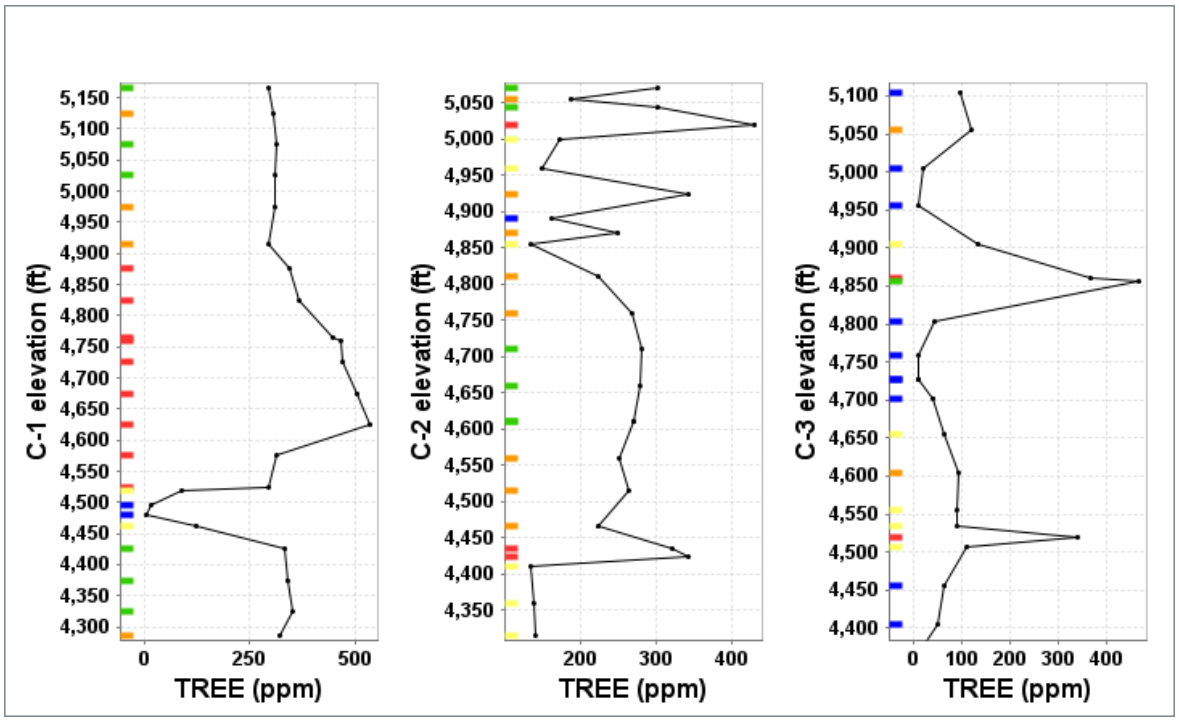

FIGURE 129. Downhole profile showing concentrations of total REE for Chess Draw drill holes. The colored bars reflect concentrations of Zr (ppm) (legend in Fig. 127).

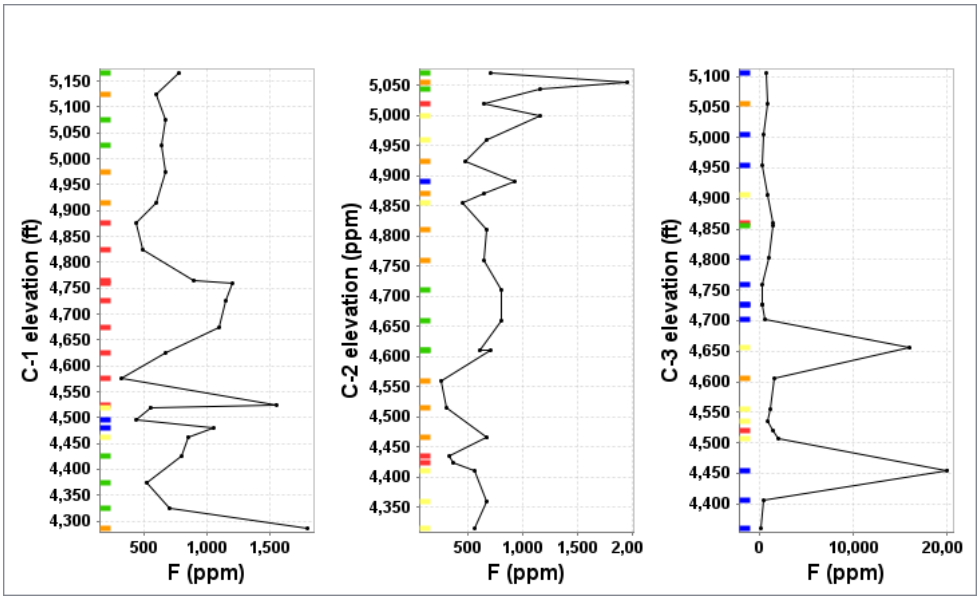

FIGURE 130. Downhole profile showing concentrations of F for Chess Draw drill holes. The colored bars reflect concentrations of Zr (ppm) (legend in Fig. 127).

Prospects in McVeigh Hills

Two shallow prospect pits were found in the altered Hueco limestones in the McVeigh Hills (NMOt0436, NMOt0438). Fractures zones and lenses consist of iron oxides, calcite, and recrystallized limestones in the vicinity of syenite, nepheline syenite, and quartz syenite. Nine samples from the McVeigh Hills ranged from 11 to 480 ppm total REE, 17-1525 ppm Zr, 3-229 ppm Nb, and 120-1130 ppm F. Although the total REE is low in these samples (Fig. 131), hydrothermal fluids from a deeper source may have altered the rocks and more enriched REE-bearing source could be at depth. More sampling and mapping, and ultimately drilling is recommended to assess the economic potential for total REE-bearing zones.

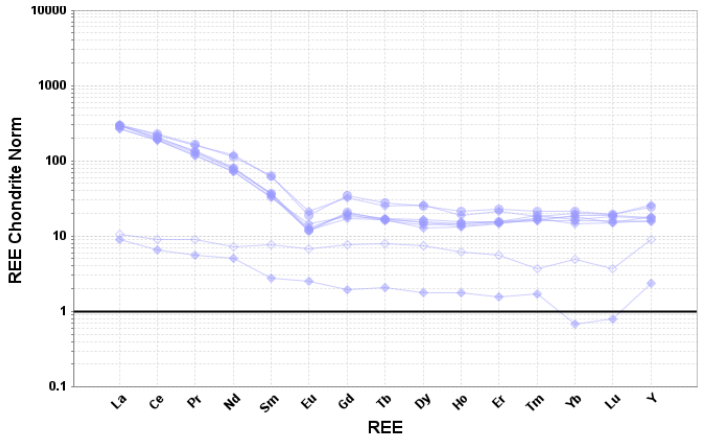

FIGURE 131. REE chondrite normalized plot of samples from McVeigh Hills (chondrite values from Taylor and McLennan, 1985). Open diamonds=altered limestones. Closed diamonds=syenite, nepheline syenite, and syenite quartz dikes. Closed circles=phonolite dikes.

$^{40}Ar/^{39}Ar$ GEOCHRONOLGY RESULTS

Prior to this study, only six of the intrusions had been dated, focusing on Wind Mountain and intrusions in Chess Draw. Only one of the ages used high precision $^{40}Ar/^{39}Ar$ geochronology. These data show a range of ages from 38.6-31.6 Ma (Table 26, 27).

To better understand the emplacement history of the Cornudas Mountains, 21 different intrusions were dated using the $^{40}Ar/^{39}Ar$ dating method (Table 27). Figure 132 shows a summary of the new $^{40}Ar/^{39}Ar$ ages compared to the range of ages from McLemore (2018) and Baker, et al. (1977). All new geochronology figures (spectra, isochron) and tables can be found in Appendix 7. In total, 27 samples were dated, some with two aliquots, and they display a range of spectra complexities from alteration or ^{40}Ar loss, excess ^{40}Ar and/or ^{39}Ar recoil. Two samples (CORN20-24-11.5m and CORN804) did not provide meaningful ages and were dominated by discordant spectra and isochrons dominated by excess ^{40}Ar and were resampled.

TABLE 26. Previous K-Ar and $^{40}Ar/^{39}Ar$ dating results.

Intrusion	Age (Ma)	Method		Source
Augite Syenite	35.0 ± 1.1	K-Ar		Barker et al. 1977
Deer Mtn	31.6 ± 0.9	K-Ar		Barker et al. 1977
Deer Mtn	33.0 ± 1.4	K-Ar		McLemore, 2018
Alamo Mtn	36.0 ± 1.1	K-Ar		Barker et al. 1977
Alamo Mtn	36.8 ± 0.6	K-Ar		McLemore, 2018
Cornudas Mtn	33.9 ± 1.0	K-Ar		Barker et al. 1977
Cornudas Mtn	34.6 ± 1.5	K-Ar		McLemore, 2018
Wind Mtn	36.32 ± 0.15	$^{40}Ar/^{39}Ar$		McLemore, 2018
Unnamed Hill	36.8 ± 0.6	K-Ar		McLemore, 2018

All ages are considered to be minimum emplacement ages as textural and field relationships do not suggest any of the igneous rocks were erupted subaerially. Some of the intrusions were dated using multiple materials (biotite, amphibole and groundmass concentrate) to assess cooling history that may be present because of closure temperature differences between mineral phases. Deer Mountain (CORN2000) was the only intrusion that produced meaningful ages on two mineral phases (amphibole (36.67±0.04 Ma) and biotite (36.71±0.05 Ma). Both ages are indistinguishable and suggest rapid cooling of the intrusion. We were not able to assess mineral pair cooling or reheating histories in any other intrusion, because the pairs were not present or one phase did not provide an acceptable age. Wind Mountain was the only intrusion where all four phase were dated and required multiple samples to produce a preferred age (CORN20-24-11.5m, biotite and amphibole and CORN814, amphibole and groundmass). The best age for Wind Mountain that we could determine is 37.14±0.65 Ma, which does not overlap at 2σ with the previous $^{40}Ar^{39}Ar$ age from Wind Mountain 36.32±0.15 Ma (McLemore, 2018). We still consider the McLemore (2018) age of Wind Mountain to be the best possible age because our samples appear to contain excess argon.

Biotite (36.52±0.93 Ma) and groundmass (31.07±0.16 Ma) were extracted and dated from Alamo Mountain and only the groundmass produced an acceptable age. Barker (1977) suggest that all biotite in the Cornudas Mountains are xenocrystic and the old and scatter biotite from Alamo Mountain may exhibit inherited ^{40}Ar. Amphibole and groundmass were dated from Black Mountain and only the groundmass sample produced an acceptable age (26.95±0.04 Ma).

The amphibole age was considerable older and had a discordant spectra. Electron microprobe analysis of this sample showed that the sample was predominantly arfvedsonite and contained little potassium. Flat Top has the same issue as Black Mountain and only the groundmass sample produced a preferred age (28.49±0.35 Ma).

The majority of the samples only contained one viable phase to target for $^{40}Ar^{39}Ar$ dating. Groundmass concentrates produced the most accepted ages (14 of 21), followed by biotite (5 of 21) and amphibole (2 of 21). Groundmass samples predominantly had climbing spectra for the first few steps and then stabilized at a plateau. This can be because of ^{40}Ar loss because of alteration or could be because of slow cooling of the intrusions. This shape of spectra is common for laccoliths, sills and dikes hinting that it could be an alteration or reheating events and not slow cooling. CORN117 (Dike East of Float Top, 32.48±0.03 Ma), CORN226 (McVeigh Hills, 34.96±0.07 Ma) and CORN4002 (Alamo Mountain) are the only samples that appear to have ^{39}Ar recoil (young first few steps followed by older steps and then a slightly younger plateau). This was not expected because all of the groundmass samples are sieved to the same grain-size. One ground mass sample, CORN4019 (Sill West of Cornudas, 36.46±0.04 Ma) contained excess ^{40}Ar. Both aliquots of CORN4019 had a distinctive "saddle shaped" spectra (old low wattage steps that get younger at middle wattage steps and then progressively get older at high wattage steps) (Kelley, 2002).

Biotite samples were the most complex and varied from some samples producing considerably old ages (i.e. CORN20-24-11.5m). Biotite samples CORN112 (Cornudas Mountain, 35.77±0.07 Ma), CORN177 (South Chess Draw Dike, 35.93±.0.06 Ma) and CORN4015 (Chattfield Mountain, 36.80±0.04 Ma) produced the highest precision ages. CORN177 had a "saddle shaped" spectra typical of excess ^{40}Ar. CORN4015 forms a nice plateau and only the last two fusion steps (L and M) appear to contain excess ^{40}Ar. CORN112 has the same shape but does not form a plateau. CORN4005 ("Lil' Windy", 36.98±0.03 Ma) has a low first step (argon loss) followed by a rising spectra until high wattage steps (J and K) and then become discordant. CORN20-10 (35.93±0.06 Ma) has three young steps (argon loss) followed by a plateau before becoming discordant.

Amphiboles were the most difficult to date because they contained the lowest concentration of potassium. Deer Mountain produced the best amphibole age (36.67±0.04) with a near perfectly flat spectra (10 of 14 step). The Wind Mountain sample (CORN814) showed young low wattage steps (argon loss) followed by a pseudo-plateau that comprised of nearly 50% of the spectra before becoming discordant. The isochron age is the lowest precision accepted age out of all of the samples (37.14±0.65 Ma).

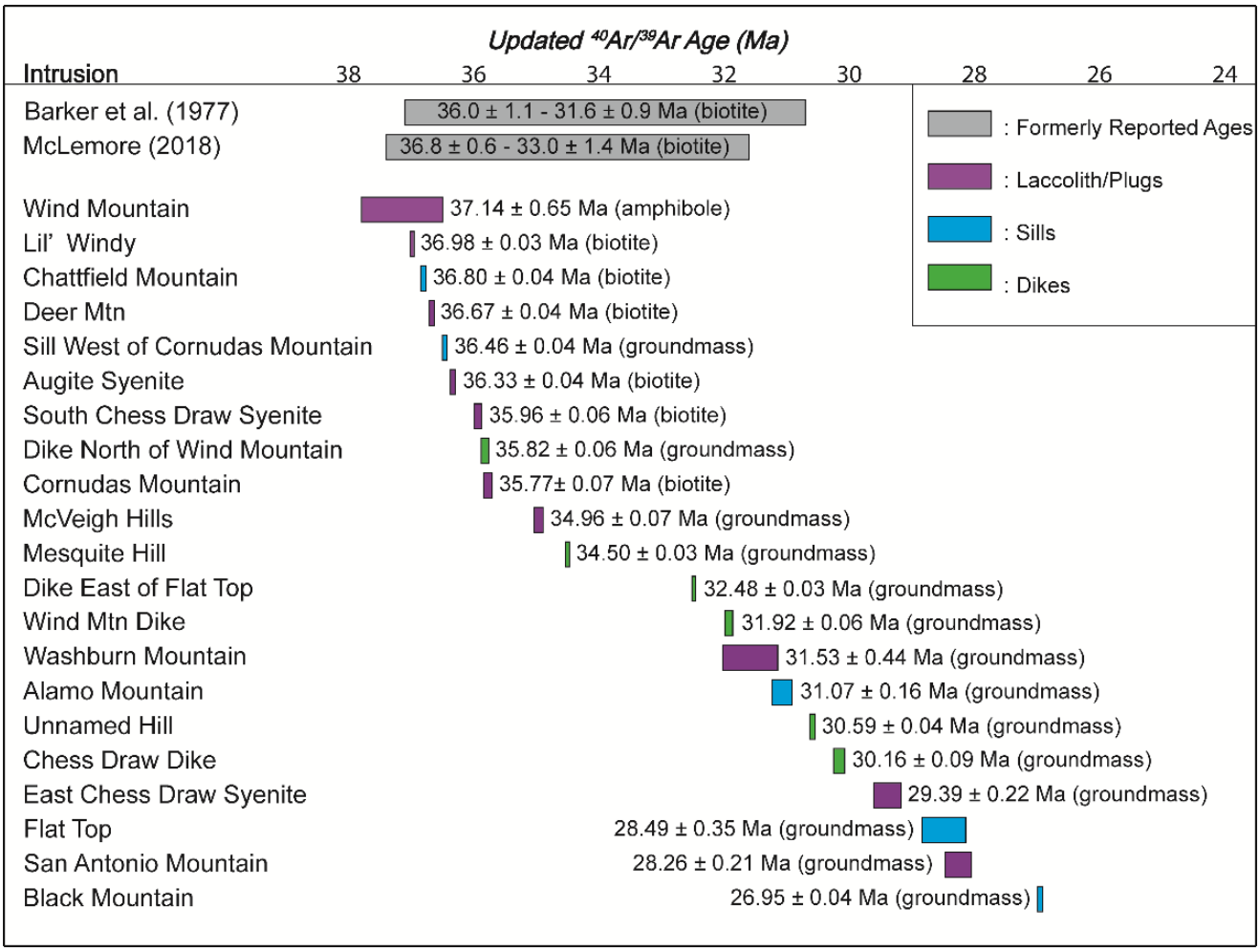

FIGURE 132. Summary view of new $^{40}Ar/^{39}Ar$ data (colored bars) and published data (gray bars from Barker et al, 1977 and McLemore, 2018). The length of the bar represents the precision of the age. Most intrusions do not overlap in time and there is no spatial or temporal relationship in the timing and type of intrusion for the Cornudas Mountains in New Mexico.

TABLE 27. $^{40}Ar/^{39}Ar$ ages from the Cornudas Mountains.

Sample	Unit	Material	Age Type	N	MSWD	Age (Ma)	±2σ	Comments
CORN2000	Deer Mtn.	Amphibole	Plateau	10/14	1.8	36.67	0.04	
CORN112	Cornudas Mtn.	Biotite	Isochron	8/12	467.6	35.77	0.07	High MSWD indicates excess ^{40}Ar
CORN805	Wind Mtn. Dike	Groundmass	Plateau	5/10	2.6	31.92	0.06	High MSWD from argon loss in first few steps
CORN814	Wind Mtn.	Amphibole	Isochron	12/14	2.8	37.14	0.65	High MSWD from argon loss in first few steps
CORN4005	Lil' Windy	Biotite	Isochron	12/12	34.7	36.98	0.03	High MSWD
CORN4006	Unnamed Hill	Groundmass	Isochron	10/10	90.0	30.59	0.04	High MSWD from argon loss in first few steps
CORN4007	Phonolite Dike	Groundmass	Plateau	7/10	0.9	30.16	0.09	

Sample	Unit	Material	Age Type	N	MSWD	Age (Ma)	±2σ	Comments
CORN4008	Mesquite Hill	Groundmass	Isochron	10/10	28.9	34.50	0.03	High MSWD indicates excess ^{40}Ar
CORN4002	Alamo Mtn.	Groundmass	Plateau	5/10	1.9	31.07	0.16	High MSWD from argon loss in first few steps and scatter due to recoil
CORN177	Augite Syenite	Biotite	Plateau	4/13	0.0	36.33	0.04	Contains excess 40Ar
CORN20-10	S. Chess Draw Dike	Biotite	Plateau	5/13	2.1	35.93	0.06	High MSWD from argon loss in first few steps
CORN4015	Chatfield Mtn.	Biotite	Plateau	9/13	0.6	36.80	0.04	Contains excess 40Ar
CORN4019	Sill W. of Cornudas	Groundmass	Isochron	10/10	108.4	36.46	0.04	High MSWD and spectra shape indicates excess ^{40}Ar
CORN79	E. Chest Draw Dike	Groundmass	Plateau	6/10	2.0	29.39	0.22	Argon loss in first few steps
CORN117	Dike E. of Flat Top	Groundmass	Plateau	6/10	0.9	32.48	0.03	High MSWD from argon loss in first few steps and scatter due to recoil
CORN181	Dike N. of Wind Mtn.	Groundmass	Isochron	6/10	26.4	35.82	0.06	High MSWD from argon loss in first few steps
CND-208	Washburn Mtn.	Groundmass	Isochron	9/10	30.5	31.53	0.44	Climbing spectra and short plateau
CORN226	McVeigh Hills	Groundmass	Plateau	4/10	2.5	34.96	0.07	High MSWD from argon loss in first few steps and scatter due to recoil
CORN4004	Flat Top	Groundmass	Plateau	4/10	1.9	28.49	0.35	
CORN4011	Black Mtn.	Groundmass	Plateau	3/10	1.6	26.95	0.04	Argon loss in first few steps
CORN4013	San Antonio	Groundmass	Plateau	4/10	1.5	28.26	0.21	Argon loss in first few steps

REE-Zr-Nb MINERALOGY

Several minerals in the Cornudas Mountains host REE, Zr, and Nb (Table 28). In addition, trace amounts of galena, sphalerite, and molybdenite are found in the Cornudas Mountains, however, these minerals are not of economic concentrations in the Cornudas Mountains. Rheniite (ReS_2) was tentatively identified by electron microprobe (WDS) but requires additional verification. Rhenium (Re) is a critical mineral, typically found associated with molybdenite.

The predominant REE-Zr mineral in the Cornudas Mountains is eudialyte, which is found as red to pink to red-brown disseminations, cavity fillings, and veins in nepheline syenite, phonolite, skarns and altered limestones in the Wind Mountain and Chess Draw areas (Fig. 94, 119, Appendix 8). Eudialyte is Greek meaning *well decomposable*, referring to high solubility with acid. Eudialyte is a group of minerals (Johnsen et al., 2003) and three species have been identified at Wind Mountain and Chess Draw: aqualite, maganoeudialyte, and sergevanite (Table 28). A eudialyte concentrate can be obtained by magnetic or flotation techniques (Vaccarezza and Anderson, 2019). REE can be recovered from eudialyte concentrates by acid leaching (Ma et al., 2019; Vaccarezza and Anderson, 2019).

Catapleiite is a red-brown hydrated zirconosilicate that also contains REE. It forms a solid solution series with calciocatapleiite, both of which have been found at Wind Mountain (Table 28, Appendix 8). Catapleiite is a dimorph of gaidonnayite (also reported at Wind Mountain). Catapleiite can be separated along with eudialyte by magnetic or flotation techniques (Silin et al., 2022).

Fine-grained REE fluoro-carbonate minerals, predominantly bastnäsite-(Ce) with minor parisite-(Ce) are found disseminated in nepheline syenite at Wind Mountain (Table 28, Appendix 8). Other REE-bearing minerals found in the Wind Mountain and Chess Draw areas include monazite, xenotime, vitusite, and zircon. Metallurgical testing is required to determine if these minerals can be easily separated.

The only Be mineral found in the Cornudas Mountains is epididmite. Be is a light element and difficult to identify by electron microprobe. The highest concentration of Be is 147 ppm (Appendix 4). Even though early exploration for Be occurred in the Cornudas Mountains, there is no evidence of economic concentrations in the area.

TABLE 28. REE-Zr-Nb minerals found in the Cornudas Mountains. *Confirmed by NMBGMR thin section, XRD (Appendix 6) or electron microprobe (Appendix 8). Additional references include Tschernich (1992) and DeMark (1989). na=not analyzed

Mineral	Occurrence	Chemical formulae	Approximate amount of total REE (wt%)	Reference
*Aqualite (Eudialyte group)	Skarn north of Wind Mountain (CORN104)	$(H_3O)_8(Na,K,Sr)_5Ca_6Zr_3Si_{26}O_{66})(OH)_9Cl$	9	This study
*Bastnäsite	Hexagonal crystals, disseminated in nepheline syenite	$(Ce,La)(CO_3)F$	66	This study
Brockite	Vugs in nepheline syenite	$(Ca,Th,Ce)PO_4 \cdot H_2O$	6	Mindat.Org

Mineral	Occurrence	Chemical formulae	Approximate amount of total REE (wt%)	Reference
*Catapleiite (calciocatapleiite)	Miarolitic cavities, platy to tabular, disseminated in nepheline syenite	$Na_2Zr(Si_3O_9)$ •$2H_2O$	2	Boggs (1985)
Elpidite	Prismatic, in miarolitic cavities	$Na_2ZrSi_6O_{15}$•$3H_2O$	na	Michayluk and Cone (2017b)
Epididmite	Psuedohexagonal plates	$Na_2Be_2Si_6O_{15}$•H2O	na	Michayluk and Cone (2017b)
*Eudialyte	Dikes, sills, and laccoliths and in miarolitic cavities	$Na_4(Ca, Ce)_2(Fe^{2+}, Mn^{2+})$ $YZrSi_8O_{22}(OH,Cl)_2$	9	Barker and Hodges (1977), Clabaugh (1950), Boggs (1985, 1987)
*Fluorite	Breccia, skarns	CaF_2	?	Barker et al. (1977), Schreiner (1994)
Gaidonnayite	Miarolitic cavities	$Na_2Zr(Si_3O_9)$ •$2H_2O$	?	Michayluk and Cone (2017b)
*Galena	Dikes, nepheline syenite Wind Mountain	PbS	na	Schreiner (1994), this study
*Georgechaoite	Miarolitic cavities, coatings on microcline or acmite, from south side of Wind Mountain	$NaKZrSi_3O_9$•$2H_2O$	na	Boggs (1985), Boggs and Ghose (1985)
*Hydroxy-manganopyrochlore	Phonolite dike	$(Mn^{2+},Th,Na,Ca,REE)_2(Nb,Ti)_2O_6($ OH)	na	This study
*Lueshite	Phonolite dike	$NaNbO_3$	na	This study
*Maganoeudialyte	Skarn east of Wind Mountain (CORN108), nepheline syenite Wind Mountain	$Na_{14}Ca_6Mn_3Zr_3[Si_{26}O_{72}(OH)_2](H_2$ O,Cl,O,OH)$_6$	9	This study
*Molybdenite	Disseminated in nepheline syenite	MoS_2	na	Michayluk and Cone (2017a)
*Monazite	Miarolitic cavities, disseminated in nepheline syenite, skarns	Ce, La, Nd(PO_4)	65	Boggs (1985)
Niobian rutile	Vugs, miarolitic cavities	$(Ti,Nb)O_2$	na	Schreiner (1994)
*Oxynatropyrochlore (Pyrochlore group)	skarn	$(Na,Ca,U)_2Nb_2O_6(O,OH)$	na	This study
Parakeldyshite	Nepheline syenite, Wind Mountain	$Na_2ZrSi_2O_7$	na	McLemore et al. (1996a)
*Parasite-Ce	Disseminated nepheline syenite	$CaCe_2(CO_3)_3F_2$	61	Michayluk and Cone (2017b)

Mineral	Occurrence	Chemical formulae	Approximate amount of total REE (wt%)	Reference
*Pyrite	Within mineral aggregates of ferromagnesian minerals in syenite dike and skarn in Chess Draw, Wind Mountain nepheline syenite	FeS_2	na	Schreiner (1994), McLemore et al. (1996a), this study
*Pyrochlore	Nepheline syenite	$(Na,Ca)_2Nb_2O_6(OH,F)$	na	This study
*Rheniite?	In Wind Mountain nepheline syenite (CORN812)	ReS_2	na	This study, needs confirmation but sample contains 0.002 ppm Re (higher than most)
*Roumaite	In Wind Mountain nepheline syenite (CORN260)	$(Ca,Na,REE)_7(Nb,Ti)[Si_2O_7]_2OF_3$	7-10	This study
*Sergevanite (eudialyte group)	Nepheline syenite	$Na_{15}(Ca_3Mn_3)(Na_2Fe)Zr_3Si_{26}O_{72}(OH)_3 \cdot H_2O$	9	This study
*Sphalerite	Disseminated in Wind Mountain nepheline syenite and dikes	(Zn,Fe)S	na	Schreiner (1994), this study
*Vitusite	Nepheline syenite Wind Mountain	$Na_3(Ce,La,Nd)(PO_4)_2$	34	This study
*Xenotime	Nepheline syenite	$(Y,Th,U,Dy,Yb.Er,Gd)PO_4$	16 (48% Y)	This study
*Zircon	Nepheline syenite, syenite	$ZrSiO_4$	4	Schreiner (1994)

DEPTH OF EMPLACEMENT

Woodard (2023) incorporated whole rock and clinopyroxene chemistry of each intrusion into the clinopyroxene-liquid geothermobarometer (Masotta, 2013) to determine the temperatures and pressures of emplacement. Application of the geothermobarometer to clinopyroxene-whole rock pairs that have equilibrium $^{Fe\text{-}Mg}K_D$ values yields temperatures ranging from 693-996°C (±31°C) and pressures from 1.2-4.0 kb (±1.7 kb). Pairing these depths with the new geochronology, the minimum exhumation rates for intrusions in the Cornudas Mountains can be estimated as 0.2-0.4 mm/yr (Woodard et al., 2022; Woodward, 2023). These emplacements are similar to the emplacement conditions of other, similar large alkaline igneous complexes such as Ilimaussaq and Nechalacho (Konnerup-Madsen and Rose-Hansen, 1984; Markl et al., 2001; Möller and Williams-Jones, 2016). A comparison of the calculated rates of the Cornudas Mountains to standard erosional rates (0.05 mm/yr) and exhumation rates within the nearby Rio Grande Rift (0.4 mm/yr) shows that the calculated rates fall between erosional and Rio Grande Rift rates. This suggests that tectonic forces during Rio Grande Rift extension played a role in exhuming the Cornudas Mountains. Estimating crystallization temperatures and exhumation rates provide additional information to aid in developing a model for the formation of REE deposits. More details are in Woodward (2023).

MINERAL-RESOURCE POTENTIAL

Summary of REE potential in the Cornudas Mountains

Over 470 surface samples (Appendix 4) and 300 drill core samples (Appendix 3) have been collected and chemically analyzed throughout the Cornudas Mountains. The highest sample in total REE (3513 ppm) is from a phonolite dike intruding the Wind Mountain nepheline syenite. All of the samples >800 ppm total REE are from Wind Mountain or Chess Draw (Table 29) from all of the lithologies (Table 30).

TABLE 29. Summary of REE concentrations by area in the Cornudas Mountains, locations shown in Figure 4.

Locality, map unit	Predominant lithology	Form	Range in REE	Mean REE	Number of samples
Wind Mountain, Ensp2	Nepheline syenite to syenite porphyry	Layered laccolith	11-3513	810	230
Chattfield Mountain, Ep	Phonolite	Sill	589-726	683	15
Deer Mountain (Little Wind Mountain), Ens	Nepheline syenite	Laccolith	1-598	305	11
Chess Draw area combined, Es-Os	various	Dikes, sills	12-2539	584	84
Cornudas Mountain, Es	Quartz syenite to syenite	Plug, laccolith, sill	312-495	357	7
McVeigh Hills, Es	Quartz syenite to syenite	Top of a laccolith or sill?	17-480	327	10
Washburn Mountain, PEns	Nepheline syenite	Sill	50-488	353	8
Alamo Mountain, Op	Phonolite	Discordant sheet or sill	434-445	440	2
Flat Top, Op	Phonolite	Sill	197-674	522	7
San Antonio Mountain, PEns	Nepheline syenite	Laccolith	31-545	402	6
Black Mountain, Ons	Nepheline syenite	Sill	458-706	550	17
Total samples			11-3513	699	360

TABLE 30. Summary of REE concentrations by lithology in the Cornudas Mountains.

Predominant lithology	Form	Range in REE	Mean REE	Number of samples
Nepheline syenite	Laccolith	144-3119	810	280
Phonolite	Sill, dike	11-3513	719	50
Syenite	Plug, laccolith, sill	17-2316	472	47
Trachyte	Dike	464-684	554	7
Breccia	Dike	329-2361	1260	5
Skarn	Skarn	21-2540	581	36
Total samples		11-3513	741	425

Total REE, Zr, and Nb are highest in the PEnsp2 portion of the Wind Mountain laccolith (lower unit) and in the Chess Draw area (Fig. 125, 133). The other areas are relatively low in total REE, Zr, and Nb. In addition, Ga, Y, Hf, and Be are relatively high. There is a strong

correlation between total REE and Zr (correlation coefficient 0.85, Fig. 133), Nb (correlation coefficient 0.69), Y (correlation coefficient 0.87), Ga (correlation coefficient 0.64), Be (correlation coefficient 0.51, Fig. 134), Hf (correlation coefficient 0.9; Fig. 135), and MnO (correlation coefficient 0.62, Fig. 136), which is consistent with the predominant mineralogy of eudialyte. There is a strong correlation between Zr and Nb (correlation coefficient 0.66, Fig. 137). Chess Draw samples have higher Nb than Wind Mountain samples, whereas Wind Mountain samples have higher Zr (Fig. 133). The strong correlation between total REE and MnO suggests Mn oxides are associated with the REE minerals.

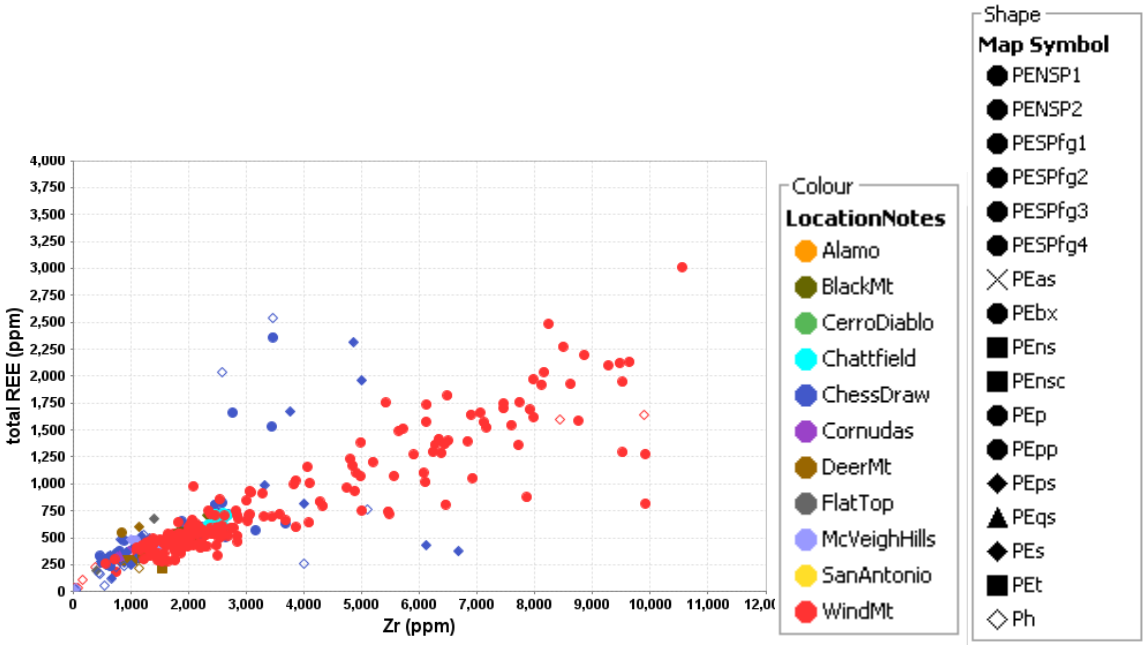

FIGURE 133. Total REE vs Zr (all samples), showing a strong correlation, which is consistent with the predominate mineralogy of eudialyte.

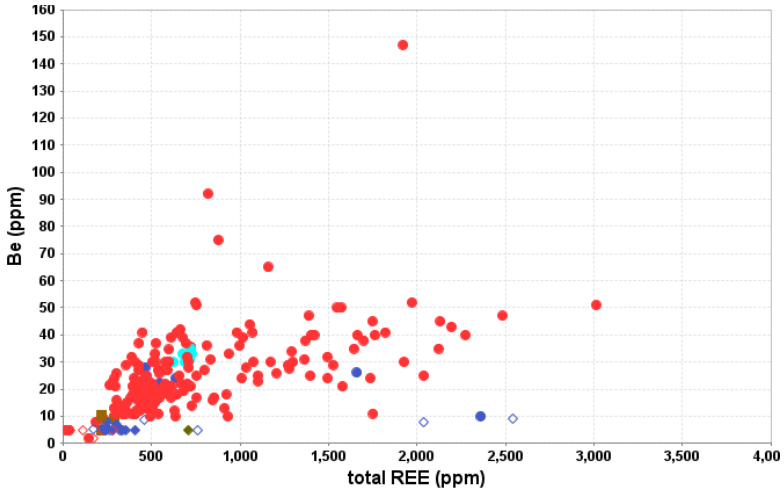

FIGURE 134. Be vs total REE for all samples. Legend in Figure 133.

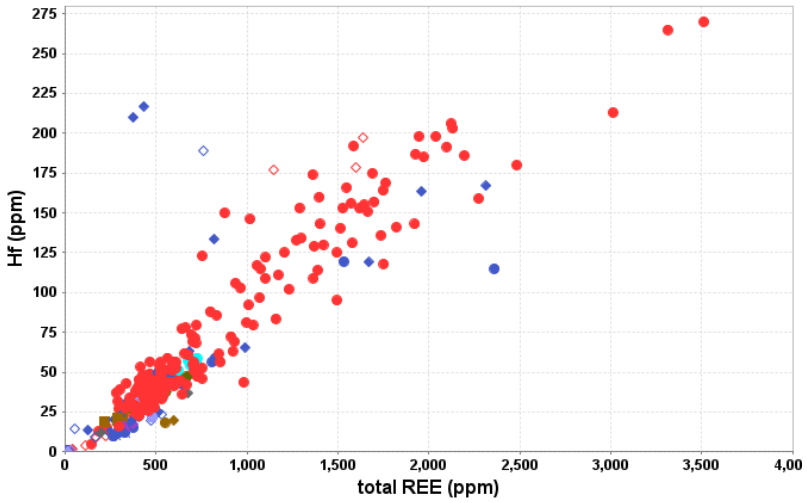

FIGURE 135. Hf vs total REE for all samples. Legend in Figure 133.

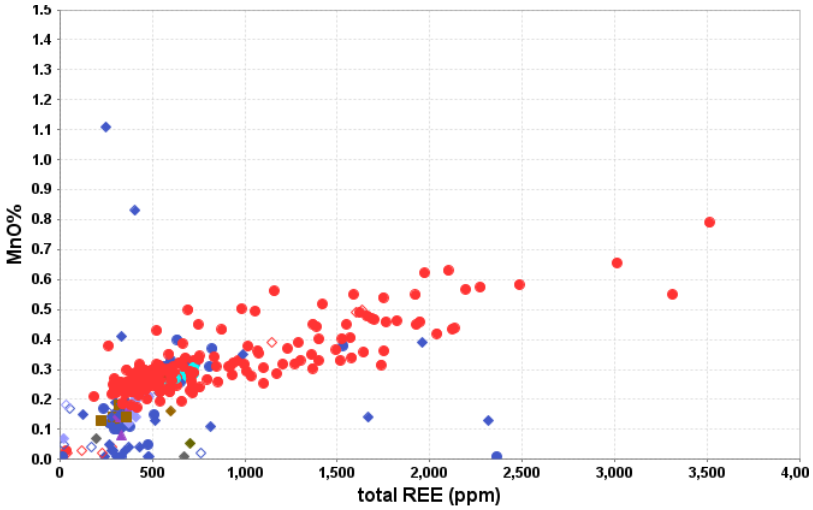

FIGURE 136. MnO vs. total REE for all samples. Legend in Figure 133

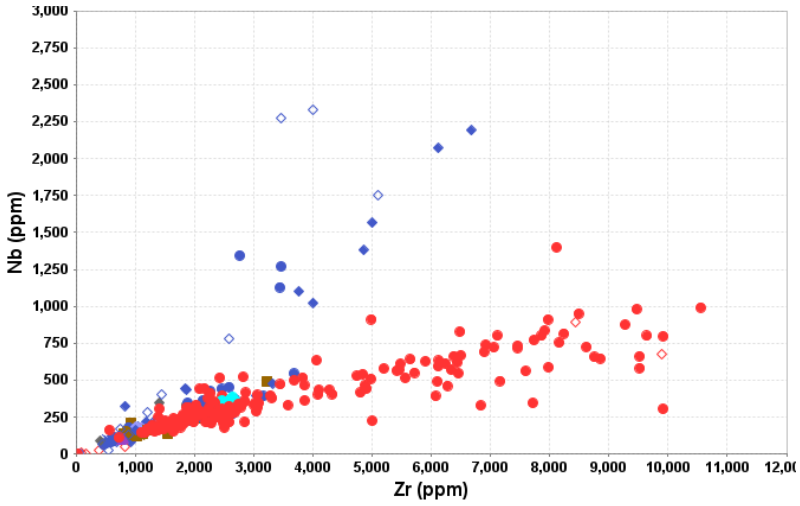

FIGURE 137. Nb vs Zr for all samples (correlation coefficient 0.66). Legend in Figure 133.

REE Potential in Wind Mountain

REE, Zr, and Nb potential is within the basal unit (PEnsp2) of Wind Mountain laccolith (Fig. 138, 139, 140). It is possible that the REE potential is only along the contact between the limestone and the basal unit (PEnsp2) of the Wind Mountain laccolith (PEnsp2). REE are found in eudialyte, zircon, monazite, bastnäsite, calciocatapleiite, vitusite, roumaite, and xenotime in nepheline syenite, phonolite dikes, and skarns. Additional sampling and drilling is needed to determine if the highest potential is along the contact or how far into the PEnsp2 unit. None of the other intrusions, outside of Chess Draw and Wind Mountain, have elevated REE, Zr or Nb. Eudialyte and other REE-bearing minerals could be concentrated using magnetic separation and provide a mineral concentration where REE could be leached.

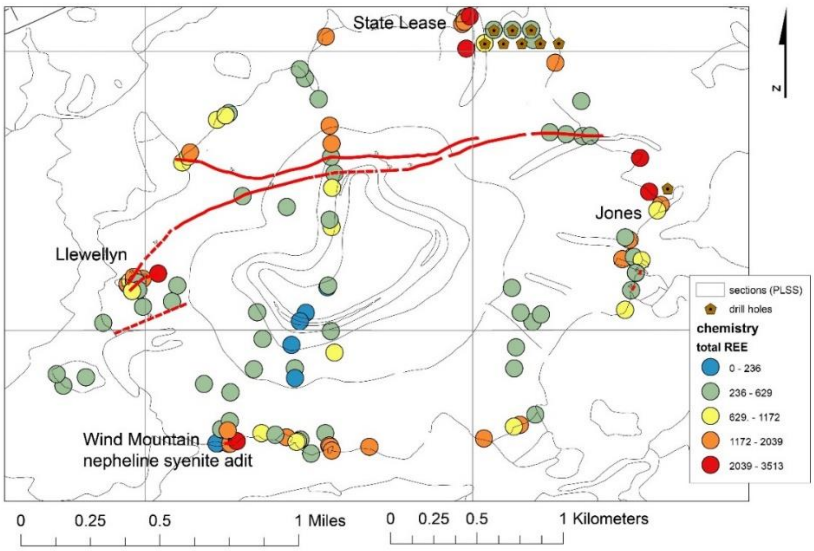

FIGURE 138. Map of Wind Mountain, showing spatial distribution of total REE. See Plate 1 for description of geology (gray lines). Red line=phonolite dike.

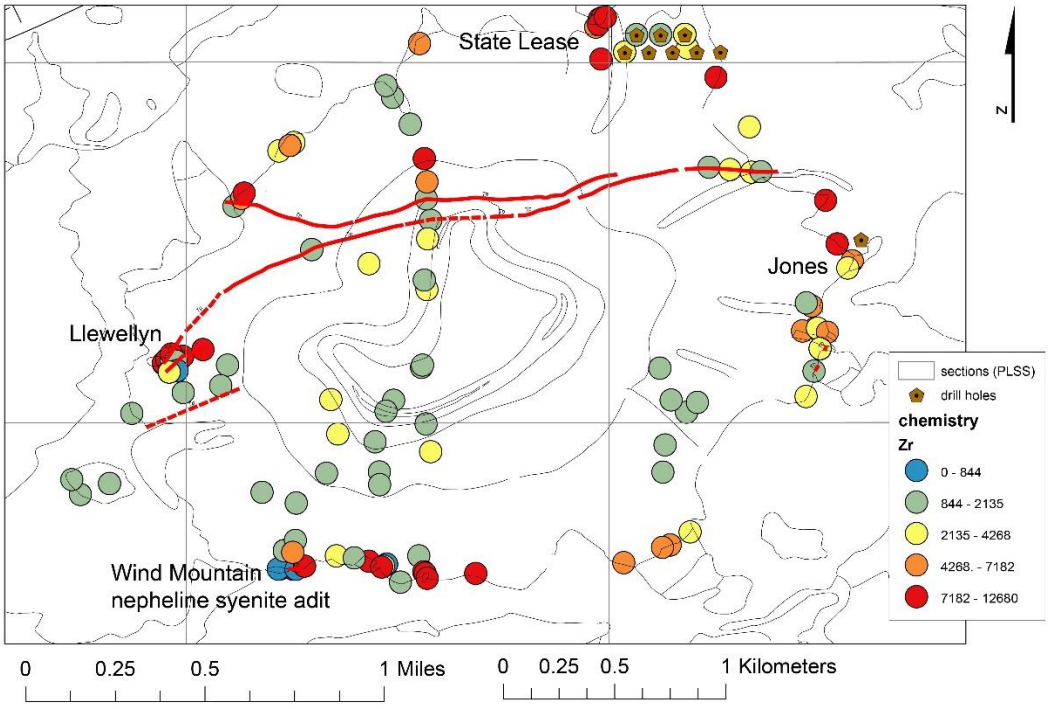

FIGURE 139. Map of Wind Mountain, showing spatial distribution of Zr. See Plate 1 for description of geology (gray lines). Red line=phonolite dike.

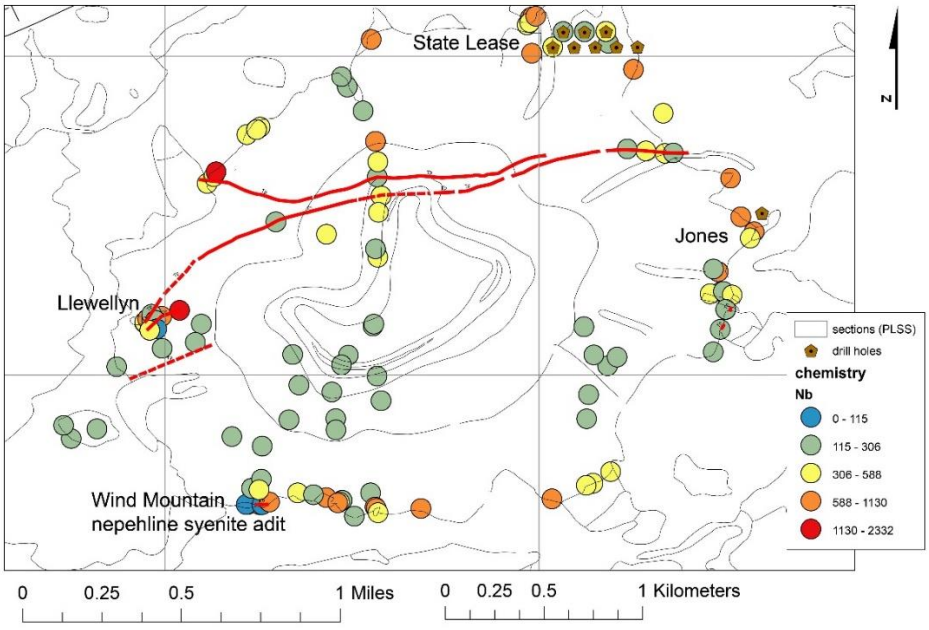

FIGURE 140. Map of Wind Mountain, showing spatial distribution of Nb. See Plate 1 for description of geology (gray lines). Red line=phonolite dike.

REE Potential in Chess Draw

New mapping and geochemical sampling in Chess Draw (Fig. 82, Plate 1) indicates the aeromagnetic anomalies could be the top of syenite and phonolite intrusions, possibly as sills, laccoliths, or plugs. The REE, Zr, and Nb potential in phonolite and breccia dikes in Chess Draw is high (Fig. 141, 142, 143; but drilling is required to locate specific areas of economic potential. The potential economic deposit is likely at depth.

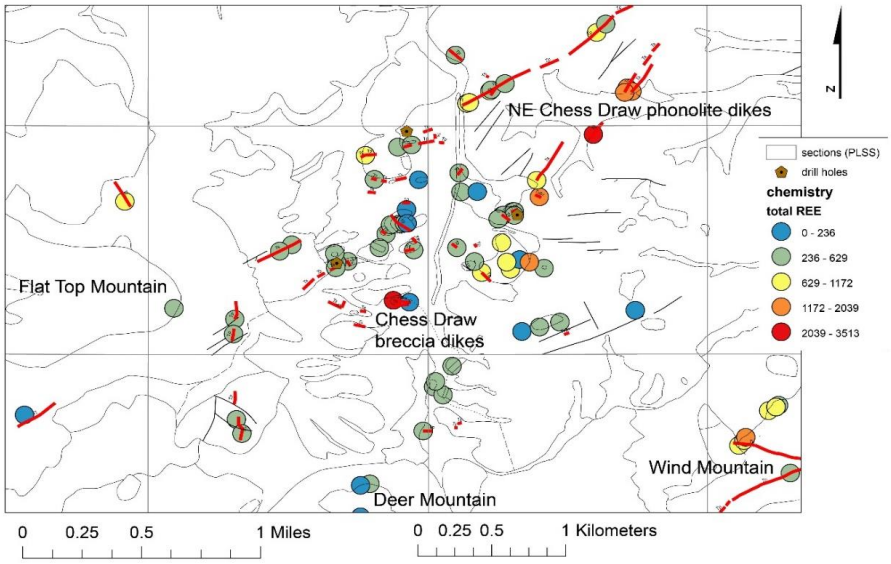

FIGURE 141. Map of Chess Draw area, showing spatial distribution of total REE. See Plate 1 for description of geology (gray lines). Red line=dikes.

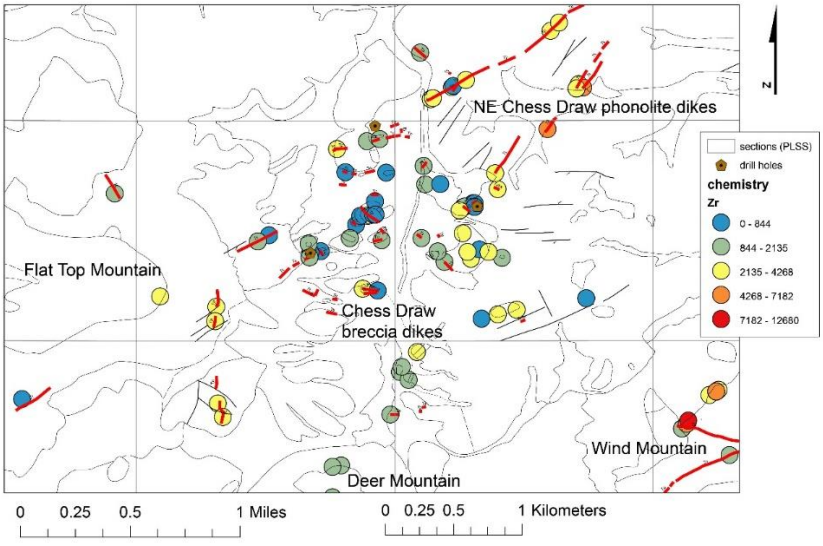

FIGURE 142. Map of Chess Draw area, showing spatial distribution of Zr. See Plate 1 for description of geology (gray lines). Red line=dikes.

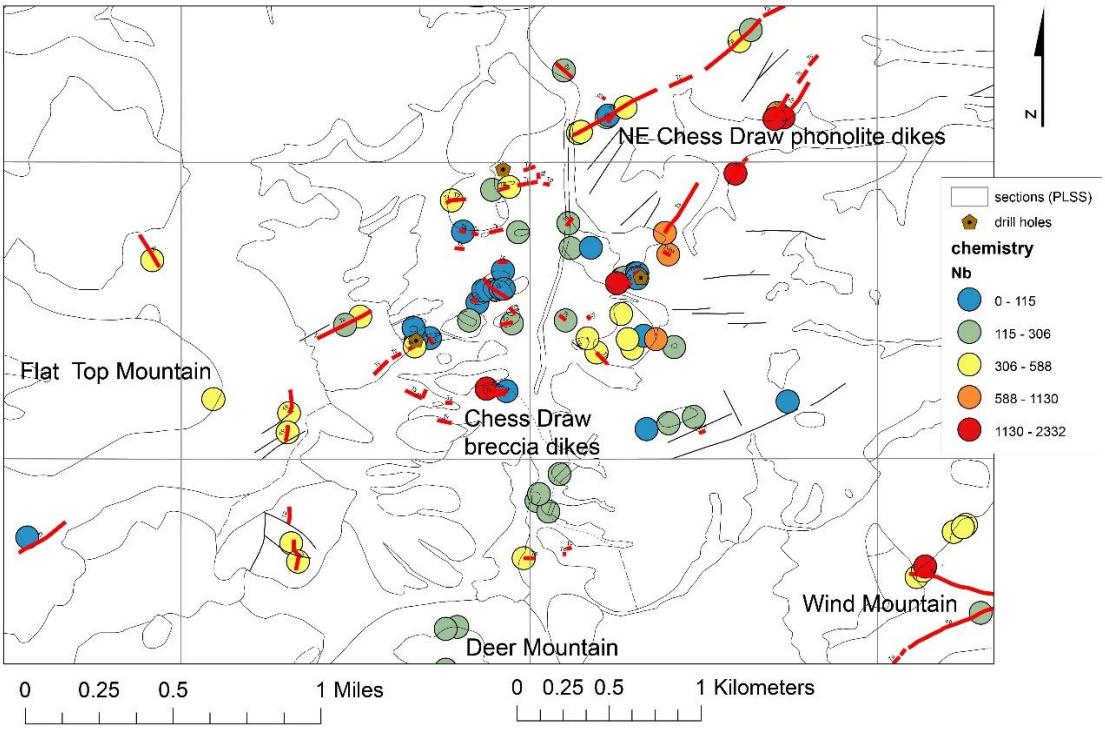

FIGURE 143. Map of Chess Draw area, showing spatial distribution of Nb. See Plate 1 for description of geology (gray lines). Red line=dikes.

Comparison of the mineral deposits in the Cornudas Mountains to other REE deposits in New Mexico and elsewhere

REE occurrences are common in the North American Cordilleran alkaline-igneous belt (Fig. 2; McLemore, 2018). Geochronology studies indicate that the Wind Mountain pluton in the Cornudas Mountains is the oldest of the four major REE deposits in New Mexico at 36.6 Ma and the Laughlin Peak district has the youngest igneous rocks at 22.8 Ma (McLemore et al., 2023). Carbonatite dikes are found in the Laughlin Peak area in northern New Mexico (Fig. 2; McLemore, 2015c), where bastnäsite and florencite are the predominant REE minerals. Allanite is the predominant REE mineral in the Capitan Mountains (McLemore and Phillips, 1991; Campbell et al., 1995). Bastnäsite is the predominant REE mineral in the Gallinas Mountains (McLemore et al., 2021). At Round Top Mountain, Sierra Blanca, Texas (Fig. 2, south of the Cornudas Mountains), the predominant REE minerals are bastnäsite, xenotime, and fluocerite (Standard Silver Corp, 2008; Pingitore et al., 2014; Elliott et al., 2017). Carbonatites are found at Villa Ahumada, Chihuahua, Mexico (Nandigam, 2000), but the REE mineralogy is not known. These occurrences reflect the complex magmatic and resulting hydrothermal activity in the North American Cordilleran alkaline-igneous belt.

Two lithologic and chemically distinct groups of igneous rocks are found in the Hueco Mountains on the McGregor Range, southern Otero County; syenite to trachyte and quartz monzonite and rhyolite (New Mexico Bureau of Mines and Mineral Resources, et al., 1998; McLemore, 2002). Alkaline and metaluminous syenite to trachyte stocks, sills, and dikes intruded Paleozoic sedimentary rocks in the northern Hueco Mountains. Only small,

discontinuous skarns and jasperoids that are low in precious and base metals and REE are found adjacent to some intrusions, thereby making the mineral-resource potential low in the McGregor Range (Kness, 1994; New Mexico Bureau of Mines and Mineral Resources, et al., 1998; McLemore, 2002).

Breccia pipes, defined as a cylindrical shaped mass of broken fragments of minerals and rocks cemented together by a fine-grained matrix, are found in many of the North American Cordilleran alkaline-igneous belt containing both gold and REE deposits (McLemore, 2018; McLemore et al., 2021). The more common breccia pipes found in the North American Cordilleran alkaline-igneous belt are intrusive and magmatic-hydrothermal breccia pipes (Sillitoe, 1985). Intrusive breccia pipes are formed directly from the subsurface movement of magmas (Sillitoe, 1985). Magmatic-hydrothermal breccia pipes are formed by the release of hydrothermal fluids from the magma chamber and can include magmatic, meteoric, connate, or ocean waters (Sillitoe, 1985). Mineral deposits are commonly found associated with breccia pipes because of their association with magmas/hydrothermal activity and porous texture, providing pathways for mineralizing fluids to migrate, as well as a providing a host for the deposits. Although breccia pipes have not been found in the Cornudas Mountains, mineralized volcanic breccia dikes are found in the Chess Draw area that could be associated with potential mineralized breccia pipes at depth. Breccia pipes are typically found at the top of magmatic system, similar to that found in Chess Draw. Future exploration should focus on identifying if such mineralized features occur in the area.

The Ilimaussaq Complex is a large Mesoproterozoic alkaline intrusion in southern Greenland that hosts REE, zirconium, niobium, and uranium deposits (Dostal, 2017; Marks and Markl, 2015), with total REE reserves reported as more than 950 Mt (million metric tonnes) (Dostal, 2017). It is mainly composed of syenites and nepheline syenites with minor peralkaline granites (Marks and Markl, 2015). The Ilimaussaq Complex hosts similar minerals as those found in the Cornudas Mountains, such as aegirine, analcime, nepheline, arfvedsonite, eudialyte, and sodalite. The mineralogy and chemical composition is similar to that in the Cornudas Mountains, but the known REE deposits are smaller in the Cornudas Mountains.

Another alkaline complex with known zirconium, REE, and niobium deposits is the Paleoproterozoic Nechalacho Layered Complex (also known as Thor Lake) in the Northwest Territories of Canada, with reported reserves of more than 300 Mt of REE, largely in eudialyte cumulate laters (Dostal, 2017; Möller and Williams-Jones, 2016). The intrusive complex is comprised predominantly of gabbros, granites, quartz syenites, and nepheline syenites, and host minerals such as albite, K-feldspar, nepheline, aegirine, sodalite, and eudialyte (Möller and Williams-Jones, 2016), which are also found in the Cornudas Mountains.

CONCLUSIONS

- $^{40}Ar/^{39}Ar$ geochronology results indicate emplacement in two pulses in the Cornudas Mountains, from 37.14-34.5 and 32.48-26.95 Ma, longer than the previously reported K/Ar ages (36.0-31.6 Ma).
- REE, Zr, and Nb have the highest potential in the Wind Mountain and Chess Draw areas, specifically the PEnsp2 portion of the Wind Mountain laccolith (lower unit), phonolite and breccia dikes, and hydrothermal skarns and altered areas. The spatial distribution of REE, Zr, and Nb is discontinuous and localized. Downhole profiles of chemical analyses of drill core indicate no increase in trace elements with depth, but suggest certain zones are more enriched in these elements than others. Drilling in areas of higher REE, Zr and Nb is required to determine if there are enough concentrations in local REE-Zr-enriched zones for economic development.
- Although the REE of the Wind Mountain and Chess Draw intrusions and altered areas are below normal economic grades (i.e. <5% total REE), some of these minerals could be separated magnetically, producing a potential economic REE concentrate. REE are found in eudialyte, zircon, monazite, bastnäsite, calcio-catapleiite, vitusite, roumaite and xenotime. Eudialyte and other REE-minerals could be concentrated using magnetic separation and provide a mineral concentration where REE could be leached.
- There is a strong correlation between total REE and Zr, Nb, Y, Ga, Be, Hf, Th and MnO, which is consistent with the predominant REE-mineralogy of eudialyte. There is a strong correlation between Zr and Nb. Fluorine is not a major constituent in these mineral deposits, unlike REE deposits at Round Top and in the Gallinas and Capitan Mountains.
- Chess Draw samples have higher Nb than Wind Mountain samples, whereas Wind Mountain samples have higher Zr. Pyrochlore is the predominant Nb mineral and zircon and eudialyte are the predominant Zr minerals.
- New mapping and chemical analyses in Chess Draw indicates that the aeromagnetic anomalies could be the top of syenite and phonolite intrusions, possibly as sills, laccoliths, or plugs. The REE, Zr, and Nb potential in this area is high, but drilling is required.
- None of the other intrusions, outside of Chess Draw and Wind Mountain, have elevated REE (>800 ppm) or Nb, although eudylite is found in the Chattfield sill.
- Calculated emplacement depths of the intrusions are estimated as 1.2-12.3 km, emplacement temperatures range from 693-996°C (±31°C), and pressures from 1.2-4.0 kb (±1.7 kb). The minimum exhumation rates for intrusions in the Cornudas Mountains can be estimated as 0.2-0.4 mm/yr. Calculated rates fall between erosional (0.05 mm/yr) and Rio Grande Rift (0.4 mm/yr) rates, suggesting that tectonic forces at the beginning of Rio Grande Rift extension played a role in exhuming the Cornudas Mountains.

RECOMMENDATIONS FOR FUTURE STUDIES

- Preliminary petrography suggest sodic alteration is present in the Wind Mountain laccolith. Additional petrographic work is needed.
- Abundances and particle size distribution of economic trace minerals should be determined, using other methods not available to this team.
- McVeigh Hills needs to be mapped in detail. New mapping in this study has shown that altered syenite and quartz syenite intrusions are found in drainages and saddles of several areas. Small skarns and altered areas also are found.
- Contacts along the northwestern Wind Mountain also should be mapped in detail. Low aeromagnetic anomalies along the northern Wind Mountain are consistent with skarn mineralization at depth, which could host eudialyte.
- Underground drilling along the AddWest Wind Mountain nepheline syenite adit is recommended to locate additional zones of high total REE in eudialyte, zircon, and other REE-bearing minerals.
- Surface drilling in the vicinity of the aeromagnetic anomalies in Chess Draw and McVeigh Hills is recommended in order to assess the potential. Although samples at the surface are not as elevated in total REE, total REE could increase with depth. The presence of REE-bearing volcanic breccia dikes in Chess Draw suggests a potential for REE-bearing breccia pipes at depth.
- The occurrence of rheniite and roumaite requires confirmation.

ACKNOWLEDGEMENTS

This work is part of ongoing research of the economic geology of mineral resources in New Mexico at NMBGMR, Nelia Dunbar, Director and State Geologist. This study was partially funded by the USGS Earth MRI Cooperative Agreement No. G20AC00170 and student grants from the NMGS and New Mexico Tech Brightstar Scholarship. A special thanks to Bobby Jones, local rancher, for his insight on the access, topography and previous studies of the area, and assistance throughout the field work. Previous mapping by U.S. Borax geologists was helpful in focusing and understanding recent new geologic mapping in Chess Draw. Geochemical analyses by U.S. Borax and Geovic-JS Group geologists provided additional analyses for interpretation. Geovic-JS Group allowed access to their core for logging and sampling and provided additional geochemical analyses. Discussions and field time with USGS geophysicists Mark Bultman and Mark Gettings were invaluable and appreciated. Laura Waters is a member of Mason Woodward's graduate committee and her comments are appreciated. Virgil Lueth and Kesley McNamara performed the XRD analyses. Peter Lyons, Stellah Cherotich, Ernest Brakohiapa, Carmin Vasquez, and other members of the Economic Geology Group at NMBGMR provided technical support. Sarah Bennett and Megan Badonie maintained organization in the laboratory, including archiving the slabs, hand samples, and thin sections. Dave Kasefang, Mark Leo-Russell, and Brandon Dennis provided database and other computer support. I would like to thank Russ Schreiner for his previous work in the area and sharing his insights and information over the years. Finally, James McLemore spent many days in the field camping, driving, mapping, and collecting samples with the senior author. Everyone's assistance is appreciated.

REFERENCES

Allen, M.S. and Foord, E.E., 1991, Geological, geochemical and isotopic characteristics of the Lincoln County porphyry belt, New Mexico: implications for regional tectonics and mineral deposits *in* Barker, J.M., Kues, B.S., Austin, G.S., and Lucas, S.G., eds., Geology of the Sierra Blanca, Sacramento, and Capitan Ranges, New Mexico: New Mexico Geological Society, 42nd Annual Field Conference, Guidebook, p. 97-113.

Barker, D.S., 1977, Northern Trans-Pecos Magmatic province: Introduction and comparison with the Kenya rift: Geological Society of America Bulletin, v. 88, p. 1421-1427.

Barker, D.S., 1979, Cenozoic magmatism in the Trans-Pecos province: Relation to Rio Grande rift; *in* Riecker, R. E., editor, Rio Grande Rift: Tectonics and magmatism: American Geophysical Union, p. 382-392.

Barker, D.S., 1980, Cenozoic igneous rocks, Sierra Blanca area, Texas: New Mexico Geological Society, Guidebook 31, p. 219-223.

Barker, D.S., 1987, Tertiary alkaline magmatism in Trans-Pecos Texas; in Fitton, J. G. and Upton, B. G. J., eds., Alkaline igneous rocks: Geological Society, Special Publication 30, p. 415-431.

Barker, D.S., and Hodges, F.N., 1977, Mineralogy of intrusions in the Diablo Plateau, northern Trans-Pecos magmatic province, Texas and New Mexico: Geological Society of America Bulletin, v. 88, p. 1428-1436.

Barker, D.S., Long, L.E., Hoops, G.K. and Hodges, F.N., 1977, Petrology and Rb-Sr isotope geochemistry of intrusions in the Diablo Plateau, northern Trans-Pecos magmatic province, Texas and New Mexico: Geological Society America, Bulletin, v. 88, p. 1437-1446.

Black, B.A., 1975, Geology and oil and gas potential of the northeast Otero platform area, New Mexico: New Mexico Geological Society, Guidebook 26, p. 323-333.

Boggs, R.C., 1985, Mineralogy of the Wind Mountain laccolith, Otero County, New Mexico (abstr.): New Mexico Geology, v. 7, p. 41-42.

Boggs, R.C., 1987, Mineralogy and textures of a eudialyte-bearing dike, Wind Mountain, Otero County, New Mexico (abstr.): New Mexico Geology, v. 9, p. 22.

Boggs, R.C. and Ghose, S., 1985, Georgechaoite, $NaKZrSi_3O_9 \cdot 2H_2O$, a new species from Wind Mountain, New Mexico: Canadian Mineralogist, v. 23, pp. 1-4.

Bonham, H.F., Jr., 1988, Models for volcanic-hosted epithermal precious metal deposits; *in* Bulk mineable precious metal deposits of the western United States: Geological Society of Nevada, Symposium Proceedings, p. 259-271.

Bultman, M.W., 2021a, Aeromagnetic and aeroradiometric data acquired over parts of the Trans-Pecos region of West Texas and Southern New Mexico: U.S. Geological Survey data release, https://doi.org/10.5066/P91GTPQL

Bultman, M.W., 2021b, Potential for concealed critical mineral deposits in the northern Trans-Pecos region of west Texas and southern New Mexico from a new aeromagnetic survey (abstr.); in Critical minerals: From discovery to supply chain, Program with abstracts, British Columbia Ministry of Energy, Mines and Low Carbon Innovation, British Columbia Geological Survey GeoFile 2021-14, p. 46-47.

Bultman, M.W., 2022, Delineating potential for concealed critical mineral deposits in the northern Trans-Pecos region of West Texas and Southern New Mexico with a new aeromagnetic/aeroradiometric survey: Geological Society of Nevada Symposium May2-5, 2022.

Chapin, C.E., 2012, Origin of the Colorado mineral belt: Geosphere, v. 8, p. 28-43.

Chapin, C.E., Wilks, M., and McIntosh, W.C., 2004, Space-time patterns of Late Cretaceous to present magmatism in New Mexico; comparison with Andean volcanism and potential for future volcanism; *in* Tectonics, geochronology and volcanism in the southern Rocky Mountains and Rio Grande rift: New Mexico Bureau of Geology and Mineral Resources, Bulletin 160, p. 13-40, http://geoinfo.nmt.edu/publications/bulletins/160/downloads/02chapin.pdf (accessed March 29, 2012).

Clabaugh, S.E., 1941, Geology of the northwestern portion of the Cornudas Mountains, New Mexico: unpublished M. S. thesis, University of Texas at Austin, 66 p.

Clabaugh, S.E., 1950, Eudialyte and eucolite from southern New Mexico (abstr.): American Mineralogist, v. 35, p. 279-280.

Collins, G. E., 1958, Preliminary reconnaissance for uranium in the Cornudas Mountains, Otero County, New Mexico and Hudspeth County, Texas: U.S. Atomic Energy Commission, Report DBO-4-TM-5, 16 p.

Committee on Critical Mineral Impacts of the U.S. Economy, 2008, Minerals, Critical Minerals, and the U.S. Economy: Committee on Earth Resources, National Research Council, ISBN: 0-309-11283-4, 264 p., http://www.nap.edu/catalog/12034.html

DeMark, R.S., 1989, Micromounting in New Mexico. The Mineralogical Record, v. 20, p. 64.

Dostal, J., 2017, Rare Earth Element Deposits of Alkaline Igneous Rocks: Resources, 6(3), Article 3, https://doi.org/10.3390/resources6030034

Fleck, R. J., Sutter, J. F., and Elliot, D. H. (1977). Interpretation of discordant 40Ar/39Ar age-spectra of Mesozoic tholeiites from Antarctica: Geochimica et Cosmochimica Acta, 41(1), 15-32. https://doi.org/10.1016/0016-7037(77)90184-3

Fleischer, M. and Cameron, E.N., 1946, U.S. Geological Survey, Trace Elements Investigative Report 29, 27 p.

Frost, B.D., Barnes, C.G., Collins, W.J., Arculus, R.J., Ellis, D.J., and Frost, C.D., 2001, A geochemical classification for granitic rocks: Journal of Petrology, v. 42, no. 11, p. 2033-2048.

Fulp, M.S. and Woodward, L.A., 1991, Mineral deposits of the New Mexico alkalic province (abstr.): Geological Society of America, Abstracts with Programs, v. 23, p. 23.

Ghose, S. and Thakur, P., 1985, The crystal structure of georgechaoite $NaKZrSi_3O_9 \cdot 2H_2O$: Canadian Mineralogist, v. 23, pp. 5-10.

Goodell, P.C., Lueth, V.W., and Willsie, T.C., 2002, The Chess Draw depression, Otero County, New Mexico: A hydrothermally-altered sublaccolithic, alkalic system: New Mexico Geological Society, Guidebook 53, p. 357-361.

Henry, C.D. and McDowell, F.W., 1986, Geochronology of magmatism in the Tertiary volcanic field, Trans-Pecos, Texas: Texas Bureau of Economic geology, guidebook 23, p. 99-122.

Henry, C.D., McDowell, F.W., Price, J.G., and Smyth, R.C., 1986, Compilation of potassium-argon ages of Tertiary igneous rocks, Trans Pecos Texas: University of Texas at Austin, Bureau of Economic Geology, Geologic Circular 86-2, 34 p.

Henry, C.D., McIntosh, W., McDowell, F.W., Lipman, P.W., Chapin, C.E., and Richardson, M.T., 2010, Distribution, timing, and controls of the Mid-Cenozoic ignimbrite flareup in western North America (abstr.): Geological Society of America Abstracts with Programs, v. 42, no. 5, p. 144.

Holser, W.T., 1959, Trans-Pecos region, Texas and New Mexico; *in* Warner, L. A., Holser, W. T., Wilmarth, V. R., and Cameron, E. N., eds., Occurrence of non-pegmatitic beryllium in the United States: U.S. Geological Survey, Professional Paper 318,197 p.

Industrial Minerals, 1995, Newcomer to nepheline syenite: Industrial Minerals, no. 332, p.17.

Johnsen, O., Ferraris, G., Gault, R.A., Grice, J.D., Kampf, A.R., and Pekov, I.V., 2003, The nomenclature of eudialyte-group minerals: Canadian Mineralogist, v. 41, p. 785-794.
Kelley, K.D. and Luddington, S., 2002, Cripple Creek and other alkaline-related gold deposits in the southern Rocky Mountains, USA: influence of regional tectonics: Mineralium Deposita, v. 37, p. 38-60.
Kelley, K.D., and Sry, P.G., 2016, Critical elements in alkaline igneous rock-related epithermal gold deposits; Verplank, P.L. and Hitzman, M.W., eds., Rare earth and critical elements in ore deposits: Society of Economic Geologists, Reviews in Economic Geology 18, p. 195-216.
Kelley, S**.,** Fichera, M., Evenocheck, E., Eberle, B.A., Person, M., Cadol, D., Newton, B.T., Timmons, S., and Pokorny, C., 2020, Assessment of Water Resources in the Salt Basin Region of New Mexico and Texas: Data Summary Report: New Mexico Bureau of Geology and Mineral Resources, Open-file report 608, https://geoinfo.nmt.edu/publications/openfile/details.cfml?Volume=608
King, P.B., 1934, Permian stratigraphy of Trans-Pecos, Texas: Geological Society of America Bulletin, v. 45, p. 697-798.
King, W.E., and Harder, V.M., 1985, Oil and gas potential of the Tularosa Basin-Otero platform-Salt Basin graben area, New Mexico and Texas: New Mexico Bureau of Mines and Mineral Resources, Circular 198, 36 p.
Klein, D.P. and Rodrigues, B.D., 1997, Electrical resistivity survey in the Cornudas Mountains area, Otero County, New Mexico: U.S. Geological Survey, Open-file Report 97-149, 25 p.
Kness, R. F., 1994, Mineral resource investigation of part of the Fort Bliss Military Reservation (McGregor Range), Caballo Resource Area, Otero County, New Mexico: U.S. Bureau of Mines, Mineral Land Assessment Report MLA-19-94, 46 pp.
Konnerup-Madsen, J., and Rose-Hansen, J., 1984, Composition and significance of fluid inclusions in the Ilímaussaq peralkaline granite, South Greenland: Bulletin de Minéralogie, 107(2), p. 317–326, https://doi.org/10.3406/bulmi.1984.7761
Korzeb, S. L., and Kness, R. F., 1994, Mineral resources in areas of critical environmental concern in the Caballo Resource Area, Otero County, New Mexico: U. S. Bureau of Mines, Mineral Land Assessment Report MLA 20-94, 72 pp.
Korzeb, S. L., Kness, R. F., Geroyan, R. I., and Ward, D. A., 1995, Mineral resource assessment of the Caballo Resource Area, Sierra and Otero Counties, New Mexico: U.S. Bureau of Mines, Mineral Land Assessment Report MLA 5–95, 177 p.
Kues, B.S., and Lucas, S.G., 1993, Stratigraphy, paleontology and correlation of Lower Cretaceous exposures in southeastern New Mexico; *in* Love, D. L., Hawley, J. W., Kues, B. S., Adams, J. W., Austin, G., S., and Barker, J. M., eds., Carlsbad Region, New Mexico and Texas: New Mexico Geological Society, Guidebook 44, p. 245-260.
Kuiper, K. F., Deino, A., Hilgen, F. J., Krijgsman, W., Renne, P. R., and Wijbrans, J. R., 2008, Synchronizing rock clocks of earth history: Science, v. 320, p. 500-504.
LeMaitre, R.W., ed., 1989, A classification of igneous rocks and glossary of terms: Blackwell Scientific Publications, Oxford, Great Britain, 193 p.
Leung, D.D. and McDonald, A.M., 2020, Windmountainite, $Fe^{+3}{}_2Mg_2\,2Si_8O_{20}(OH)_2(H_2O)_4{\cdot}4H_2O$, a new modulated, layered Fe3+-Mg-silicate-hydrate from Wind Mountain, New Mexico: Characterization and origin, with comments on the classification of palygorskite-group minerals: The Canadian Mineralogist, v. 58, p. 477-509, DOI: 10.3749/canmin.1900063.

Lindgren, W., 1933, Mineral deposits, 4th edition: New York, McGraw-Hill, 930 p.
Long, K.R., van Gosen, B.S., Foley, N.K. and Cordier, D., 2010, The principle rare earth elements deposits of the United States—A summary of domestic deposits and a global perspective: U.S. Geological Survey, Scientific Investigations Report 2010-5220, 104 p., http://pubs.usgs.gov/sir/2010/5220/ (accessed 5/1/12).
Ma, Y., Stopic, S., and Friedrich, B., 2019, Hydrometallurgical treatment of an eudialyte concentrate for preparation of rare earth carbonate: Johnson Matthey Technology Review, v. 63, 12 p., Hydrometallurgical Treatment of an Eudialyte Concentrate for Preparation of Rare Earth Carbonate - technology.matthey.com
Markl, G., Marks, M., Schwinn, G., and Sommer, H., 2001, Phase Equilibrium Constraints on Intensive Crystallization Parameters of the Il´ımaussaq Complex, South Greenland. 42(12).
Mason, G.T., Jr. and Arndt, R.E., 1996, Mineral resources data system (MRDS): U.S. Geological Survey, Digital Data Series DDS-20, CD-ROM.
Masotta, M., Mollo, S., Freda, C., Gaeta, M., and Moore, G., 2013, Clinopyroxene-liquid thermometers and barometers specific to alkaline differentiated magmas: Contributions to Mineralogy and Petrology, v. 166, p. 1545-1561.
Maynard, S.R., 2002, Laccoliths of the Ortiz porphyry belt, Santa Fe County, New Mexico: New Mexico Geology, v. 27, p. 3-21.
McLemore, V. T., 1983, Uranium and thorium occurrences in New Mexico: distribution, geology, production, and resources; with selected bibliography: New Mexico Bureau of Mines and Mineral Resources, Open-file Report OF-182, 950 pp., also; U.S. Department of Energy Report GJBX-11 (83).
McLemore, V.T., 1996, Great Plains Margin (alkalic-related) gold deposits in New Mexico; *in* Cyner, A.R. and Fahey, P.L. (eds.), Geology and ore deposits of the American Cordillera: Geological Society of Nevada Symposium Proceedings, Reno/Sparks, Nevada, April 1995, p. 935-950.
McLemore, V.T., 2001, Silver and gold resources in New Mexico: New Mexico Bureau of Mines and Mineral Resources, Resource Map 21, 60 p.
McLemore, V.T., 2002, Geology and geochemistry of the Mid-Tertiary alkaline to calc-alkaline intrusions in the northern Hueco Mountains and adjacent areas, McGregor Range, southern Otero County, New Mexico: New Mexico Geological Society, Guidebook 52, p. 129-137.
McLemore, V.T., 2010, Use of the New Mexico Mines Database and ArcMap in Uranium Reclamation Studies: Society of Mining, Metallurgy and Exploration Annual Convention, Phoenix, Feb 2010, Preprint 10-125, 10 p., http://www.onemine.org/view/?d=8E55DAEA43EE7D5BA01638DB9CFBD177001A9F1C5B76 7B62C0A1D7A061509FCB169983 (accessed 8/22/11)
McLemore, V.T., 2011, Rare earth elements for emerging technologies: New Mexico Earth Matters, summer, 4 p., http://geoinfo.nmt.edu/publications/periodicals/earthmatters/11/EM11n2.pdf
McLemore, V.T., 2014, Rare Earth Elements Deposits in New Mexico, *in* Conway, F.M., ed., Proceedings of the 48th Annual Forum on the Geology of Industrial Minerals, Phoenix, Arizona, April 30 - May 4, 2012. Arizona Geological Survey Special Paper #9, Chapter 3, p. 1-16, http://repository.azgs.az.gov/uri_gin/azgs/dlio/1568
McLemore, V.T., 2015a, Mineral deposits associated with Tertiary alkaline igneous rocks in New Mexico: Society for Mining, Metallurgy, and Exploration, 2015 Annual meeting preprint, 13 p.

McLemore, V.T., 2015b, Great Plains Margin (alkaline-related) gold deposits in New Mexico: twenty years later: Geological Society of Nevada, New concepts and discoveries, 2013 Symposium volume.

McLemore, V.T., 2015c, Geology and Mineral Resources of the Laughlin Peak Mining District, Colfax County, New Mexico: New Mexico Geological Society, Guidebook 66, p. 277-288**.**

McLemore, V.T., 2017, Mining districts and prospect areas of New Mexico: New Mexico Bureau of Geology and Mineral Resources, Resource Map 24, 65 p., scale 1:1,000,000.

McLemore, V.T., 2018, Rare Earth Elements (REE) Deposits Associated with Great Plain Margin Deposits (Alkaline-Related), Southwestern United States and Eastern Mexico: Resources, 7(1), 8; 44 p., doi:10.3390/resources7010008; http://www.mdpi.com/2079-9276/7/1/8 link http://www.mdpi.com/2079-9276/7/1/8

McLemore, V.T., and Guilinger, J. R., 1993, Geology and mineral resources of the Cornudas Mountains, Otero County, New Mexico and Hudspeth County, Texas: New Mexico Geological Society, Guidebook 44, p. 145-154.

McLemore, V. T. and Guilinger, J. R., 1996, Industrial specifications of the Wind Mountain nepheline- syenite deposit, Cornudas Mountains, Otero County, New Mexico; *in* Austin, G. S., Barker, J.M., Hoffman, G., Gilson, N., and Zidec, J., eds., Proceedings of the 31st Forum on the Geology of Industrial Minerals, Borderland Forum: New Mexico Bureau of Mines and Mineral Resources, Bulletin 154, pp. 121-126.

McLemore, V. T., Guilinger, J. R., and Oumiette, M. A., 1994, Geology of the Wind Mountain nepheline syenite deposit, Cornudas Mountains, Otero County, New Mexico: Society Mining, Metallurgy, and Exploration, Preprint 94-63, 10 p.

McLemore, V.T., Hoffman, G., Smith, M., Mansell, M., and Wilks, M., 2005a, Mining districts of New Mexico: New Mexico Bureau of Mines and Mineral Resources, OF-494, CD-ROM.

McLemore, V.T., Haft, E., Owen, E., Woodard, M., and Iverson, N., 2023**,** Mineralogy and Geochemistry of Selected Rare Earth Elements (REE) Deposits in the North American Cordilleran alkaline-igneous belt in New Mexico (abstr.): Minexchange, 2023 SME Annual Conference Technical Program, p.76.

McLemore, V.T., Kelley, S., Zimmerer, M.J., Owen, E., Haft, E., Cantrell, T., Gysi, A., Haley, D., Cherotich, S., and Trivett, A., 2021, Geology and mineral resources of the Gallinas Mountains, Lincoln and Torrance Counties, New Mexico: New Mexico Bureau of Geology and Minerals Resources, Open-file Report 617, 164 p., https://geoinfo.nmt.edu/publications/openfile/details.cfml?Volume=617

McLemore, V.T., Krueger, C.B., Johnson, P., Raugust, J.S., Jones, G.E., Hoffman, G.K. and Wilks, M., 2005b, New Mexico Mines Database: Mining Engineering, February, p. 42-47.

McLemore, V.T., Leo-Russell, M., Trivitt, A., Dennis, B., and Kasefang, D., 2022, Development of Data Systems to Support Critical Mineral Research in New Mexico (abstr.): Society of Economic Geologists (SEG) annual meeting Aug., STV4-11, https://geoinfo.nmt.edu/staff/mclemore/projects/mining/REE/documents/SEG-2022-Speed-Talk-McLemorev2.pdf

McLemore, V.T., Lueth, V.W., Pease, T.C., and Gulinger, J.R., 1996a, Petrology and mineral resources of the Wind Mountain laccolith, Cornudas Mountains, New Mexico and Texas: Canadian Mineralogist, v. 34, pt. 2, p. 335-347

McLemore, V. T., Lueth, V. W., Guilinger, J. R., and Pease, T. C., 1996b, Geology, mineral resources, and marketing of the Wind Mountain nepheline-syenite porphyry, Cornudas Mountains, New Mexico and Texas; *in* Austin, G. S., Barker, J. M., Hoffman, G., Gilson, N., and Zidec, J., eds., Proceedings of the 31st Forum on the Geology of Industrial Minerals, Borderland Forum: New Mexico Bureau of Mines and Mineral Resources, Bulletin 154, pp. 127-136.

McLemore, V.T., North, R.M., and Leppert, S., 1988a, Rare-earth elements (REE), niobium and thorium districts and occurrences in New Mexico: New Mexico Bureau of Mines and Mineral Resources, Open-file Report OF-324, 28 p.

McLemore, V.T., North, R.M., and Leppert, S., 1988b, Rare-earth elements (REE) in New Mexico: New Mexico Geology, v. 10, p. 33-38.

McMillan, N.J., Dickin, A.P. and Haag, D., 2000, Evolution of magma source regions in the Rio Grande rift, southern New Mexico: Geological Society of America Bulletin, v. 112, p. 1582-1593.

Michayluk, M.C., and Cone, J., 2017a, Collecting Wind Mountain (in the Cornudas Mountains, NM, USA): part 1: https://www.mindat.org/a/windmountain_pt1

Michayluk, M.C., and Cone, J., 2017b, Collecting Wind Mountain (in the Cornudas Mountains, NM, USA): part 2: https://www.mindat.org/a/windmountain_pt2

Miller, W.R., 1997, Environmental geochemistry and processes controlling water chemistry, Cornudas Mountains, New Mexico: U.S. Geological Survey, Open-file Report 97-158, 29 p.

Min, K., Mundil, R., Renne, P.L., and Ludwig, K.R., 2000, A test for systematic errors in $^{40}Ar/^{39}Ar$ geochronology through comparison with U/Pb analysis of a 1.1-Ga rhyolite: Geochimica et Cosmochimica Acta, v. 64, p. 73-98.

Möller, V., and Williams-Jones, A.E., 2016, Petrogenesis of the Nechalacho Layered Suite, Canada: Magmatic Evolution of a REE–Nb-rich Nepheline Syenite Intrusion: Journal of Petrology, *57*(2), p. 229–276, https://doi.org/10.1093/petrology/egw003

Mutschler, F.E., Griffin, M.E., Stevens, D.S. and Shannon, S.S., Jr., 1985, Precious metal deposits related to alkaline rocks in the North American Cordillera-an interpretive review: Transactions Geological Society of America, v. 88, p. 355-377.

Mutschler, F.E., Mooney, T.C., and Johnson, D.C., 1991, Precious metal deposits related to alkaline igneous rocks-a space-time trip through the Cordillera: Mining Engineering, v. 43, p. 304-309.

New Mexico Bureau of Mines and Mineral Resources, New Mexico State University Southwest Technology Institute, and TRC Mariah Associates, Inc., 1998, Mineral and energy resource assessment of the McGregor Range (Fort Bliss), Otero County, New Mexico: New Mexico Bureau of Mines and Mineral Resources OF- 458, 543 p.

New Southwest and Grant County Herald, 1882, Mining Department: Las Cruces, January 21, 1882, p. 1.

Neir, A.O., 1950, A redetermination of the relative abundances of the isotopes of carbon, nitrogen, oxygen, argon, and potassium: Physical Reviews, v. 77, p. 789-793.

North, R.M., and McLemore, V.T., 1988, A classification of the precious metal deposits of New Mexico; *in* Bulk mineable precious metal deposits of the western United States Symposium Volume: Geological Society of Nevada, Reno, Symposium held April 6-8, 1987, p. 625-660.

Northrop, S.A., 1996, Minerals of New Mexico: University of New Mexico Press, Albuquerque, New Mexico, 356 p.

Nutt, C.J., O'Neille, J.M., Kleinkopf, M.D., Klein, D.P., Miller, W.R., Rodriquez, B.D., and McLemore, V.T., 1997, Geology and mineral resources of the Cornudas Mountains, New Mexico: U.S. Geological Survey, Open file Report OF97-282, 46 p., http://pubs.usgs.gov/of/1997/0282/report.pdf (accessed 8/22/14).

Nutt, C.J. and O'Neill, J.M., 1998, Geologic framework of Tertiary intrusions of the Cornudas Mountains, southern New Mexico: New Mexico Geological Society, Guidebook 49, p. 129-134.

O'Neill, J.M. and Nutt, C.J., 1998, Geologic map of the Cornudas Mountains, Otero County, New Mexico: U.S. Geological Survey, Miscellaneous Geologic Investigations Map, I-2631.

Pearce, J.A., Harris, N.B.W. and Tindle, A.G., 1984, Trace element discrimination diagrams for the tectonic interpretation of granitic rocks: Journal of Petrology, v. 24, p. 956–983.

Pingitore, N., Clague, J., and Gorski, D., 2014, Round Top Mountain rhyolite (Texas, USA), a massive Y-bearing-fluorite-hosted heavy rare earth element (HRRE) deposit: Journal of Rare Earths, v. 32, no.1, p. 90-96.

Potter, L.S., 1996a, Chemical variation along strike in feldspathoidal rocks of the eastern alkali belt, Trans-Pecos magmatic province, Texas and New Mexico: The Canadian Mineralogist, v. 34, p. 241-264.

Potter, L.S., 1996b, Chemical and isotopic variation along strike in the eastern alkali belt, Trans-Pecos magmatic province, Texas and New Mexico: PhD. Dissertation, University of Texas at Austin, 267 p.

Pray, L.C., 1961, Geology of the Sacramento Mountains escarpment, Otero County, New Mexico, New Mexico Bureau of Mining and Mineral Resources, Bulletin 35, 144p.

Price, J.G., Henry, C.D., Barker, D.S., and Parker, D.F., 1987, Alkalic rocks of contrasting tectonic settings in trans-Pecos, Texas: Geological Society of America, Special Paper no. 215, p. 335-346.

Price, J.G., Rubin, J.N., Henry, C.D., Pinkston, T.L., Tweedy, S.W. and Koppenaal, D.W., 1990, Rare-metal enriched peraluminous rhyolites in a continental arc, Sierra Blanca area, Trans-Pecos Texas; chemical modification by vapor-phase crystallization; *in* H.J. Stein and Hannah, J.L., Ore-bearing granite systems; Petrogenesis and mineralizing processes: Geological Society of America, Special Paper 246, p. 103-120.

Prodehl, C. and Lipman, P.W., 1989, Crustal structure of the Rocky Mountain region; *in* Pakiser, L.C. and Mooney, W.D., eds., Geophysical framework of the continental United States: Boulder, Colorado, Geological Society of America Memoir 172, p. 249-284.

Richards, J.P., 1995, Alkalic-type epithermal gold deposits—a review; *in* Thompson, J.F.H. (ed.), Magmas, fluids, and ore deposits: Mineralogical Association of Canada, Short Course Series, v. 23, p. 367-400.

Ross, J., 2014, Geochronology of southern McMurdo Sound and development of pychron: a $^{40}Ar/^{39}Ar$ data collection and processing software suite [dissertation]: New Mexico Institute of Mining and Technology.

Rubin, J.N., Price, J.G., Henry, C.D. and Koppenaal, D.W., 1987, Cryolite-bearing and rare metal-enriched rhyolite, Sierra Blanca Peaks, Hudspeth County, Texas: American Mineralogist, v. 72, p. 1122-1130.

Rubin, J.N., Price, J.G., Henry, C.D., Pinkston, T.L., Tweedy, S.W., Koppenaal, D.W., Peterson, S.B., Harlan, H.M., Miller, W.T., Thompson, R.J., Grabowski, R.G., Laybourn, P.D., Schrock, G.E., Johnson, A., Staes, D.G., Gains, R.V., and Miller, T.H., 1988, Mineralogy

of beryllium deposits near Sierra Blanca, Texas; in A.E. Torma and I.H. Gundiler, eds. Precious and rare metals technologies: Elsevier, Amsterdam, p. 601-614.
Rubin, J.N., Henry, C.D., and Price, J.G., 1989**,** Hydrothermal zircons and zircon overgrowths, Sierra Blanca Peaks, Texas: American Mineralogist, v. 74, p. 865-869.
Rubin, J.N., Price, J.G., Henry, C.D. and Kyle, J.R., 1990, Geology of the beryllium-rare earth element deposits at Sierra Blanca, west Texas; *in* J.R. Kyle, Industrial minerals of the Delaware Basin, Texas and New Mexico: Society of Economic Geologists, Guidebook 8, p. 191-203.
Scaar, I.C., 1986, Results of drilling the Chess Draw prospect, Otero County, New Mexico: U.S. Borax, unpublished report.
Schandl, E.S. and Gorton, M.P., 2002, Application of high field strength elements to discriminate tectonic settings in VMS environments: Economic Geology, v. 97, p. 629-642
Schreiner, R.A., 1994, Mineral investigation of Wind Mountain and the Chess Draw area, Cornudas Mountains, Otero County, New Mexico: U.S. Bureau of Mines, MLA 26-94, 51 p.
Shumard, G.G., 1886, A partial report on the geology of West Texas: Austin State Printing Office, p. 98-99.
Silin, I., Gürsel, D., Bütchter, C., Weitkämper, L. and Wotruba, H., 2022, Recovery of catapleiite and eudialyte from non-magnetic fraction of eudialyte ore processing of Norra Karr deposit: Minerals, v. 12, 19 p.
Sillitoe, R.H. 1985, Ore-related breccias in volcanoplutonic arcs: Economic Geology, v. 80, p. 1467-1515.
Sims, P.K., Stein, H.J., and Finn, C.A., 2002, New Mexico structural zone—an analogue of the Colorado mineral belt: Ore Geology Reviews, v. 21, p. 211-225.
Standard Silver Corporation, 2008, Round Top beryllium, uranium, rare earth project: unpublished company report, 34 p., http://www.standardsilvercorp.com/main-sect/uploads/08/round_top_presentation.pdf, accessed February 3, 2010.
Subcommittee on Critical and Strategic Mineral Supply Chains Committee on Environment, Natural Resources, and Sustainability, 2018, Assessment of critical minerals: Updated application of screening methodology: National Science and Technology Council, 7 p., https://www.whitehouse.gov/wp-content/uploads/2018/02/Assessment-of-Critical-Minerals-Update-2018.pdf
Taylor, S.R. and McLennan, S.M., 1985, The Continental Crust: Its Composition and Evolution. Blackwell Scientific Publication, Carlton, 312 p.
Timm, B.C., 1941, The geology of the southern Cornudas Mountains, Texas and New Mexico: unpublished M. S. thesis, University of Texas at Austin, 55 p.
Thompson, T.B, 1991a, Genesis of gold associated with alkaline igneous rocks (abstr.): Geological Society of America, Abstracts with Programs, v. 23, p. 99-100.
Thompson, T.B., 1991b, The Lincoln County porphyry belt, New Mexico (abstr.): Geological Society of America, Abstracts with Programs, v. 23, p. 99.
Tschernich, R., 1992, Zeolites of the World, 67 p.
U.S. Borax, 1986, Geologic map of Chess Draw: unpublished map.
U.S. Bureau of Mines, 1995, MAS/MILS CD-ROM: U.S. Bureau of Mines, Special Publication 12-95, CD-ROM.

U.S. Executive Order No. 13817, 2017, Presidential executive order on a federal strategy to ensure secure and reliable supplies of critical minerals: Federal Register :: A Federal Strategy To Ensure Secure and Reliable Supplies of Critical Minerals.

Vaccarezza, V. and Anderson, C., 2019, An overview of beneficiation and hydrometallurgical techniques on eudialyte group minerals: Mining, Metallurgy, and Exploration, v. 37, p. 39-50.

Walker, J.D. and Cohen, H.A., 2009, Geoscience Handbook: The AGI data sheets: American Geological Institute, 4th edition, ISBN 10: 0922152756 / ISBN 13: 9780922152759

Wilson, R. and Kyser, T.K., 1988, Geochemistry of porphyry-hosted Au-Ag deposits in the Little Rocky Mountains, Montana: Economic Geology Bulletin 3, p. 1329-1346.

Warner, L.A., Holser, W.T., Wilmarth, V.R., and Cameron, E.N., 1959, Occurrence of nonpegmatite beryllium in the United States: U.S. Geological Survey, Professional Paper, v. 318, 198 p.

Wilson, M., 1989, Igneous Petrogenesis: London, Unwin Hyman, 499 p.

Woodward, M., 2023, Using $^{40}Ar/^{39}Ar$ Geochronology and clinopyroxene geothermometry to re-evaluate the emplacement history and tectonics of the Cornudas Mountains, Southern New Mexico: New Mexico Institute of Mining and Technology, M.S. thesis, 89 p.

Woodward, M., Iverson, N., Waters, L., and McLemore, V.T., 2022, Re-evaluating the emplacement history and tectonics of the Cornudas Mountains, southern New Mexico (abstr.): Geological Society of America, Connects 2022, annual conference, https://gsa.confex.com/gsa/2022AM/meetingapp.cgi/Paper/383081

Woodrome, L.S., 1980, Uranium: Trans-Pecos, Texas Tertiary intrusive and groundwater anomalies: University of Texas at El Paso, M.S. thesis, 234 p.

Woolley, A.R., 1987, Alkaline rocks and carbonatites of the world, Part 1: North and South America: University of Texas Press, Austin.

Zapp, A.D., 1941, Geology of the northeastern Cornudas Mountains, New Mexico: unpublished M. S. Thesis, University of Texas at Austin, 63 p.

Zimmerer, M.J., Ramos, F.C., and Orozco, S., 2019, Possible origins of dikes exposed in northeastern New Mexico and implications for Mid-Tertiary alkali magmatism in the region: New Mexico Geological Society, Guidebook 70, p. 161-168.